

# A phase field model for droplets suspended in viscous liquids under the influence of electric fields

Yuzhe Qin<sup>a</sup>, Huaxiong Huang<sup>b,c,\*</sup>, Zilong Song<sup>d</sup> and Shixin Xu<sup>e,\*</sup>

<sup>a</sup>*Key Laboratory of Complex Systems and Data Science of Ministry of Education and School of Mathematical Sciences, Shanxi University, Taiyuan, 030006, China;*

<sup>b</sup>*Advanced Institute of Natural Sciences, Beijing Normal University, Zhuhai, 519087, China*

<sup>c</sup>*BNU-HKBU United International College, Zhuhai, 519087, China*

<sup>d</sup>*Department of Mathematics and Statistics, Utah State University, Logan, UT, 84322, US*

<sup>e</sup>*Duke Kunshan University, 8 Duke Ave, Kunshan, Jiangsu, China*

*\*Corresponding authors, shixin.xu@dukekunshan.edu.cn; hhuang@uic.edu.cn*

## Abstract

In this paper, we propose a Poisson-Nernst-Planck-Navier-Stokes-Cahn-Hilliard (PNP-NS-CH) model for an electrically charged droplet suspended in a viscous fluid subjected to an external electric field. Our model incorporates spatial variations of electric permittivity and diffusion constants, as well as interfacial capacitance. Based on a time scale analysis, we derive two approximations of the original model, namely a dynamic model for the net charge (by assuming conductance remains unchanged) and a leaky-dielectric model (by assuming both conductance and net charge remain unchanged). For the leaky-dielectric model, we conduct a detailed asymptotic analysis to demonstrate the convergence of the diffusive-interface leaky-dielectric model to the sharp interface model as the interface thickness approaches zero. Numerical computations are performed to validate the asymptotic analysis and demonstrate the model's effectiveness in handling topology changes, such as electro-coalescence. Our numerical results of these two approximation models reveal that the polarization force, which is induced by the spatial variation of electric permittivity in the direction perpendicular to the external electric field, consistently dominates the Lorentz force, which arises from the net charge. The equilibrium shape of droplets is determined by the interplay between these two forces along the direction of the electric field. Furthermore, in the presence of the interfacial capacitance, local variation of effective permittivity leads to an accumulation of counter-ions near the interface, resulting in a reduction in droplet deformation. Our numerical solutions also confirm that the leaky-dielectric model serves as a reasonable approximation of the original PNP-NS-CH model when the electric relaxation time is sufficiently short. The Lorentz force and droplet deformation both decrease when diffusion of net charge is significant.

**Keyword:** Electrohydrodynamics, leaky-dielectric, sharp interface limit, phase field method

## 1 Introduction

When a charged droplet is suspended in a viscous fluid, it can exhibit complex behaviors, such as forming prolate or oblate shapes, pearling, and breaking up, under the influence of an externally applied electric field. Understanding and predicting droplet shape evolution are essential for many applications, including microfluidics ([25]), printing ([34]), emulsion stability ([1]), and biophysical systems ([10, 8, 29]). A more comprehensive review of this topic can be found in [26].

Various mathematical models have been developed to investigate the dynamics of droplets under electric fields, ranging from simplified leaky-dielectric models to more sophisticated models that consider charge transport, fluid flow, and interfacial dynamics. One of the very first models was proposed by [17], known as the Melcher-Taylor (TM) model. It is a mathematical framework that describes the behavior of electrically charged fluids in the presence of electric fields, assuming electroneutrality, quasi-static electric field, leaky-dielectric fluids, weak deformation with no charge convection. The TM model has been experimentally validated and further extended by [22], [14], and others to explore large drop deformations, stability, and breakup.

Another class of models are based on the Poisson-Nernst-Planck (PNP) system ([30, 5, 4, 27]), which has been applied successfully to problems involving ion transport. Ryham et al. ([21, 20]) proposed a coupled PNP-Navier Stokes (PNP-NS) system to model the motion of electrolyte droplets. Other researchers

([36, 23, 18]) have tried to build a link between PNP-NS and TM models. Most theoretical models are limited to small deformation while under the influence of a strong electric field, however, droplets may exhibit large deformation and topology changes, resulting in droplets merge (electro-coalescence, [15]) and breakup ([13]).

Various numerical methods are proposed to analyze complex flows of droplets with large deformation. [35]) proposed a Lattice Boltzmann method to solve leaky-dielectric problem and reveal the flow pattern. Boundary integral method is proposed by [14]) to study droplet breakup. Most of the investigations can be classified into two main categories, sharp interface and diffusive interface methods. In sharp interface approach, there are level set method ([6, 2]), front tracking method ([12]) and finite volume methods ([16, 9]), as well as hybrid immersed boundary (IB) and immersed interface method (IIM) [11] (for droplets) and [10] (for vesicles). Thanks to its ability to handle complex deformations and topological changes, diffusive interface models [15, 32, 33] have also been widely used for droplets with certain types of interfacial forces/energies. On the other hand, the capacitance and conductivity of droplet interface play important roles on their deformation and dynamics ([3, 7, 10]) since they change the continuity of electric potential and distribution of ions near the interface. How to integrate capacitance and conductance with spacial variation electric permittivity and diffusion consistently remains a challenge task.

In this paper, we propose a Poisson-Nernst-Planck-Navier-Stokes-Cahn-Hilliard (PNP-NS-CH) model for an electrically charged droplet suspended in a viscous fluid subjected to an external electric field, with the following specific features and objectives.

1. We propose a thermodynamically consistent model for electrohydrodynamics (EHD) of two-phase flow, considering different electric conductance and permittivity, within the framework of the diffusive interface model. In this model, the capacitance of the interface will be taken into consideration;
2. Based on an asymptotic analysis, we show that the obtained the diffusive-interface leaky dielectric model converges to the sharp interface one as the interface thickness tends to zero;
3. We compare and analyze the differences between the leaky dielectric model (where both net charge and conductivity remain unchanged) and a net charge model where both diffusion and convection of net charge are considered. By examining these differences, a deeper understanding of the roles of various forces and processes in the system can be gained;
4. We investigate the influence of electric forces on the equilibrium profile of the droplets. Particularly, we explore how variations in permittivity across the interface impact the distribution of ions and the resulting forces. This analysis provides insights into the mechanisms governing the behavior of the system under different conditions.

The rest of the paper is organized as follows. In section 2, we derive the phase field Poisson-Nernst-Planck-Navier-Stokes model based on the energy variational method. Then, the phase field leaky dielectric model is derived based on the time scale assumption. In section 3, the sharp interface limit is conducted to show our model could converge to the former sharp interface leaky dielectric model. In section 4, a series of numerical experiments are presented to verify the effectiveness of our phase field leaky dielectric model and study the capacitance effect at the interface. The comparison of the results from leaky dielectric and net charge dynamic models are given in section 5. Conclusions and the limitation of the current models and future directions are given in section 6.

## 2 Model derivation

In this section, energy variation method is used to derive a thermal dynamically consistent phase field model for a droplet suspended in a viscous fluid under an external electric field. We define two functionals for the total energy and dissipation of the system and introduce the corresponding kinematic equations based on physical laws of conservation. The specific forms of the flux and stress functions in the kinematic equations are obtained by taking the time derivative of the total energy functional and comparing with the dissipation functional. More details of this method can be found in [24].

### 2.1 Phase field model for a droplet suspended in electrolyte under electric field

Let  $\Omega$  represent the computational domain that consists of the droplet and ambient fluid.  $\psi$  is an order parameter function which is equal to 1 in the droplet region and -1 in the ambient fluid region. The

interface between two domains can be described by the zero level set  $\Gamma = \{\mathbf{x} : \psi(\mathbf{x}, t) = 0\}$ . Let  $c_i, i = 1 \dots N$  be the concentration of the  $i_{th}$  ion,  $\phi$  be the electric potential, and  $\mathbf{u}$  be the fluid velocity. Based the the laws of conservation, we have the following kinematic assumptions

$$\frac{\partial \psi}{\partial t} + \nabla \cdot (\mathbf{u} \psi) + \nabla \cdot \mathbf{j}_\psi = 0, \quad \text{in } \Omega, \quad (2.1a)$$

$$\frac{\partial c_i}{\partial t} + \nabla \cdot (\mathbf{u} c_i) + \nabla \cdot \mathbf{j}_i = 0, \quad i = 1, \dots, N, \quad \text{in } \Omega, \quad (2.1b)$$

$$\nabla \cdot \mathbf{D} = \sum_{i=1}^N z_i e c_i, \quad \text{in } \Omega, \quad (2.1c)$$

$$\mathbf{D} = \epsilon_{eff} \mathbf{E} = -\epsilon_{eff} \nabla \phi, \quad \text{in } \Omega, \quad (2.1d)$$

$$\rho \left( \frac{\partial \mathbf{u}}{\partial t} + (\mathbf{u} \cdot \nabla) \mathbf{u} \right) = \nabla \cdot \boldsymbol{\sigma}_\eta + \nabla \cdot \boldsymbol{\sigma}_e + \nabla \cdot \boldsymbol{\sigma}_\psi, \quad \text{in } \Omega, \quad (2.1e)$$

$$\nabla \cdot \mathbf{u} = 0, \quad \text{in } \Omega, \quad (2.1f)$$

where  $z_i$  is the valency of  $i$ th ion,  $\mathbf{D}$  is the electric displacement,  $\mathbf{E}$  is the electric field intensity,  $e$  is the elementary charge, and  $\rho$  is the density of fluid. The first two equations are the conservation of each phase and ion with two unknown flux  $\mathbf{j}_\psi$  and  $\mathbf{j}_i$ . The third and fourth equations are based on Maxwell equation. The last two equations are the law of conservation of momentum for incompressible fluid with unknowns stresses induced by viscosity  $\boldsymbol{\sigma}_\eta$ , electricity  $\boldsymbol{\sigma}_e$  and interface  $\boldsymbol{\sigma}_\psi$ , respectively.  $\epsilon_{eff}$  is the dielectric coefficient, which is defined by the harmonic average [19]

$$\epsilon_{eff}^{-1} = \frac{1 - \psi}{2\epsilon^-} + \frac{1 + \psi}{2\epsilon^+} + \frac{(1 - \psi^2)^2}{\delta C_m}, \quad (2.2)$$

where  $C_m$  is the capacitance of the interface, and  $\epsilon^\pm$  is the dielectric constant of the droplet and ambient fluid, respectively.

Here we consider a closed system during the derivation, i.e. the boundary condition is taken into account as

$$\mathbf{u}|_{\partial\Omega} = 0, \quad \mathbf{j}_i \cdot \mathbf{n}|_{\partial\Omega} = 0, \quad \mathbf{j}_\psi \cdot \mathbf{n}|_{\partial\Omega} = 0, \quad \phi|_{\partial\Omega} = 0, \quad \frac{\partial \psi}{\partial \mathbf{n}}|_{\partial\Omega} = 0, \quad \frac{\partial \mu_\psi}{\partial \mathbf{n}}|_{\partial\Omega} = 0. \quad (2.3)$$

In the next, energy variational method is used to derive those unknown terms. The total energy functional consists of kinetic energy, electrical static energy, entropy and phase mixing energy,

$$\begin{aligned} E_{total} &= E_{kin} + E_{es} + E_{ion} + E_{mix} \\ &= \int_{\Omega} \left( \frac{\rho}{2} |\mathbf{u}|^2 + \frac{1}{2} \mathbf{E} \cdot \mathbf{D} + k_B T \sum_{i=1}^N c_i \left( \ln \frac{c_i}{\tilde{c}} - 1 \right) + \lambda \left( \frac{\delta^2}{2} |\nabla \psi|^2 + F(\psi) \right) \right) d\mathbf{x}, \end{aligned} \quad (2.4)$$

where  $k_B$  and  $T$  are Boltzmann constant and temperature respectively,  $\tilde{c}$  is a reference concentration,  $\lambda$  is the energy density for phase mixing energy,  $\delta$  is the thickness of diffuse interface and  $F(\psi) = \frac{1}{4} (1 - \psi^2)^2$  is the double well potential.

According to the total energy, the chemical potentials are given by

$$\mu_i = z_i e \phi + k_B T \ln \frac{c_i}{\tilde{c}}, \quad i = 1 \dots N \quad (2.5a)$$

$$\mu_\psi = \lambda (-\delta^2 \nabla^2 \psi + F'(\psi)) - \frac{1}{2} \frac{\partial \epsilon_{eff}}{\partial \psi} |\mathbf{E}|^2. \quad (2.5b)$$

The dissipation is mainly induced by viscosity of fluid in macroscale, invertible ions and interface diffusion in microscale

$$\Delta = \int_{\Omega} 2\eta |\mathbf{D}_\eta|^2 d\mathbf{x} + \int_{\Omega} \sum_{i=1}^N \frac{D_i c_i}{k_B T} |\nabla \mu_i|^2 d\mathbf{x} + \int_{\Omega} \mathcal{M} |\nabla \mu_\psi|^2 d\mathbf{x}, \quad (2.6)$$

where  $\eta$  is fluid viscosity,  $\mathbf{D}_\eta = \frac{\nabla \mathbf{u} + (\nabla \mathbf{u})^T}{2}$  is the rate of strain,  $\mu_i$  is the chemical potential of  $i$ th ion,  $\mathcal{M}$  and  $\mu_\psi$  are the phenomenological mobility and chemical potential for  $\psi$  respectively.  $D_i$  is the diffusion coefficient of  $i_{th}$  ion

$$D_i^{-1} = \frac{1 - \psi}{2D_i^-} + \frac{1 + \psi}{2D_i^+}, \quad (2.7)$$

where  $D_i^\pm$  is the diffusion coefficient of  $i_{th}$  ion in two regions, respectively.

For a closed system, the total energy satisfies the following energy dissipation law [24, 30]

$$\begin{aligned}\frac{dE_{total}}{dt} &= \frac{dE_{kin}}{dt} + \frac{dE_{es}}{dt} + \frac{dE_{ion}}{dt} + \frac{dE_{mix}}{dt} \\ &= I_1 + I_2 + I_3 + I_4 \\ &= -\Delta.\end{aligned}\quad (2.8)$$

For the first term, using the Eqs.(2.1e)-(2.1f) yields

$$\begin{aligned}I_1 &= \frac{d}{dt} \int_{\Omega} \frac{1}{2} \rho |\mathbf{u}|^2 d\mathbf{x} \\ &= \frac{1}{2} \int_{\Omega} \left( \frac{\partial \rho}{\partial t} |\mathbf{u}|^2 + 2\rho \mathbf{u} \cdot \frac{\partial \mathbf{u}}{\partial t} \right) d\mathbf{x} \\ &= \frac{1}{2} \int_{\Omega} \left( \frac{\partial \rho}{\partial t} |\mathbf{u}|^2 + 2\rho \mathbf{u} \cdot \left( \frac{\partial \mathbf{u}}{\partial t} + \mathbf{u} \cdot \nabla \mathbf{u} - \mathbf{u} \cdot \nabla \mathbf{u} \right) \right) d\mathbf{x} \\ &= \int_{\Omega} \rho \mathbf{u} \cdot \left( \frac{\partial \mathbf{u}}{\partial t} + \mathbf{u} \cdot \nabla \mathbf{u} \right) d\mathbf{x} + \frac{1}{2} \int_{\Omega} \left( \frac{\partial \rho}{\partial t} |\mathbf{u}|^2 - 2\rho \mathbf{u} \cdot (\mathbf{u} \cdot \nabla \mathbf{u}) \right) d\mathbf{x} \\ &= \int_{\Omega} \mathbf{u} \cdot (\nabla \cdot \sigma_{\eta} + \nabla \cdot \sigma_e + \nabla \cdot \sigma_{\psi}) d\mathbf{x} + \frac{1}{2} \int_{\Omega} \left( \frac{\partial \rho}{\partial t} |\mathbf{u}|^2 - \rho \mathbf{u} \cdot \nabla |\mathbf{u}|^2 \right) d\mathbf{x} \\ &= - \int_{\Omega} \nabla \mathbf{u} : (\sigma_{\eta} + \sigma_e + \sigma_{\psi}) d\mathbf{x} + \frac{1}{2} \int_{\Omega} \left( \frac{\partial \rho}{\partial t} |\mathbf{u}|^2 + \nabla \cdot (\rho \mathbf{u}) |\mathbf{u}|^2 \right) d\mathbf{x} \\ &\quad - \frac{1}{2} \int_{\partial \Omega} \rho \mathbf{u} |\mathbf{u}|^2 \cdot \mathbf{n} ds + \int_{\partial \Omega} \mathbf{u} \cdot (\sigma_{\eta} + \sigma_e + \sigma_{\psi}) \cdot \mathbf{n} ds \\ &= - \int_{\Omega} \nabla \mathbf{u} : (\sigma_{\eta} + \sigma_e + \sigma_{\psi}) d\mathbf{x} - \int_{\Omega} p \nabla \cdot \mathbf{u} d\mathbf{x} \\ &\quad - \frac{1}{2} \int_{\partial \Omega} \rho \mathbf{u} |\mathbf{u}|^2 \cdot \mathbf{n} ds + \int_{\partial \Omega} \mathbf{u} \cdot (\sigma_{\eta} + \sigma_e + \sigma_{\psi}) \cdot \mathbf{n} ds,\end{aligned}\quad (2.9)$$

where  $\mathbf{n}$  is the unit outer normal vector of domain  $\Omega$ .

For electric potential energy, we have

$$\begin{aligned}\frac{dE_{es}}{dt} &= \frac{d}{dt} \int_{\Omega} \frac{1}{2} \mathbf{E} \cdot \mathbf{D} d\mathbf{x} \\ &= \frac{1}{2} \int_{\Omega} \left( \mathbf{D} \cdot \frac{\partial}{\partial t} \mathbf{E} + \mathbf{E} \cdot \frac{\partial}{\partial t} \mathbf{D} \right) d\mathbf{x} \\ &= \frac{1}{2} \int_{\Omega} \left( \mathbf{D} \cdot \frac{\partial}{\partial t} \mathbf{E} + \frac{\partial \epsilon_{eff}}{\partial \psi} \frac{\partial \psi}{\partial t} \mathbf{E} \cdot \mathbf{E} + \mathbf{D} \cdot \frac{\partial}{\partial t} \mathbf{E} \right) d\mathbf{x} \\ &= \int_{\Omega} \mathbf{D} \cdot \frac{\partial}{\partial t} \mathbf{E} d\mathbf{x} + \frac{1}{2} \int_{\Omega} \frac{\partial \epsilon_{eff}}{\partial \psi} \frac{\partial \psi}{\partial t} \mathbf{E} \cdot \mathbf{E} d\mathbf{x} \\ &= \int_{\Omega} \mathbf{E} \cdot \frac{\partial}{\partial t} \mathbf{D} d\mathbf{x} + \frac{1}{2} \int_{\Omega} \frac{\partial \epsilon_{eff}}{\partial \psi} \frac{\partial \psi}{\partial t} \mathbf{E} \cdot \mathbf{E} d\mathbf{x} \\ &= \int_{\Omega} \mathbf{E} \cdot \left( \frac{\partial \mathbf{D}}{\partial t} - \frac{\partial \epsilon_{eff}}{\partial \psi} \frac{\partial \psi}{\partial t} \mathbf{E} \right) d\mathbf{x} + \frac{1}{2} \int_{\Omega} \frac{\partial \epsilon_{eff}}{\partial \psi} \frac{\partial \psi}{\partial t} \mathbf{E} \cdot \mathbf{E} d\mathbf{x} \\ &= - \int_{\Omega} \nabla \phi \cdot \frac{\partial \mathbf{D}}{\partial t} d\mathbf{x} - \frac{1}{2} \int_{\Omega} \frac{\partial \epsilon_{eff}}{\partial \psi} \frac{\partial \psi}{\partial t} \mathbf{E} \cdot \mathbf{E} d\mathbf{x} \\ &= - \int_{\partial \Omega} \phi \frac{\partial \mathbf{D}}{\partial t} \cdot \mathbf{n} ds + \int_{\Omega} \phi \nabla \cdot \frac{\partial \mathbf{D}}{\partial t} d\mathbf{x} - \frac{1}{2} \int_{\Omega} \frac{\partial \epsilon_{eff}}{\partial \psi} \frac{\partial \psi}{\partial t} \mathbf{E} \cdot \mathbf{E} d\mathbf{x} \\ &= - \int_{\partial \Omega} \phi \frac{\partial \mathbf{D}}{\partial t} \cdot \mathbf{n} ds + \int_{\Omega} \phi \left( \sum_{i=1}^N z_i e \frac{\partial c_i}{\partial t} \right) d\mathbf{x} - \frac{1}{2} \int_{\Omega} \frac{\partial \epsilon_{eff}}{\partial \psi} \frac{\partial \psi}{\partial t} |\mathbf{E}|^2 d\mathbf{x} \\ &= - \int_{\partial \Omega} \phi \frac{\partial \mathbf{D}}{\partial t} \cdot \mathbf{n} ds + \int_{\Omega} \left( \sum_{i=1}^N z_i e \phi \frac{\partial c_i}{\partial t} \right) d\mathbf{x} - \frac{1}{2} \int_{\Omega} \frac{\partial \epsilon_{eff}}{\partial \psi} \frac{\partial \psi}{\partial t} |\mathbf{E}|^2 d\mathbf{x},\end{aligned}\quad (2.10)$$

where we used Eqs.(2.1b), (2.1d), and

$$\frac{\partial \mathbf{D}}{\partial t} = \frac{\partial \epsilon_{eff}}{\partial \psi} \frac{\partial \psi}{\partial t} \mathbf{E} + \epsilon_{eff} \frac{\partial \mathbf{E}}{\partial t}. \quad (2.11)$$

The derivative of entropy is given by

$$\begin{aligned} \frac{dE_{ion}}{dt} &= \frac{d}{dt} \int_{\Omega} k_B T \sum_{i=1}^N c_i \left( \ln \frac{c_i}{\tilde{c}} - 1 \right) d\mathbf{x} \\ &= \int_{\Omega} k_B T \sum_{i=1}^N \frac{\partial c_i}{\partial t} \ln \frac{c_i}{\tilde{c}} d\mathbf{x}. \end{aligned} \quad (2.12)$$

For the mixing energy, the Eq. (2.1a) yields

$$\begin{aligned} \frac{dE_{mix}}{dt} &= \frac{d}{dt} \int_{\Omega} \lambda \left( \frac{\delta^2}{2} |\nabla \psi|^2 + F(\psi) \right) d\mathbf{x} \\ &= \int_{\Omega} \lambda \frac{\partial}{\partial t} \left( \frac{\delta^2}{2} |\nabla \psi|^2 + F(\psi) \right) d\mathbf{x} \\ &= \int_{\Omega} \lambda \left( \delta^2 \nabla \psi \cdot \frac{\partial \nabla \psi}{\partial t} + F'(\psi) \frac{\partial \psi}{\partial t} \right) d\mathbf{x} \\ &= \int_{\Omega} \lambda \left( \delta^2 \nabla \psi \cdot \nabla \frac{\partial \psi}{\partial t} + F'(\psi) \frac{\partial \psi}{\partial t} \right) d\mathbf{x} \\ &= \int_{\Omega} \lambda \delta^2 \nabla \psi \cdot \nabla \frac{\partial \psi}{\partial t} d\mathbf{x} + \int_{\Omega} \lambda F'(\psi) \frac{\partial \psi}{\partial t} d\mathbf{x} \\ &= \int_{\partial\Omega} \lambda \delta^2 \nabla \psi \frac{\partial \psi}{\partial t} \cdot \mathbf{n} ds - \int_{\Omega} \lambda \delta^2 \nabla^2 \psi \frac{\partial \psi}{\partial t} d\mathbf{x} + \int_{\Omega} \lambda F'(\psi) \frac{\partial \psi}{\partial t} d\mathbf{x} \\ &= \int_{\partial\Omega} \lambda \delta^2 \nabla \psi \frac{\partial \psi}{\partial t} \cdot \mathbf{n} ds + \int_{\Omega} \lambda (-\delta^2 \nabla^2 \psi + F'(\psi)) \frac{\partial \psi}{\partial t} d\mathbf{x}. \end{aligned} \quad (2.13)$$

In summary, for the total energy, we have

$$\begin{aligned} &\frac{dE_{total}}{dt} \\ &= I_1 + I_2 + I_3 + I_4 \\ &= - \int_{\Omega} \nabla \mathbf{u} : (\sigma_{\eta} + \sigma_e + \sigma_{\psi}) d\mathbf{x} - \int_{\Omega} p \nabla \cdot \mathbf{u} d\mathbf{x} - \frac{1}{2} \int_{\partial\Omega} \rho \mathbf{u} |\mathbf{u}|^2 \cdot \mathbf{n} ds + \int_{\partial\Omega} \mathbf{u} \cdot (\sigma_{\eta} + \sigma_e + \sigma_{\psi}) \cdot \mathbf{n} ds \\ &\quad - \int_{\partial\Omega} \phi \frac{\partial \mathbf{D}}{\partial t} \cdot \mathbf{n} ds + \int_{\Omega} \left( \sum_{i=1}^N z_i e \phi \frac{\partial c_i}{\partial t} \right) d\mathbf{x} - \frac{1}{2} \int_{\Omega} \frac{\partial \epsilon_{eff}}{\partial \psi} \frac{\partial \psi}{\partial t} |\mathbf{E}|^2 d\mathbf{x} + \int_{\Omega} k_B T \sum_{i=1}^N \frac{\partial c_i}{\partial t} \ln \frac{c_i}{\tilde{c}} d\mathbf{x} \\ &\quad + \int_{\partial\Omega} \lambda \delta^2 \nabla \psi \frac{\partial \psi}{\partial t} \cdot \mathbf{n} ds + \int_{\Omega} \lambda (-\delta^2 \nabla^2 \psi + F'(\psi)) \frac{\partial \psi}{\partial t} d\mathbf{x} \\ &= - \int_{\Omega} \nabla \mathbf{u} : (\sigma_{\eta} + \sigma_e + \sigma_{\psi}) d\mathbf{x} - \int_{\Omega} p \nabla \cdot \mathbf{u} d\mathbf{x} + \int_{\Omega} \left( \sum_{i=1}^N z_i e \phi \frac{\partial c_i}{\partial t} \right) d\mathbf{x} + \int_{\Omega} k_B T \sum_{i=1}^N \frac{\partial c_i}{\partial t} \ln \frac{c_i}{\tilde{c}} d\mathbf{x} \\ &\quad + \int_{\Omega} \lambda (-\delta^2 \nabla^2 \psi + F'(\psi)) \frac{\partial \psi}{\partial t} d\mathbf{x} - \frac{1}{2} \int_{\Omega} \frac{\partial \epsilon_{eff}}{\partial \psi} \frac{\partial \psi}{\partial t} |\mathbf{E}|^2 d\mathbf{x} \\ &\quad - \frac{1}{2} \int_{\partial\Omega} \rho \mathbf{u} |\mathbf{u}|^2 \cdot \mathbf{n} ds + \int_{\partial\Omega} \mathbf{u} \cdot (\sigma_{\eta} + \sigma_e + \sigma_{\psi}) \cdot \mathbf{n} ds - \int_{\partial\Omega} \phi \frac{\partial \mathbf{D}}{\partial t} \cdot \mathbf{n} ds + \int_{\partial\Omega} \lambda \delta^2 \nabla \psi \frac{\partial \psi}{\partial t} \cdot \mathbf{n} ds \\ &= - \int_{\Omega} \nabla \mathbf{u} : (\sigma_{\eta} + \sigma_e + \sigma_{\psi}) d\mathbf{x} - \int_{\Omega} p \nabla \cdot \mathbf{u} d\mathbf{x} + \int_{\Omega} \sum_{i=1}^N \left( \left( z_i e \phi + k_B T \ln \frac{c_i}{\tilde{c}} \right) \frac{\partial c_i}{\partial t} \right) d\mathbf{x} \\ &\quad + \int_{\Omega} \left( \lambda (-\delta^2 \nabla^2 \psi + F'(\psi)) - \frac{1}{2} \frac{\partial \epsilon_{eff}}{\partial \psi} |\mathbf{E}|^2 \right) \frac{\partial \psi}{\partial t} d\mathbf{x} \\ &\quad - \frac{1}{2} \int_{\partial\Omega} \rho \mathbf{u} |\mathbf{u}|^2 \cdot \mathbf{n} ds + \int_{\partial\Omega} \mathbf{u} \cdot (\sigma_{\eta} + \sigma_e + \sigma_{\psi}) \cdot \mathbf{n} ds - \int_{\partial\Omega} \phi \frac{\partial \mathbf{D}}{\partial t} \cdot \mathbf{n} ds + \int_{\partial\Omega} \lambda \delta^2 \nabla \psi \frac{\partial \psi}{\partial t} \cdot \mathbf{n} ds \end{aligned}$$

$$\begin{aligned}
&= - \int_{\Omega} \nabla \mathbf{u} : (\sigma_{\eta} + \sigma_e + \sigma_{\psi}) \mathbf{d}x - \int_{\Omega} p \nabla \cdot \mathbf{u} \mathbf{d}x + \int_{\Omega} \sum_{i=1}^N \mu_i \frac{\partial c_i}{\partial t} \mathbf{d}x + \int_{\Omega} \mu_{\psi} \frac{\partial \psi}{\partial t} \mathbf{d}x \\
&\quad - \frac{1}{2} \int_{\partial\Omega} \rho \mathbf{u} \cdot \mathbf{u} \mathbf{n} ds + \int_{\partial\Omega} \mathbf{u} \cdot (\sigma_{\eta} + \sigma_e + \sigma_{\psi}) \cdot \mathbf{n} ds - \int_{\partial\Omega} \phi \frac{\partial \mathbf{D}}{\partial t} \cdot \mathbf{n} ds + \int_{\partial\Omega} \lambda \delta^2 \nabla \psi \frac{\partial \psi}{\partial t} \cdot \mathbf{n} ds \\
&= - \int_{\Omega} \nabla \mathbf{u} : (\sigma_{\eta} + \sigma_e + \sigma_{\psi}) \mathbf{d}x - \int_{\Omega} p \nabla \cdot \mathbf{u} \mathbf{d}x \\
&\quad + \int_{\Omega} \sum_{i=1}^N \mu_i (-\nabla \cdot (\mathbf{u} c_i) - \nabla \cdot \mathbf{j}_i) \mathbf{d}x + \int_{\Omega} \mu_{\psi} (-\nabla \cdot (\mathbf{u} \psi) - \nabla \cdot \mathbf{j}_{\psi}) \mathbf{d}x \\
&\quad - \frac{1}{2} \int_{\partial\Omega} \rho \mathbf{u} \cdot \mathbf{u} \mathbf{n} ds + \int_{\partial\Omega} \mathbf{u} \cdot (\sigma_{\eta} + \sigma_e + \sigma_{\psi}) \cdot \mathbf{n} ds - \int_{\partial\Omega} \phi \frac{\partial \mathbf{D}}{\partial t} \cdot \mathbf{n} ds + \int_{\partial\Omega} \lambda \delta^2 \nabla \psi \frac{\partial \psi}{\partial t} \cdot \mathbf{n} ds \\
&= - \int_{\Omega} \nabla \mathbf{u} : (\sigma_{\eta} + \sigma_e + \sigma_{\psi}) \mathbf{d}x + \int_{\Omega} p \nabla \cdot \mathbf{u} \mathbf{d}x \\
&\quad + \underbrace{\int_{\Omega} \sum_{i=1}^N c_i \mathbf{u} \cdot \nabla \mu_i \mathbf{d}x}_{H_1} + \int_{\Omega} \sum_{i=1}^N \nabla \mu_i \cdot \mathbf{j}_i \mathbf{d}x \quad (:= I_1 + I_2) \\
&\quad + \underbrace{\int_{\Omega} \psi \mathbf{u} \cdot \nabla \mu_{\psi} \mathbf{d}x}_{H_2} + \int_{\Omega} \nabla \mu_{\psi} \cdot \mathbf{j}_{\psi} \mathbf{d}x \quad (:= I_3 + I_4) \\
&\quad - \int_{\partial\Omega} \sum_{i=1}^N c_i \mu_i \mathbf{u} \cdot \mathbf{n} ds - \int_{\partial\Omega} \sum_{i=1}^N \mu_i \mathbf{j}_i \cdot \mathbf{n} ds - \int_{\partial\Omega} \psi \mu_{\psi} \mathbf{u} \cdot \mathbf{n} ds - \int_{\partial\Omega} \mu_{\psi} \mathbf{j}_{\psi} \cdot \mathbf{n} ds \\
&\quad - \frac{1}{2} \int_{\partial\Omega} \rho \mathbf{u} \cdot \mathbf{u} \mathbf{n} ds + \int_{\partial\Omega} \mathbf{u} \cdot (\sigma_{\eta} + \sigma_e + \sigma_{\psi}) \cdot \mathbf{n} ds \\
&\quad - \int_{\partial\Omega} \phi \frac{\partial \mathbf{D}}{\partial t} \cdot \mathbf{n} ds + \int_{\partial\Omega} \lambda \delta^2 \nabla \psi \frac{\partial \psi}{\partial t} \cdot \mathbf{n} ds. \tag{2.14}
\end{aligned}$$

For  $H_1$ , combining the definition of chemical potential  $\mu_i$  and Eq. (2.1d) yields

$$\begin{aligned}
&\int_{\Omega} \sum_{i=1}^N c_i \mathbf{u} \cdot \nabla \mu_i \mathbf{d}x \\
&= \int_{\Omega} \left( \sum_{i=1}^N z_i e c_i \right) \mathbf{u} \cdot \nabla \phi \mathbf{d}x + \int_{\Omega} \sum_{i=1}^N k_B T \mathbf{u} \cdot \nabla c_i \mathbf{d}x \\
&= \int_{\Omega} (\nabla \cdot \mathbf{D}) \mathbf{u} \cdot \nabla \phi \mathbf{d}x + \int_{\Omega} \sum_{i=1}^N k_B T \mathbf{u} \cdot \nabla c_i \mathbf{d}x \\
&= - \int_{\Omega} \mathbf{D} \cdot \nabla (\mathbf{u} \cdot \nabla \phi) \mathbf{d}x + \int_{\partial\Omega} \sum_{i=1}^N k_B T c_i \mathbf{u} \cdot \mathbf{n} ds + \int_{\partial\Omega} (\mathbf{u} \cdot \nabla \phi) \mathbf{D} \cdot \mathbf{n} ds \\
&= \int_{\Omega} \epsilon_{eff} \nabla \phi \cdot \nabla \mathbf{u} \cdot \nabla \phi \mathbf{d}x + \int_{\Omega} \epsilon_{eff} \nabla \phi \cdot \nabla \nabla \phi \cdot \mathbf{u} \mathbf{d}x + \int_{\partial\Omega} \sum_{i=1}^N k_B T c_i \mathbf{u} \cdot \mathbf{n} ds + \int_{\partial\Omega} (\mathbf{u} \cdot \nabla \phi) \mathbf{D} \cdot \mathbf{n} ds \\
&= \int_{\Omega} \epsilon_{eff} \nabla \phi \cdot \nabla \mathbf{u} \cdot \nabla \phi \mathbf{d}x + \int_{\Omega} \epsilon_{eff} \frac{1}{2} \nabla |\nabla \phi|^2 \cdot \mathbf{u} \mathbf{d}x + \int_{\partial\Omega} \sum_{i=1}^N k_B T c_i \mathbf{u} \cdot \mathbf{n} ds + \int_{\partial\Omega} (\mathbf{u} \cdot \nabla \phi) \mathbf{D} \cdot \mathbf{n} ds \\
&= \int_{\Omega} \epsilon_{eff} \nabla \phi \cdot \nabla \mathbf{u} \cdot \nabla \phi \mathbf{d}x - \int_{\Omega} \frac{1}{2} |\nabla \phi|^2 \nabla \cdot (\epsilon_{eff} \mathbf{u}) \mathbf{d}x \\
&\quad + \int_{\partial\Omega} \sum_{i=1}^N k_B T c_i \mathbf{u} \cdot \mathbf{n} ds + \int_{\partial\Omega} (\mathbf{u} \cdot \nabla \phi) \mathbf{D} \cdot \mathbf{n} ds + \int_{\partial\Omega} \epsilon_{eff} \frac{1}{2} |\nabla \phi|^2 \mathbf{u} \cdot \mathbf{n} ds \\
&= \int_{\Omega} \epsilon_{eff} \nabla \phi \cdot \nabla \mathbf{u} \cdot \nabla \phi \mathbf{d}x - \int_{\Omega} \frac{1}{2} |\nabla \phi|^2 \nabla \epsilon_{eff} \cdot \mathbf{u} \mathbf{d}x - \int_{\Omega} \frac{1}{2} |\nabla \phi|^2 \epsilon_{eff} \nabla \cdot \mathbf{u} \mathbf{d}x \\
&\quad + \int_{\partial\Omega} \sum_{i=1}^N k_B T c_i \mathbf{u} \cdot \mathbf{n} ds + \int_{\partial\Omega} (\mathbf{u} \cdot \nabla \phi) \mathbf{D} \cdot \mathbf{n} ds + \int_{\partial\Omega} \epsilon_{eff} \frac{1}{2} |\nabla \phi|^2 \mathbf{u} \cdot \mathbf{n} ds
\end{aligned}$$

$$\begin{aligned}
&= \int_{\Omega} \epsilon_{eff} \left( \nabla \phi \otimes \nabla \phi - \frac{1}{2} |\nabla \phi|^2 \mathbf{I} \right) : \nabla \mathbf{u} d\mathbf{x} - \int_{\Omega} \frac{1}{2} |\nabla \phi|^2 \nabla \epsilon_{eff} \cdot \mathbf{u} d\mathbf{x} \\
&\quad + \int_{\partial\Omega} \sum_{i=1}^N k_B T c_i \mathbf{u} \cdot \mathbf{n} ds + \int_{\partial\Omega} (\mathbf{u} \cdot \nabla \phi) \mathbf{D} \cdot \mathbf{n} ds + \int_{\partial\Omega} \epsilon_{eff} \frac{1}{2} |\nabla \phi|^2 \mathbf{u} \cdot \mathbf{n} ds. \tag{2.15}
\end{aligned}$$

Similarly, for  $H_2$  terms, the chemical potential of  $\mu_\psi$  gives

$$\begin{aligned}
&\int_{\Omega} \psi \mathbf{u} \cdot \nabla \mu_\psi d\mathbf{x} \\
&= \int_{\Omega} \psi \mathbf{u} \cdot \nabla \left( \lambda (-\delta^2 \nabla^2 \psi + F'(\psi)) - \frac{1}{2} \frac{\partial \epsilon_{eff}}{\partial \psi} |\mathbf{E}|^2 \right) d\mathbf{x} \\
&= - \int_{\Omega} \nabla \cdot (\psi \mathbf{u}) \left( \lambda (-\delta^2 \nabla^2 \psi + F'(\psi)) - \frac{1}{2} \frac{\partial \epsilon_{eff}}{\partial \psi} |\mathbf{E}|^2 \right) d\mathbf{x} \\
&\quad + \int_{\partial\Omega} \left( \lambda (-\delta^2 \nabla^2 \psi + F'(\psi)) - \frac{1}{2} \frac{\partial \epsilon_{eff}}{\partial \psi} |\mathbf{E}|^2 \right) \psi \mathbf{u} \cdot \mathbf{n} ds \\
&= - \int_{\Omega} \mathbf{u} \cdot \nabla \psi \left( \lambda (-\delta^2 \nabla^2 \psi + F'(\psi)) - \frac{1}{2} \frac{\partial \epsilon_{eff}}{\partial \psi} |\mathbf{E}|^2 \right) d\mathbf{x} \\
&\quad + \int_{\partial\Omega} \left( \lambda (-\delta^2 \nabla^2 \psi + F'(\psi)) - \frac{1}{2} \frac{\partial \epsilon_{eff}}{\partial \psi} |\mathbf{E}|^2 \right) \psi \mathbf{u} \cdot \mathbf{n} ds \\
&= - \int_{\Omega} \left( \lambda (-\delta^2 \mathbf{u} \cdot \nabla \psi \nabla^2 \psi + \mathbf{u} \cdot \nabla F(\psi)) - \frac{1}{2} |\mathbf{E}|^2 \mathbf{u} \cdot \nabla \epsilon_{eff} \right) d\mathbf{x} \\
&\quad + \int_{\partial\Omega} \left( \lambda (-\delta^2 \nabla^2 \psi + F'(\psi)) - \frac{1}{2} \frac{\partial \epsilon_{eff}}{\partial \psi} |\mathbf{E}|^2 \right) \psi \mathbf{u} \cdot \mathbf{n} ds \\
&= - \int_{\Omega} \left( -\lambda \delta^2 \mathbf{u} \cdot \left( \nabla \cdot (\nabla \psi \otimes \nabla \psi) - \frac{1}{2} \nabla |\nabla \psi|^2 \right) + \lambda \mathbf{u} \cdot \nabla F(\psi) - \frac{1}{2} |\mathbf{E}|^2 \mathbf{u} \cdot \nabla \epsilon_{eff} \right) d\mathbf{x} \\
&\quad + \int_{\partial\Omega} \left( \lambda (-\delta^2 \nabla^2 \psi + F'(\psi)) - \frac{1}{2} \frac{\partial \epsilon_{eff}}{\partial \psi} |\mathbf{E}|^2 \right) \psi \mathbf{u} \cdot \mathbf{n} ds \\
&= \int_{\Omega} \lambda \delta^2 \mathbf{u} \cdot \nabla \cdot (\nabla \psi \otimes \nabla \psi) d\mathbf{x} - \int_{\Omega} \lambda \mathbf{u} \cdot \nabla \left( \frac{\delta^2}{2} |\nabla \psi|^2 - F(\psi) \right) d\mathbf{x} + \int_{\Omega} \frac{1}{2} |\mathbf{E}|^2 \mathbf{u} \cdot \nabla \epsilon_{eff} d\mathbf{x} \\
&\quad + \int_{\partial\Omega} \left( \lambda (-\delta^2 \nabla^2 \psi + F'(\psi)) - \frac{1}{2} \frac{\partial \epsilon_{eff}}{\partial \psi} |\mathbf{E}|^2 \right) \psi \mathbf{u} \cdot \mathbf{n} ds \\
&= - \int_{\Omega} \nabla \mathbf{u} : (\lambda \delta^2 \nabla \psi \otimes \nabla \psi) d\mathbf{x} + \int_{\Omega} \frac{1}{2} |\mathbf{E}|^2 \mathbf{u} \cdot \nabla \epsilon_{eff} d\mathbf{x} - \int_{\partial\Omega} \lambda \left( \frac{\delta^2}{2} |\nabla \psi|^2 - F(\psi) \right) \mathbf{u} \cdot \mathbf{n} ds \\
&\quad + \int_{\partial\Omega} \left( \lambda (-\delta^2 \nabla^2 \psi + F'(\psi)) - \frac{1}{2} \frac{\partial \epsilon_{eff}}{\partial \psi} |\mathbf{E}|^2 \right) \psi \mathbf{u} \cdot \mathbf{n} ds + \int_{\partial\Omega} \lambda \delta^2 \mathbf{u} \cdot \nabla \psi \otimes \nabla \psi \cdot \mathbf{n} ds. \tag{2.16}
\end{aligned}$$

Substituting Eqs. (2.15) and (2.16) into Eq. (2.14) yields

$$\begin{aligned}
&\frac{dE_{total}}{dt} \\
&= - \int_{\Omega} \nabla \mathbf{u} : (\sigma_\eta + \sigma_\psi + \sigma_e) d\mathbf{x} - \int_{\Omega} p \nabla \cdot \mathbf{u} d\mathbf{x} + \int_{\Omega} \sum_{i=1}^N \nabla \mu_i \cdot \mathbf{j}_i d\mathbf{x} + \int_{\Omega} \nabla \mu_\psi \cdot \mathbf{j}_\psi d\mathbf{x} \\
&\quad + \int_{\Omega} \epsilon_{eff} \left( \nabla \phi \otimes \nabla \phi - \frac{1}{2} |\nabla \phi|^2 \mathbf{I} \right) : \nabla \mathbf{u} d\mathbf{x} - \int_{\Omega} \frac{1}{2} |\nabla \phi|^2 \nabla \epsilon_{eff} \cdot \mathbf{u} d\mathbf{x} \\
&\quad - \int_{\Omega} \nabla \mathbf{u} : (\lambda \delta^2 \nabla \psi \otimes \nabla \psi) d\mathbf{x} + \int_{\Omega} \frac{1}{2} |\mathbf{E}|^2 \mathbf{u} \cdot \nabla \epsilon_{eff} d\mathbf{x} + \int_{\partial\Omega} \lambda \left( \frac{\delta^2}{2} |\nabla \psi|^2 - F(\psi) \right) \mathbf{u} \cdot \mathbf{n} ds \\
&\quad + \int_{\partial\Omega} \left( \lambda (-\delta^2 \nabla^2 \psi + F'(\psi)) - \frac{1}{2} \frac{\partial \epsilon_{eff}}{\partial \psi} |\mathbf{E}|^2 \right) \psi \mathbf{u} \cdot \mathbf{n} ds + \int_{\partial\Omega} \lambda \delta^2 \mathbf{u} \cdot \nabla \psi \otimes \nabla \psi \cdot \mathbf{n} ds \\
&\quad + \int_{\partial\Omega} \sum_{i=1}^N k_B T c_i \mathbf{u} \cdot \mathbf{n} ds + \int_{\partial\Omega} (\mathbf{u} \cdot \nabla \phi) \mathbf{D} \cdot \mathbf{n} ds + \int_{\partial\Omega} \epsilon_{eff} \frac{1}{2} |\nabla \phi|^2 \mathbf{u} \cdot \mathbf{n} ds \\
&\quad - \int_{\partial\Omega} \sum_{i=1}^N c_i \mu_i \mathbf{u} \cdot \mathbf{n} ds - \int_{\partial\Omega} \sum_{i=1}^N \mu_i \mathbf{j}_i \cdot \mathbf{n} ds - \int_{\partial\Omega} \psi \mu_\psi \mathbf{u} \cdot \mathbf{n} ds - \int_{\partial\Omega} \mu_\psi \mathbf{j}_\psi \cdot \mathbf{n} ds
\end{aligned}$$

$$\begin{aligned}
& -\frac{1}{2} \int_{\partial\Omega} \rho \mathbf{u} \cdot \mathbf{u}^2 \cdot \mathbf{n} \, ds + \int_{\partial\Omega} \mathbf{u} \cdot (\sigma_\eta + \sigma_e) \cdot \mathbf{n} \, ds - \int_{\partial\Omega} \phi \frac{\partial \mathbf{D}}{\partial t} \cdot \mathbf{n} \, ds + \int_{\partial\Omega} \lambda \delta^2 \nabla \psi \frac{\partial \psi}{\partial t} \cdot \mathbf{n} \, ds, \\
& = - \int_{\Omega} \nabla \mathbf{u} : (\sigma_\eta + \sigma_\psi + \sigma_e) \, d\mathbf{x} - \int_{\Omega} p \mathbf{I} : \nabla \mathbf{u} \, d\mathbf{x} + \int_{\Omega} \sum_{i=1}^N \nabla \mu_i \cdot \mathbf{j}_i \, d\mathbf{x} + \int_{\Omega} \nabla \mu_\psi \cdot \mathbf{j}_\psi \, d\mathbf{x} \\
& \quad + \int_{\Omega} \epsilon_{eff} \left( \nabla \phi \otimes \nabla \phi - \frac{1}{2} |\nabla \phi|^2 \mathbf{I} \right) : \nabla \mathbf{u} \, d\mathbf{x} - \int_{\Omega} \nabla \mathbf{u} : (\lambda \delta^2 \nabla \psi \otimes \nabla \psi) \, d\mathbf{x}, \tag{2.17}
\end{aligned}$$

where the close boundary conditions (2.3) are used.

Comparing with the predefined dissipation functional (2.6), we obtain the expression for those unknowns variables,

$$\mathbf{j}_i = - \frac{D_i c_i}{k_B T} \nabla \mu_i, \tag{2.18a}$$

$$\mathbf{j}_\psi = - \mathcal{M} \nabla \mu_\psi, \tag{2.18b}$$

$$\boldsymbol{\sigma}_\eta = 2\eta \mathbf{D}_\eta - p \mathbf{I}, \tag{2.18c}$$

$$\boldsymbol{\sigma}_\psi = - \lambda \delta^2 \nabla \psi \otimes \nabla \psi, \tag{2.18d}$$

$$\boldsymbol{\sigma}_e = \epsilon_{eff} \left( \nabla \phi \otimes \nabla \phi - \frac{1}{2} |\nabla \phi|^2 \mathbf{I} \right). \tag{2.18e}$$

Therefore, the Poisson-Nernst-Planck-Navier-Stokes-Cahn-Hilliard system for a droplet in electrolyte under electric fields is summarized as follows

$$\frac{\partial \psi}{\partial t} + \nabla \cdot (\mathbf{u} \psi) = \nabla \cdot (\mathcal{M} \nabla \mu_\psi), \quad \text{in } \Omega, \tag{2.19a}$$

$$\mu_\psi = \lambda (-\delta^2 \nabla^2 \psi + F'(\psi)) - \frac{1}{2} \frac{\partial \epsilon_{eff}}{\partial \psi} |\mathbf{E}|^2, \quad \text{in } \Omega, \tag{2.19b}$$

$$\frac{\partial c_i}{\partial t} + \nabla \cdot (\mathbf{u} c_i) = \nabla \cdot \left( \frac{D_i c_i}{k_B T} z_i e \nabla \phi + D_i \nabla c_i \right), \quad i = 1, \dots, N, \quad \text{in } \Omega, \tag{2.19c}$$

$$-\nabla \cdot (\epsilon_{eff} \nabla \phi) = \sum_{i=1}^N z_i e c_i, \quad \text{in } \Omega, \tag{2.19d}$$

$$\rho \left( \frac{\partial \mathbf{u}}{\partial t} + (\mathbf{u} \cdot \nabla) \mathbf{u} \right) = \nabla \cdot \boldsymbol{\sigma}_\eta + \nabla \cdot \boldsymbol{\sigma}_\psi + \nabla \cdot \boldsymbol{\sigma}_e, \quad \text{in } \Omega, \tag{2.19e}$$

$$\nabla \cdot \mathbf{u} = 0, \quad \text{in } \Omega, \tag{2.19f}$$

$$\boldsymbol{\sigma}_\eta = 2\eta \mathbf{D}_\eta - p \mathbf{I}, \quad \text{in } \Omega, \tag{2.19g}$$

$$\boldsymbol{\sigma}_\psi = - \lambda \delta^2 \nabla \psi \otimes \nabla \psi, \quad \text{in } \Omega, \tag{2.19h}$$

$$\boldsymbol{\sigma}_e = \epsilon_{eff} \left( \nabla \phi \otimes \nabla \phi - \frac{1}{2} |\nabla \phi|^2 \mathbf{I} \right), \quad \text{in } \Omega, \tag{2.19i}$$

$$\epsilon_{eff}^{-1} = \frac{1 - \psi}{2\epsilon^-} + \frac{1 + \psi}{2\epsilon^+} + \frac{(1 - \psi^2)^2}{\delta C_m}, \quad \text{in } \Omega, \tag{2.19j}$$

with boundary condition (2.3).

## 2.2 Time scale analysis and approximation models

Following previous work [11], if  $R$  is the radius of the initial drop, the characteristic length scale, velocity, time, pressure are set to be  $L = R$ ,  $\tilde{u} = \sqrt{\frac{\lambda \delta}{\rho R}}$ ,  $\tilde{t} = \sqrt{\frac{\rho R^3}{\lambda \delta}}$ , and  $\tilde{p} = \frac{\lambda \delta}{L} = \frac{\sigma_s}{L}$ , respectively. Here we define  $\sigma_s$  as the surface tension. The characteristic dielectric constant is set to be the one in the outer region  $\epsilon^-$ . And the characteristic electric field intensity is defined as  $E_\infty$ .

The dimensionless Navier-Stokes equations are given by

$$\begin{aligned}
\left( \frac{\partial \mathbf{u}'}{\partial t'} + (\mathbf{u}' \cdot \nabla) \mathbf{u}' \right) + \nabla p' &= \frac{1}{Re} \nabla \cdot (\eta' (\nabla \mathbf{u}' + (\nabla \mathbf{u}')^T) \\
&\quad - \delta' \nabla \cdot (\nabla \psi \otimes \nabla \psi) + Ca_E \nabla \cdot \epsilon'_{eff} \left( \mathbf{E}' \otimes \mathbf{E}' - \frac{1}{2} |\mathbf{E}'|^2 \mathbf{I} \right)). \tag{2.20}
\end{aligned}$$

Here  $Re = \frac{\rho \tilde{u} L}{\tilde{\eta}}$  is the Reynolds number,  $\delta' = \frac{\delta}{L}$  is the non-dimensional thickness of diffuse interface,  $Ca_E$  is the electrical capillary number defined as  $Ca_E = \epsilon^- R |E_\infty|^2 / \lambda \delta$ , which measures the strength of the electric field relative to the surface tension force.

The non-dimensional effective dielectric coefficient is as follows,

$$\epsilon'_{eff} = \frac{1}{\frac{(1-\psi^2)^2}{\delta' C'_m} + \frac{1-\psi}{2} + \frac{1+\psi}{2\epsilon_r}} \left( \text{where } \epsilon_r = \frac{\epsilon^+}{\epsilon^-} \text{ and } C'_m = \frac{C_m R}{\epsilon^-} \sim o\left(\frac{1}{\delta'}\right) \right). \quad (2.21)$$

For the Cahn-Hilliard equation, if let  $\tilde{\mu} = \frac{\sigma_s}{L}$  be the characteristic chemical potential, we have the Cahn-Hilliard equations as follows,

$$\frac{\partial \psi}{\partial t'} + \nabla \cdot (\mathbf{u}' \psi) = M' \nabla^2 \mu'_\psi, \quad (2.22)$$

$$\mu'_\psi = -\delta' \nabla^2 \psi + \frac{1}{\delta'} F'(\psi) - \frac{Ca_E}{2} \frac{\partial \epsilon'_{eff}}{\partial \psi} |\mathbf{E}'|^2, \quad (2.23)$$

where  $M' = \frac{\mathcal{M} \tilde{\mu}}{L \tilde{u}}$ .

We define net charge as  $\rho_e = \sum_{i=1}^N z_i c_i e$  and the characteristic electric potential as  $\tilde{\phi} = E_\infty L$ , the dimensionless of Poisson equation is given by

$$-\zeta^2 \nabla \cdot (\epsilon'_{eff} \nabla \phi') = \rho'_e \quad (2.24)$$

where  $\zeta = \frac{\lambda_D}{L}$  and  $\lambda_D = \sqrt{\frac{\epsilon^- E_\infty L}{\tilde{c} e}}$  is the Debye length.

For the ion concentration, multiplying above equation (2.19c) by  $z_i e$  respectively and summing up from 1 to  $N$  give

$$\frac{\partial \left( \sum_{i=1}^N z_i c_i e \right)}{\partial t} + \nabla \cdot \left( \mathbf{u} \left( \sum_{i=1}^N z_i c_i e \right) \right) = \nabla \cdot \left( \frac{\left( \sum_{i=1}^N D_i z_i^2 c_i \right) e^2}{k_B T} \nabla \phi + \sum_{i=1}^N D_i \nabla (z_i c_i e) \right). \quad (2.25)$$

For simplicity, we assume that  $D_i = D$  for all ionic species for the rest of the paper and the case of different  $D_i$  will be considered in a follow up paper. The equation above could be rewritten as

$$\frac{\partial \rho_e}{\partial t} + \nabla \cdot (\mathbf{u} \rho_e) = \nabla \cdot (\sigma_c \nabla \phi + D \nabla \rho_e). \quad (2.26)$$

where  $\sigma_c = \frac{D \sum_{i=1}^N z_i^2 c_i e^2}{k_B T}$  is the effective conductivity. If we define the diffusion time  $\tilde{t}_D = \frac{L^2}{D}$  and electric relaxation time  $\tilde{t}_E = \frac{\epsilon^-}{\sigma^2}$ , then the dimensionless of charge density is

$$\frac{1}{\tilde{t}} \left( \frac{\partial \rho'_e}{\partial t} + \nabla \cdot (\mathbf{u} \rho'_e) \right) = \frac{\zeta^2}{\tilde{t}_E} \nabla \cdot (\sigma'_c \nabla \phi') + \frac{1}{\tilde{t}_D} \nabla \cdot (D \nabla \rho'_e). \quad (2.27)$$

When the electric relaxation time is much shorter than the diffusion time and macro time scale, i.e.  $\tilde{t}_E \ll \tilde{t}_D$  and  $\tilde{t}_E \ll \tilde{t}$ , the ions in bulk attain steady state simultaneously and conductivity could be treated as constants  $\sigma^\pm$  in the bulk region.

### 2.2.1 Leaky-dielectric model

In the leaky-dielectric model, we assume that the conductivities  $\sigma^\pm$  remains as constants, and the conductivity in phase field frame work could be defined as follows

$$\sigma'_{eff} = \frac{1-\psi}{2} + \frac{1+\psi}{2\sigma^+/\sigma^-} = \frac{1-\psi}{2} + \frac{1+\psi}{2\sigma_r}. \quad (2.28)$$

Equation (2.27) can be approximated by

$$\nabla \cdot (\sigma_{eff} \nabla \phi') = 0. \quad (2.29)$$

Replacing (2.27) by the equation above, we obtain the non-dimensional leaky-dielectric phase field system as follows,

$$\begin{aligned} \left( \frac{\partial \mathbf{u}}{\partial t} + (\mathbf{u} \cdot \nabla) \mathbf{u} \right) + \nabla p &= \frac{1}{Re} \nabla^2 \mathbf{u} - \delta \nabla \cdot (\nabla \psi \otimes \nabla \psi) \\ &+ Ca_E \nabla \cdot \epsilon_{eff} \left( \mathbf{E} \otimes \mathbf{E} - \frac{1}{2} |\mathbf{E}|^2 \mathbf{I} \right), \end{aligned} \quad (2.30a)$$

$$\nabla \cdot \mathbf{u} = 0, \quad (2.30b)$$

$$\nabla \cdot (\sigma_{eff} \nabla \phi) = 0, \quad (2.30c)$$

$$\frac{\partial \psi}{\partial t} + \nabla \cdot (\mathbf{u} \psi) = M \nabla^2 \mu_\psi, \quad (2.30d)$$

$$\mu_\psi = -\delta \nabla^2 \psi + \frac{1}{\delta} F'(\psi) - \frac{Ca_E}{2} \frac{\partial \epsilon_{eff}}{\partial \psi} |\mathbf{E}|^2. \quad (2.30e)$$

where we omit superscript  $\prime$  for simplicity's sake.

Note that the following fact,

$$\nabla \cdot (\nabla \psi \otimes \nabla \psi) = \nabla^2 \psi \nabla \psi + \frac{1}{2} \nabla |\nabla \psi|^2 = -\frac{1}{\delta} \mu \nabla \psi + \nabla \left( \frac{1}{2} |\nabla \psi|^2 + \frac{1}{\delta^2} F(\psi) \right). \quad (2.31)$$

Then, if we define a new variable

$$\mu = -\delta \nabla^2 \psi + \frac{1}{\delta} F(\psi), \quad (2.32)$$

and let

$$\hat{p} = p + \frac{1}{\delta} F(\psi) + \frac{\delta}{2} |\nabla \psi|^2, \quad (2.33)$$

we can rewrite the above system as follows,

$$\left( \frac{\partial \mathbf{u}}{\partial t} + (\mathbf{u} \cdot \nabla) \mathbf{u} \right) + \nabla p = \frac{1}{Re} \nabla^2 \mathbf{u} + \mu \nabla \psi + Ca_E \nabla \cdot \epsilon_{eff} \left( \mathbf{E} \otimes \mathbf{E} - \frac{1}{2} |\mathbf{E}|^2 \mathbf{I} \right), \quad (2.34a)$$

$$\nabla \cdot \mathbf{u} = 0, \quad (2.34b)$$

$$\nabla \cdot \mathbf{J} = 0, \quad (2.34c)$$

$$\mathbf{J} = \sigma_{eff} \nabla \phi, \quad (2.34d)$$

$$\frac{\partial \psi}{\partial t} + \nabla \cdot (\mathbf{u} \psi) = M \nabla^2 \mu_\psi, \quad (2.34e)$$

$$\mu_\psi = -\delta \nabla^2 \psi + \frac{1}{\delta} F'(\psi) - \frac{Ca_E}{2} \frac{\partial \epsilon_{eff}}{\partial \psi} |\mathbf{E}|^2, \quad (2.34f)$$

$$\mu = -\delta \nabla^2 \psi + \frac{1}{\delta} F(\psi), \quad (2.34g)$$

where  $\hat{\cdot}$  is omitted for simplicity.

## 2.2.2 Net charge model

In this model, we also assume that the conductivities  $\sigma^\pm$  remain as constants and the effective conductivity given by

$$\sigma_{eff} = \frac{1 - \psi}{2} + \frac{1 + \psi}{2\sigma^+/\sigma^-} = \frac{1 - \psi}{2} + \frac{1 + \psi}{2\sigma_r}. \quad (2.35)$$

However, we keep all the terms in (2.27) and use it to computer  $\rho_e$  instead of  $\phi$ . The electric potential can be computed with the Poisson equation, which was ignored in the leaky-dielectric model. The phase field system including the evolution of net charge is given as follows,

$$\left( \frac{\partial \mathbf{u}}{\partial t} + (\mathbf{u} \cdot \nabla) \mathbf{u} \right) + \nabla p = \frac{1}{Re} \nabla^2 \mathbf{u} + \mu \nabla \psi + Ca_E \nabla \cdot \epsilon_{eff} \left( \mathbf{E} \otimes \mathbf{E} - \frac{1}{2} |\mathbf{E}|^2 \mathbf{I} \right), \quad (2.36a)$$

$$\nabla \cdot \mathbf{u} = 0, \quad (2.36b)$$

$$\frac{1}{\tilde{t}} \left( \frac{\partial \rho_e}{\partial t} + \nabla \cdot (\mathbf{u} \rho_e) \right) = \frac{\zeta^2}{\tilde{t}_E} \nabla \cdot (\sigma_{eff} \nabla \phi) + \frac{1}{\tilde{t}_D} \nabla \cdot (D \nabla \rho_e), \quad (2.36c)$$

$$-\zeta^2 \nabla \cdot (\epsilon_{eff} \nabla \phi) = \rho_e \quad (2.36d)$$

$$\frac{\partial \psi}{\partial t} + \nabla \cdot (\mathbf{u} \psi) = M \nabla^2 \mu_\psi, \quad (2.36e)$$

$$\mu_\psi = -\delta \nabla^2 \psi + \frac{1}{\delta} F'(\psi) - \frac{Ca_E}{2} \frac{\partial \epsilon_{eff}}{\partial \psi} |\mathbf{E}|^2, \quad (2.36f)$$

$$\mu = -\delta \nabla^2 \psi + \frac{1}{\delta} F(\psi). \quad (2.36g)$$

**Remark 2.1.** Here in Eq. (2.34a) or Eq. (2.36a), the electric force term  $\nabla \cdot \boldsymbol{\sigma}_e$  could be written as follows

$$\begin{aligned} & \nabla \cdot \epsilon_{eff} \left( \nabla \phi \otimes \nabla \phi - \frac{1}{2} |\nabla \phi|^2 \mathbf{I} \right) \\ &= \nabla \cdot (\epsilon_{eff} \nabla \phi \otimes \nabla \phi) - \nabla \cdot \left( \frac{\epsilon_{eff}}{2} |\nabla \phi|^2 \mathbf{I} \right) \\ &= \nabla \cdot (\epsilon_{eff} \nabla \phi) \nabla \phi + \frac{\epsilon_{eff}}{2} \nabla |\nabla \phi|^2 - \frac{1}{2} |\nabla \phi|^2 \nabla \epsilon_{eff} - \frac{\epsilon_{eff}}{2} \nabla |\nabla \phi|^2 \\ &= \nabla \cdot (\epsilon_{eff} \nabla \phi) \nabla \phi - \frac{1}{2} |\nabla \phi|^2 \nabla \epsilon_{eff} \\ &= \nabla \cdot (\epsilon_{eff} \nabla \phi) \nabla \phi - \frac{1}{2} |\nabla \phi|^2 \frac{\partial \epsilon_{eff}}{\partial \psi} \nabla \psi \\ &= -\frac{1}{\zeta^2} \rho_e \nabla \phi - \frac{1}{2} |\nabla \phi|^2 \frac{\partial \epsilon_{eff}}{\partial \psi} \nabla \psi \\ &= \mathbf{F}_L + \mathbf{F}_p \end{aligned} \quad (2.37)$$

where the first term  $\mathbf{F}_L$  is the Lorentz force due to the interaction of net charges with electric field and the second term  $\mathbf{F}_p$  is due to the polarization stress. Then Eq.(2.34a) or Eq. (2.36a) could be rewritten as

$$\left( \frac{\partial \mathbf{u}}{\partial t} + (\mathbf{u} \cdot \nabla) \mathbf{u} \right) + \nabla p = \frac{1}{Re} \nabla^2 \mathbf{u} + \mu_\psi \nabla \psi - \frac{Ca_E}{\zeta^2} \rho_e \nabla \phi. \quad (2.38)$$

### 3 Sharp interface limit of the diffuse leaky-dielectric interface model

In this section, a detailed asymptotic analysis is presented to show that as  $\delta \rightarrow 0$ , the limit of the obtained system (2.34) is consistent with the sharp interface Taylor–Melcher model [22, 17, 11]. Here the mobility is assumed as  $M = \alpha_1 \delta^2$  and capacitance  $C_m = \alpha_2 \delta^{-1}$ , where  $\alpha_1$  and  $\alpha_2$  are constants independent of  $\delta$ . In the following,  $\llbracket f \rrbracket = f^+ - f^-$  denotes the jump across the interface.

#### 3.1 Outer expansions

In the outer region for the bulk fluids away from the interface defined by  $\Gamma = \{\mathbf{x} : \psi(\mathbf{x}, t) = 0\}$ , we consider the sharp interface limit by taking  $\delta \rightarrow 0$ , and using the expansions as follows,

$$\psi^\pm = \psi_0^\pm + \delta \psi_1^\pm + \delta^2 \psi_2^\pm + o(\delta^2), \quad (3.1a)$$

$$\mu_\psi^\pm = \delta^{-1} \mu_{\psi 0}^\pm + \mu_{\psi 1}^\pm + \delta \mu_{\psi 2}^\pm + \delta^2 \mu_{\psi 3}^\pm + o(\delta^2), \quad (3.1b)$$

$$\mu^\pm = \delta^{-1} \mu_0^\pm + \mu_1^\pm + \delta \mu_2^\pm + \delta^2 \mu_3^\pm + o(\delta^2), \quad (3.1c)$$

$$\phi^\pm = \phi_0^\pm + \delta \phi_1^\pm + \delta^2 \phi_2^\pm + o(\delta^2), \quad (3.1d)$$

$$\mathbf{u}^\pm = \mathbf{u}_0^\pm + \delta \mathbf{u}_1^\pm + \delta^2 \mathbf{u}_2^\pm + o(\delta^2), \quad (3.1e)$$

$$p^\pm = p_0^\pm + \delta p_1^\pm + \delta^2 p_2^\pm + o(\delta^2), \quad (3.1f)$$

$$\boldsymbol{\sigma}_e^\pm = \boldsymbol{\sigma}_{e0}^\pm + \delta \boldsymbol{\sigma}_{e1}^\pm + \delta^2 \boldsymbol{\sigma}_{e2}^\pm + o(\delta^2), \quad (3.1g)$$

$$\mathbf{J}^\pm = \mathbf{J}_0^\pm + \delta \mathbf{J}_1^\pm + \delta^2 \mathbf{J}_2^\pm + o(\delta^2), \quad (3.1h)$$

For the Cahn–Hilliard equation, we first consider the chemical potential of  $\psi$ . Substituting (3.1a) into (2.34f) and (2.34g) yields

$$\delta^{-1} \mu_0^\pm + \mu_1^\pm + \delta \mu_2^\pm + \delta^2 \mu_3^\pm + o(\delta^2) = -\delta \nabla^2 (\psi_0^\pm + \delta \psi_1^\pm + \delta^2 \psi_2^\pm + o(\delta^2))$$

$$+ \delta^{-1} (\psi_0^\pm + \delta\psi_1^\pm + \delta^2\psi_2^\pm + o(\delta^2)) \left( (\psi_0^\pm + \delta\psi_1^\pm + \delta^2\psi_2^\pm + o(\delta^2))^2 - 1 \right), \quad (3.2a)$$

$$\begin{aligned} \delta^{-1} \mu_{\psi 0}^\pm + \mu_{\psi 1}^\pm + \delta\mu_{\psi 2}^\pm + \delta^2\mu_{\psi 3}^\pm + o(\delta^2) &= \delta^{-1} \mu_0^\pm + \mu_1^\pm + \delta\mu_2^\pm + \delta^2\mu_3^\pm + o(\delta^2) \\ - \frac{Ca_E}{2} \frac{\partial \epsilon_{eff}}{\partial \psi} |\nabla (\phi_0^\pm + \delta\phi_1^\pm + \delta^2\phi_2^\pm + o(\delta^2))|^2. \end{aligned} \quad (3.2b)$$

The leading order of Eq. (3.2a) yields

$$\mu_0^\pm = \psi_0^\pm ((\psi_0^\pm)^2 - 1). \quad (3.3)$$

According to the definition of  $\epsilon_{eff}$ , we have

$$\frac{\partial \epsilon_{eff}}{\partial \psi} = \frac{\frac{1}{2} - \frac{1}{2\epsilon_r} + \frac{4\psi(1-\psi^2)}{\delta C_m}}{\left(\frac{1-\psi}{2} + \frac{1+\psi}{2\epsilon_r} + \frac{(1-\psi^2)^2}{\delta C_m}\right)^2}, \quad (3.4)$$

which means

$$\begin{aligned} & \left( \frac{1-\psi}{2} + \frac{1+\psi}{2\epsilon_r} + \frac{(1-\psi^2)^2}{\delta C_m} \right)^2 \left( \delta^{-1} \mu_{\psi 0}^\pm + \mu_{\psi 1}^\pm + \delta\mu_{\psi 2}^\pm + \delta^2\mu_{\psi 3}^\pm + o(\delta^2) \right) \\ &= \left( \frac{1-\psi}{2} + \frac{1+\psi}{2\epsilon_r} + \frac{(1-\psi^2)^2}{\delta C_m} \right)^2 \left( \delta^{-1} \mu_0^\pm + \mu_1^\pm + \delta\mu_2^\pm + \delta^2\mu_3^\pm + o(\delta^2) \right) \\ & \quad - \frac{Ca_E}{2} \left( \frac{1}{2} - \frac{1}{2\epsilon_r} + \frac{4\psi(1-\psi^2)}{\delta C_m} \right) |\nabla (\phi_0^\pm + \delta\phi_1^\pm + \delta^2\phi_2^\pm + o(\delta^2))|^2. \end{aligned} \quad (3.5)$$

The leading order of above equation (3.5) gives

$$\mu_{\psi 0}^\pm = \mu_0^\pm = \psi_0^\pm \left( (\psi_0^\pm)^2 - 1 \right). \quad (3.6)$$

For Navier-Stokes equations, when substituting the outer expansion of  $\mathbf{u}$ ,  $p$  and  $\mu$  into momentum equation (2.34a) and incompressibility (2.34b), we have

$$\begin{aligned} & \frac{\partial (\mathbf{u}_0^\pm + \delta\mathbf{u}_1^\pm + \delta^2\mathbf{u}_2^\pm + o(\delta^2))}{\partial t} + ((\mathbf{u}_0^\pm + \delta\mathbf{u}_1^\pm + \delta^2\mathbf{u}_2^\pm + o(\delta^2)) \cdot \nabla) (\mathbf{u}_0^\pm + \delta\mathbf{u}_1^\pm + \delta^2\mathbf{u}_2^\pm + o(\delta^2)) \\ & + \nabla (p_0^\pm + \delta p_1^\pm + \delta^2 p_2^\pm + o(\delta^2)) \\ &= \frac{1}{Re} \nabla^2 (\mathbf{u}_0^\pm + \delta\mathbf{u}_1^\pm + \delta^2\mathbf{u}_2^\pm + o(\delta^2)) \\ & + (\delta^{-1} \mu_0^\pm + \mu_1^\pm + \delta\mu_2^\pm + \delta^2\mu_3^\pm + o(\delta^2)) \nabla (\psi_0^\pm + \delta\psi_1^\pm + \delta^2\psi_2^\pm + o(\delta^2)) \\ & + Ca_E \nabla \cdot (\boldsymbol{\sigma}_{e0}^\pm + \delta\boldsymbol{\sigma}_{e1}^\pm + \delta^2\boldsymbol{\sigma}_{e2}^\pm + o(\delta^2)). \end{aligned}$$

and

$$\nabla \cdot (\mathbf{u}_0^\pm + \delta\mathbf{u}_1^\pm + \delta^2\mathbf{u}_2^\pm + o(\delta^2)) = 0. \quad (3.7)$$

The leading order yields

$$\mu_0^\pm \nabla \psi_0^\pm = 0, \quad (3.8)$$

which means

$$\nabla \left( 1 - (\psi_0^\pm)^2 \right)^2 = 0, \quad (3.9)$$

i.e.  $\psi_0^\pm = C_0^\pm$  and  $\mu_{\psi 0}^\pm = \mu_0^\pm = (C_0^\pm)^3 - C_0^\pm$ . The next order is

$$\frac{\partial \mathbf{u}_0^\pm}{\partial t} + \mathbf{u}_0^\pm \cdot \nabla \mathbf{u}_0^\pm + \nabla p_0^\pm = \frac{1}{Re} \nabla^2 \mathbf{u}_0^\pm + \mu_0^\pm \nabla \psi_1^\pm + Ca_E \nabla \cdot \boldsymbol{\sigma}_{e0}^\pm.$$

For equation (2.34c) and (2.34d), the leading order term gives us that

$$\nabla \cdot \mathbf{J}_0^\pm = 0,$$

and

$$\mathbf{J}_0^\pm = \frac{1}{\frac{1-C_0^\pm}{2} + \frac{1+C_0^\pm}{2\sigma_r}} \nabla \phi_0^\pm.$$

For the Maxwell stress, we have

$$\begin{aligned} & \left( \frac{1-\psi}{2} + \frac{1+\psi}{2\epsilon_r} + \frac{(1-(\psi)^2)^2}{\delta C_m} \right) (\boldsymbol{\sigma}_{e,0}^\pm + \delta \boldsymbol{\sigma}_{e,0}^\pm + o(\delta^2)) \\ &= \nabla (\phi_0^\pm + \delta \phi_1^\pm + o(\delta^2)) \otimes \nabla (\phi_0^\pm + \delta \phi_1^\pm + o(\delta^2)) - \frac{1}{2} |\nabla (\phi_0^\pm + \delta \phi_1^\pm + o(\delta^2))|^2 \mathbf{I}. \end{aligned}$$

Since  $C_m = \alpha_2 \delta^{-1}$ , the leading order of above equation is

$$\left( \frac{1-\psi^\pm}{2} + \frac{1+\psi^\pm}{2\epsilon_r} + \frac{(1-(\psi^\pm)^2)^2}{\alpha_2} \right) \boldsymbol{\sigma}_{e,0}^\pm = \nabla \phi_0^\pm \otimes \nabla \phi_0^\pm - \frac{1}{2} |\nabla \phi_0^\pm|^2 \mathbf{I}.$$

In summary, for the outer region,  $(\mathbf{u}_0^\pm, p_0^\pm, \mu_0^\pm, \psi_0^\pm, \phi_0^\pm)$  satisfy

$$\frac{\partial \mathbf{u}_0^\pm}{\partial t} + \mathbf{u}_0^\pm \cdot \nabla \mathbf{u}_0^\pm + \nabla p_0^\pm = \frac{1}{Re} \nabla^2 \mathbf{u}_0^\pm + \mu_0^\pm \nabla \psi_1^\pm + Ca_E \nabla \cdot \boldsymbol{\sigma}_{e,0}^\pm, \quad (3.10a)$$

$$\nabla \cdot (\mathbf{u}_0^\pm) = 0, \quad (3.10b)$$

$$\frac{\partial \psi_0^\pm}{\partial t} + \nabla \cdot (\mathbf{u}_0^\pm \psi_0^\pm) = 0, \quad (3.10c)$$

$$\psi_0^\pm = C_0^\pm, \quad \mu_{\psi 0}^\pm = \mu_0^\pm = (C_0^\pm)^3 - C_0^\pm, \quad (3.10d)$$

$$\nabla \cdot \left( \frac{1}{\frac{1-C_0^\pm}{2} + \frac{1+C_0^\pm}{2\sigma_r}} \nabla \phi_0^\pm \right) = 0, \quad (3.10e)$$

$$\left( \frac{1-\psi^\pm}{2} + \frac{1+\psi^\pm}{2\epsilon_r} + \frac{(1-(\psi^\pm)^2)^2}{\alpha_2} \right) \boldsymbol{\sigma}_{e,0}^\pm = \nabla \phi_0^\pm \otimes \nabla \phi_0^\pm - \frac{1}{2} |\nabla \phi_0^\pm|^2 \mathbf{I}. \quad (3.10f)$$

### 3.2 Inner expansions

Firstly, we introduce the signed distance function  $d(\mathbf{x})$  to the interface  $\Gamma$ . Immediately, we have  $\nabla d = \mathbf{n}$ . After defining a new rescaled variable

$$\xi = \frac{d(\mathbf{x})}{\delta}, \quad (3.11)$$

for any scalar function  $f(\mathbf{x})$ , we can rewrite it as

$$f(\mathbf{x}) = \tilde{f}(\mathbf{x}, \xi), \quad (3.12)$$

and the relevant operators are

$$\nabla f(\mathbf{x}) = \nabla_{\mathbf{x}} \tilde{f} + \delta^{-1} \partial_\xi \tilde{f} \mathbf{n}, \quad (3.13a)$$

$$\nabla^2 f(\mathbf{x}) = \nabla_{\mathbf{x}}^2 \tilde{f} + \delta^{-1} \partial_\xi \tilde{f} \kappa + 2\delta^{-1} (\mathbf{n} \cdot \nabla_{\mathbf{x}}) \partial_\xi \tilde{f} + \delta^{-2} \partial_{\xi\xi} \tilde{f}, \quad (3.13b)$$

$$\partial_t f = \partial_t \tilde{f} + \delta^{-1} \partial_\xi \tilde{f} \partial_t d, \quad (3.13c)$$

and for a vector function  $\mathbf{g}(\mathbf{x})$ , we have

$$\nabla \cdot \tilde{\mathbf{g}}(\mathbf{x}) = \nabla_{\mathbf{x}} \cdot \tilde{\mathbf{g}} + \delta^{-1} \partial_\xi \tilde{\mathbf{g}} \cdot \mathbf{n}. \quad (3.14)$$

Here the  $\nabla_{\mathbf{x}}$  and  $\nabla_{\mathbf{x}}^2$  stand for the gradient and Laplace with respect to  $\mathbf{x}$ , respectively. And we use the fact that  $\nabla_{\mathbf{x}} \cdot \mathbf{n} = \kappa$ .  $\kappa(\mathbf{x})$  for  $\mathbf{x} \in \Gamma(t)$  is the mean curvature of the interface and is positive if the domain  $\Omega_-$  is convex near  $\mathbf{x}$ . In the inner region, we assume that

$$\tilde{\psi} = \tilde{\psi}_0 + \delta \tilde{\psi}_1 + \delta^2 \tilde{\psi}_2 + o(\delta^2), \quad (3.15a)$$

$$\tilde{\mu}_\psi = \delta^{-1} \tilde{\mu}_{\psi 0} + \tilde{\mu}_{\psi 1} + \delta \tilde{\mu}_{\psi 2} + \delta^2 \tilde{\mu}_{\psi 3} + o(\delta^2), \quad (3.15b)$$

$$\tilde{\mu} = \delta^{-1} \tilde{\mu}_0 + \tilde{\mu}_1 + \delta \tilde{\mu}_2 + \delta^2 \tilde{\mu}_3 + o(\delta^2), \quad (3.15c)$$

$$\tilde{\phi} = \tilde{\phi}_0 + \delta\tilde{\phi}_1 + \delta^2\tilde{\phi}_2 + o(\delta^2), \quad (3.15d)$$

$$\tilde{\mathbf{u}} = \tilde{\mathbf{u}}_0 + \delta\tilde{\mathbf{u}}_1 + \delta^2\tilde{\mathbf{u}}_2 + o(\delta^2), \quad (3.15e)$$

$$\tilde{p} = \tilde{p}_0 + \delta\tilde{p}_1 + \delta^2\tilde{p}_2 + o(\delta^2), \quad (3.15f)$$

$$\tilde{\mathbf{J}} = \tilde{\mathbf{J}}_0 + \delta\tilde{\mathbf{J}}_1 + \delta^2\tilde{\mathbf{J}}_2 + o(\delta^2), \quad (3.15g)$$

$$\tilde{\boldsymbol{\sigma}}_e = \tilde{\boldsymbol{\sigma}}_{e0} + \delta\tilde{\boldsymbol{\sigma}}_{e1} + \delta^2\tilde{\boldsymbol{\sigma}}_{e2} + o(\delta^2), \quad (3.15h)$$

and the following matching conditions for inner and outer expansions:

$$\lim_{\xi \rightarrow \pm\infty} \tilde{f}_i(\mathbf{x}, \xi) = f_i^\pm(\mathbf{x}), \quad (3.16a)$$

$$\lim_{\xi \rightarrow \pm\infty} \left( \nabla_{\mathbf{x}} \tilde{f}_i(\mathbf{x}, \xi) + \partial_\xi \tilde{f}_{i+1}(\mathbf{x}, \xi) \mathbf{n} \right) = \nabla f_i^\pm(\mathbf{x}). \quad (3.16b)$$

Firstly, for the electric potential, we have

$$\nabla_{\mathbf{x}} \cdot \left( \tilde{\mathbf{J}}_0 + \delta\tilde{\mathbf{J}}_1 + \delta^2\tilde{\mathbf{J}}_2 + o(\delta^2) \right) + \delta^{-1} \partial_\xi \left( \tilde{\mathbf{J}}_0 + \delta\tilde{\mathbf{J}}_1 + \delta^2\tilde{\mathbf{J}}_2 + o(\delta^2) \right) \cdot \mathbf{n} = 0, \quad (3.17a)$$

$$\begin{aligned} & \left( \frac{1 - (\tilde{\psi}_0 + \delta\tilde{\psi}_1 + \delta^2\tilde{\psi}_2 + o(\delta^2))}{2} + \frac{1 + \tilde{\psi}_0 + \delta\tilde{\psi}_1 + \delta^2\tilde{\psi}_2 + o(\delta^2)}{2\sigma_r} \right) \left( \tilde{\mathbf{J}}_0 + \delta\tilde{\mathbf{J}}_1 + \delta^2\tilde{\mathbf{J}}_2 + o(\delta^2) \right) \\ &= \nabla_{\mathbf{x}} \left( \tilde{\phi}_0 + \delta\tilde{\phi}_1 + \delta^2\tilde{\phi}_2 + o(\delta^2) \right) + \delta^{-1} \partial_\xi \left( \tilde{\phi}_0 + \delta\tilde{\phi}_1 + \delta^2\tilde{\phi}_2 + o(\delta^2) \right) \mathbf{n}, \end{aligned} \quad (3.17b)$$

where we used the definition of  $\sigma_{eff}$ .

The leading order of two equations are

$$\partial_\xi \tilde{\mathbf{J}}_0 \cdot \mathbf{n} = 0 \quad (3.18a)$$

$$\partial_\xi \tilde{\phi}_0 = 0, \quad (3.18b)$$

which yields  $\tilde{\phi}_0$  does not depends on  $\xi$  in the inner region

$$\tilde{\phi}_0(\xi, x) = \tilde{\phi}_0(x), \quad (3.19)$$

and the continuity of electric potential and flux

$$[\![\tilde{\phi}_0]\!] = 0, \quad [\![\tilde{\mathbf{J}}_0 \cdot \mathbf{n}]\!] = 0. \quad (3.20)$$

We have

$$\nabla_{\mathbf{x}} \tilde{\phi} + \delta^{-1} \partial_\xi \tilde{\phi} \mathbf{n} = -\tilde{\epsilon}_{eff} \tilde{\mathbf{D}} = - \left( \frac{1 - \tilde{\psi}}{2} + \frac{1 + \tilde{\psi}}{2\epsilon_r} \right) \tilde{\mathbf{D}}. \quad (3.21)$$

So  $\tilde{\mathbf{D}}$  have the following expansion

$$\tilde{\mathbf{D}} = \tilde{\mathbf{D}}_0 + \delta\tilde{\mathbf{D}}_1 + \delta^2\tilde{\mathbf{D}}_2 + o(\delta^2). \quad (3.22)$$

And due to the fact

$$\epsilon_{eff} \sigma_e = \mathbf{D} \otimes \mathbf{D} - \frac{1}{2} |\mathbf{D}|^2 \mathbf{I}, \quad (3.23)$$

we have

$$\sigma_e = \epsilon_{eff}^{-1} \left( \mathbf{D} \otimes \mathbf{D} - \frac{1}{2} |\mathbf{D}|^2 \mathbf{I} \right), \quad (3.24)$$

and the expansion (3.15h) is apparent. It is the same reason why (3.15g) is established.

For the chemical potential, substituting expansions (3.15c), (3.15a), (3.15d) into (2.34f) and (2.34g) gives

$$\begin{aligned} \delta^{-1} \tilde{\mu}_0 + \tilde{\mu}_1 + \delta\tilde{\mu}_2 + \delta^2\tilde{\mu}_3 + o(\delta^2) &= -\delta \nabla^2 \left( \tilde{\psi}_0 + \delta\tilde{\psi}_1 + \delta^2\tilde{\psi}_2 + o(\delta^2) \right) \\ &+ \delta^{-1} \left( \tilde{\psi}_0 + \delta\tilde{\psi}_1 + \delta^2\tilde{\psi}_2 + o(\delta^2) \right) \left( \left( \tilde{\psi}_0 + \delta\tilde{\psi}_1 + \delta^2\tilde{\psi}_2 + o(\delta^2) \right)^2 - 1 \right), \end{aligned} \quad (3.25a)$$

$$\begin{aligned}
& \left( \frac{1 - (\tilde{\psi}_0 + \delta\tilde{\psi}_1 + \delta^2\tilde{\psi}_2 + o(\delta^2))}{2} + \frac{1 + (\tilde{\psi}_0 + \delta\tilde{\psi}_1 + \delta^2\tilde{\psi}_2 + o(\delta^2))}{2\epsilon_r} \right. \\
& \quad \left. + \frac{\left( 1 - (\tilde{\psi}_0 + \delta\tilde{\psi}_1 + \delta^2\tilde{\psi}_2 + o(\delta^2))^2 \right)^2}{\delta C_m} \right)^2 \times (\delta^{-1}\mu_{\psi 0} + \tilde{\mu}_{\psi 1} + \delta\tilde{\mu}_{\psi 2} + \delta^2\tilde{\mu}_{\psi 3} + o(\delta^2)) \\
= & \left( \frac{1 - (\tilde{\psi}_0 + \delta\tilde{\psi}_1 + \delta^2\tilde{\psi}_2 + o(\delta^2))}{2} + \frac{1 + (\tilde{\psi}_0 + \delta\tilde{\psi}_1 + \delta^2\tilde{\psi}_2 + o(\delta^2))}{2\epsilon_r} \right. \\
& \quad \left. + \frac{\left( 1 - (\tilde{\psi}_0 + \delta\tilde{\psi}_1 + \delta^2\tilde{\psi}_2 + o(\delta^2))^2 \right)^2}{\delta C_m} \right)^2 \times (\delta^{-1}\tilde{\mu}_0 + \tilde{\mu}_1 + \delta\tilde{\mu}_2 + \delta^2\tilde{\mu}_3 + o(\delta^2)) \\
& + \left( \frac{1}{2} - \frac{1}{2\epsilon_r} + \frac{4(\tilde{\psi}_0 + \delta\tilde{\psi}_1 + \delta^2\tilde{\psi}_2 + o(\delta^2)) \left( 1 - (\tilde{\psi}_0 + \delta\tilde{\psi}_1 + \delta^2\tilde{\psi}_2 + o(\delta^2))^2 \right)}{\delta C_m} \right) \\
& \times \left| \nabla_{\mathbf{x}} \left( \tilde{\phi}_0 + \delta\tilde{\phi}_1 + \delta^2\tilde{\phi}_2 + o(\delta^2) \right) + \delta^{-1}\partial_{\xi} \left( \tilde{\phi}_0 + \delta\tilde{\phi}_1 + \delta^2\tilde{\phi}_2 + o(\delta^2) \right) \mathbf{n} \right|^2. \tag{3.25b}
\end{aligned}$$

The leading order  $\delta^{-1}$  of above two equations gives

$$\tilde{\mu}_{\psi 0} = \tilde{\mu}_0 = -\partial_{\xi\xi}\tilde{\psi}_0 + \tilde{\psi}_0(\tilde{\psi}_0^2 - 1), \tag{3.26}$$

and the next order  $\delta^0$  of Eq. (3.25a) is

$$\tilde{\mu}_1 = -\partial_{\xi}\tilde{\psi}_0\kappa - 2(\mathbf{n} \cdot \nabla_{\mathbf{x}})\partial_{\xi}\tilde{\psi}_0 - \partial_{\xi\xi}\tilde{\psi}_1 + 3\tilde{\psi}_0^2\tilde{\psi}_1 - \tilde{\psi}_1. \tag{3.27}$$

For the Cahn-Hilliard equation, we substitute expansions (3.15a), (3.15b) and (3.15e) into (2.34e), then we have

$$\begin{aligned}
& \partial_t \left( \tilde{\psi}_0 + \delta\tilde{\psi}_1 + \delta^2\tilde{\psi}_2 + o(\delta^2) \right) + \delta^{-1}\partial_{\xi} \left( \tilde{\psi}_0 + \delta\tilde{\psi}_1 + \delta^2\tilde{\psi}_2 + o(\delta^2) \right) \partial_t d \\
& + (\tilde{\mathbf{u}}_0 + \delta\tilde{\mathbf{u}}_1 + \delta^2\tilde{\mathbf{u}}_2 + o(\delta^2)) \cdot \nabla_{\mathbf{x}} \left( \left( \tilde{\psi}_0 + \delta\tilde{\psi}_1 + \delta^2\tilde{\psi}_2 + o(\delta^2) \right) \right) \\
& + \delta^{-1}(\tilde{\mathbf{u}}_0 + \delta\tilde{\mathbf{u}}_1 + \delta^2\tilde{\mathbf{u}}_2 + o(\delta^2)) \partial_{\xi} \left( \left( \tilde{\psi}_0 + \delta\tilde{\psi}_1 + \delta^2\tilde{\psi}_2 + o(\delta^2) \right) \right) \cdot \mathbf{n} \\
& - M \left[ \nabla_{\mathbf{x}}^2 (\delta^{-1}\tilde{\mu}_{\psi 0} + \tilde{\mu}_{\psi 1} + \delta\tilde{\mu}_{\psi 2} + \delta^2\tilde{\mu}_{\psi 3} + o(\delta^2)) \right. \\
& \quad \left. + \delta^{-1}\partial_{\xi} (\delta^{-1}\tilde{\mu}_{\psi 0} + \tilde{\mu}_{\psi 1} + \delta\tilde{\mu}_{\psi 2} + \delta^2\tilde{\mu}_{\psi 3} + o(\delta^2)) \kappa \right. \\
& \quad \left. + 2\delta^{-1}(\mathbf{n} \cdot \nabla_{\mathbf{x}})\partial_{\xi} (\delta^{-1}\tilde{\mu}_{\psi 0} + \tilde{\mu}_{\psi 1} + \delta\tilde{\mu}_{\psi 2} + \delta^2\tilde{\mu}_3 + o(\delta^2)) \right. \\
& \quad \left. + \delta^{-2}\partial_{\xi\xi} (\delta^{-1}\tilde{\mu}_{\psi 0} + \tilde{\mu}_{\psi 1} + \delta\tilde{\mu}_{\psi 2} + \delta^2\tilde{\mu}_3 + o(\delta^2)) \right] = 0. \tag{3.28}
\end{aligned}$$

Since  $M = \alpha_1\delta^2$ , then the leading order of above equation is

$$\partial_{\xi}\tilde{\psi}_0\partial_t d + \tilde{\mathbf{u}}_0 \cdot \mathbf{n}\partial_{\xi}(\tilde{\psi}_0) - \alpha_1\partial_{\xi\xi}\tilde{\mu}_{\psi 0} = 0, \tag{3.29}$$

If We integrate (3.29) with respect to  $\xi$  in  $(-\infty, +\infty)$ , and use the matching condition  $\lim_{\xi \rightarrow \pm\infty} \partial_{\xi}\tilde{\mu}_0 = 0$ , then above equation yields

$$\partial_t d + \tilde{\mathbf{u}}_0 \cdot \mathbf{n} = 0. \tag{3.30}$$

This implies that the normal velocity of the interface  $\Gamma$  is

$$V_n = \mathbf{u}_0 \cdot \mathbf{n}, \tag{3.31}$$

and  $\tilde{\mu}_{\psi 0}$  is a linear function about  $\xi$ , it is  $\tilde{\mu}_0 = c_1\xi + c_0$ . Because of the matching condition

$$\lim_{\xi \rightarrow \pm\infty} \tilde{\mu}_0 = \mu_0^{\pm}, \tag{3.32}$$

$\tilde{\mu}_0 = c_0$  is obvious.

For the Navier-Stokes equations, when we substitute (3.15e), (3.15f), (3.15a), (3.15c), (3.15d) and (3.15h) into (2.34a) and (2.34b), we have

$$\begin{aligned}
& \partial_t (\tilde{\mathbf{u}}_0 + \delta \tilde{\mathbf{u}}_1 + \delta^2 \tilde{\mathbf{u}}_2 + o(\delta^2)) + \delta^{-1} \partial_\xi (\tilde{\mathbf{u}}_0 + \delta \tilde{\mathbf{u}}_1 + \delta^2 \tilde{\mathbf{u}}_2 + o(\delta^2)) \partial_t d \\
& + (\tilde{\mathbf{u}}_0 + \delta \tilde{\mathbf{u}}_1 + \delta^2 \tilde{\mathbf{u}}_2 + o(\delta^2)) \cdot \nabla_{\mathbf{x}} (\tilde{\mathbf{u}}_0 + \delta \tilde{\mathbf{u}}_1 + \delta^2 \tilde{\mathbf{u}}_2 + o(\delta^2)) \\
& + (\tilde{\mathbf{u}}_0 + \delta \tilde{\mathbf{u}}_1 + \delta^2 \tilde{\mathbf{u}}_2 + o(\delta^2)) \cdot \delta^{-1} \partial_\xi (\tilde{\mathbf{u}}_0 + \delta \tilde{\mathbf{u}}_1 + \delta^2 \tilde{\mathbf{u}}_2 + o(\delta^2)) \mathbf{n} \\
& + \nabla_{\mathbf{x}} (\tilde{p}_0 + \delta \tilde{p}_1 + \delta^2 \tilde{p}_2 + o(\delta^2)) + \delta^{-1} \partial_\xi (\tilde{p}_0 + \delta \tilde{p}_1 + \delta^2 \tilde{p}_2 + o(\delta^2)) \mathbf{n} \\
& = \frac{1}{Re} [\nabla_{\mathbf{x}}^2 (\tilde{\mathbf{u}}_0 + \delta \tilde{\mathbf{u}}_1 + \delta^2 \tilde{\mathbf{u}}_2 + o(\delta^2)) + \delta^{-1} \partial_\xi (\tilde{\mathbf{u}}_0 + \delta \tilde{\mathbf{u}}_1 + \delta^2 \tilde{\mathbf{u}}_2 + o(\delta^2)) \kappa \\
& + 2\delta^{-1} (\mathbf{n} \cdot \nabla_{\mathbf{x}}) \partial_\xi (\tilde{\mathbf{u}}_0 + \delta \tilde{\mathbf{u}}_1 + \delta^2 \tilde{\mathbf{u}}_2 + o(\delta^2)) + \delta^{-2} \partial_{\xi\xi} (\tilde{\mathbf{u}}_0 + \delta \tilde{\mathbf{u}}_1 + \delta^2 \tilde{\mathbf{u}}_2 + o(\delta^2))] \\
& + (\delta^{-1} \tilde{\mu}_0 + \tilde{\mu}_1 + \delta \tilde{\mu}_2 + \delta^2 \tilde{\mu}_3 + o(\delta^2)) \nabla_{\mathbf{x}} (\tilde{\psi}_0 + \delta \tilde{\psi}_1 + \delta^2 \tilde{\psi}_2 + o(\delta^2)) \\
& + (\delta^{-1} \tilde{\mu}_0 + \tilde{\mu}_1 + \delta \tilde{\mu}_2 + \delta^2 \tilde{\mu}_3 + o(\delta^2)) \delta^{-1} \partial_\xi (\tilde{\psi}_0 + \delta \tilde{\psi}_1 + \delta^2 \tilde{\psi}_2 + o(\delta^2)) \mathbf{n} \\
& + Ca_E (\nabla_{\mathbf{x}} \cdot (\tilde{\sigma}_{e0} + \delta \tilde{\sigma}_{e1} + \delta^2 \tilde{\sigma}_{e2} + o(\delta^2)) + \delta^{-1} \partial_\xi (\tilde{\sigma}_{e0} + \delta \tilde{\sigma}_{e1} + \delta^2 \tilde{\sigma}_{e2} + o(\delta^2)) \cdot \mathbf{n}), \quad (3.33a) \\
& \nabla_{\mathbf{x}} \cdot (\tilde{\mathbf{u}}_0 + \delta \tilde{\mathbf{u}}_1 + \delta^2 \tilde{\mathbf{u}}_2 + o(\delta^2)) + \delta^{-1} \partial_\xi (\tilde{\mathbf{u}}_0 + \delta \tilde{\mathbf{u}}_1 + \delta^2 \tilde{\mathbf{u}}_2 + o(\delta^2)) \cdot \mathbf{n} = 0. \quad (3.33b)
\end{aligned}$$

The leading order of (3.33b) is

$$\partial_\xi \tilde{\mathbf{u}}_0 \cdot \mathbf{n} = 0, \quad (3.34)$$

which means  $\tilde{\mathbf{u}}_0 \cdot \mathbf{n}$  is a constant with respect to  $\xi$ . We integrate above equation (3.34) in  $(-\infty, +\infty)$ , the following result can be obtained directly,

$$\int_{-\infty}^{+\infty} \partial_\xi \tilde{\mathbf{u}}_0 \cdot \mathbf{n} d\xi = 0, \quad (3.35)$$

which means

$$[\mathbf{u}_0 \cdot \mathbf{n}] = 0. \quad (3.36)$$

So the velocity is continuous across the interface.

The leading ( $\delta^{-2}$ ) and next order ( $\delta^{-1}$ ) of equation (3.33a) are

$$\partial_{\xi\xi} \tilde{\mathbf{u}}_0 + \tilde{\mu}_0 \partial_\xi \tilde{\psi}_0 \mathbf{n} = 0, \quad (3.37a)$$

$$\begin{aligned}
& \partial_\xi \tilde{\mathbf{u}}_0 \partial_t d + \tilde{\mathbf{u}}_0 \cdot \partial_\xi \tilde{\mathbf{u}}_0 \mathbf{n} + \partial_\xi \tilde{p}_0 \mathbf{n} = \frac{1}{Re} (\partial_\xi \tilde{\mathbf{u}}_0 \kappa + 2(\mathbf{n} \cdot \nabla_{\mathbf{x}}) \partial_\xi \tilde{\mathbf{u}}_0 + \partial_{\xi\xi} \tilde{\mathbf{u}}_1) \\
& + (\tilde{\mu}_0 \nabla_{\mathbf{x}} \tilde{\psi}_0 + \tilde{\mu}_0 \partial_\xi \tilde{\psi}_1 \mathbf{n} + \tilde{\mu}_1 \partial_\xi \tilde{\psi}_0 \mathbf{n}) + Ca_E \partial_\xi \tilde{\sigma}_{e0} \cdot \mathbf{n}.
\end{aligned} \quad (3.37b)$$

Integrate equation (3.37a) in  $(-\infty, +\infty)$  yields

$$\partial_\xi \tilde{\mathbf{u}}_0|_{-\infty}^{\infty} + c_0 \tilde{\psi}_0|_{-\infty}^{+\infty} = 0, \quad (3.38)$$

where we used the result that  $\tilde{\mu}_0 = c_0$  is independence with  $\xi$ .

Multiplying  $\mathbf{n}$  on both sides of the above equation, we have

$$c_0 \tilde{\psi}_0|_{-\infty}^{+\infty} = 0, \quad (3.39)$$

which means  $c_0 (\psi_0^+ - \psi_0^-) = 0$ , and hence  $c_0 = 0$ , it is  $\tilde{\mu}_0 = 0$ .

Then equation (3.26) gives

$$\tilde{\psi}_0 = \tanh(\xi/\sqrt{2}), \quad (3.40)$$

and as  $\xi \rightarrow \pm\infty$ , the matching condition yields

$$\psi_0^+ = \lim_{\xi \rightarrow \infty} \tilde{\psi}_0 = 1, \quad (3.41a)$$

$$\psi_0^- = \lim_{\xi \rightarrow -\infty} \tilde{\psi}_0 = -1. \quad (3.41b)$$

If we integrate equation (3.37b) in  $(-\infty, +\infty)$  and use the results in [31], then we obtain

$$\left[ \left[ -p_0 \mathbf{n} + \frac{1}{Re} (\mathbf{n} \cdot \nabla \mathbf{u}_0) + Ca_E \sigma_{e0} \cdot \mathbf{n} \right] \right] = \sigma \kappa \mathbf{n}. \quad (3.42)$$

Using the results (3.20), (3.36), (3.41) and (3.42), we obtain the sharp interface limit of system (2.34)

$$\frac{\partial \mathbf{u}_0^\pm}{\partial t} + (\mathbf{u}_0^\pm \cdot \nabla) \mathbf{u}_0^\pm + \nabla p_0^\pm = \frac{1}{Re} \nabla^2 \mathbf{u}_0^\pm + Ca_E \nabla \cdot \sigma_{e0}^\pm, \quad (3.43a)$$

$$\nabla \cdot \mathbf{u}_0^\pm = 0, \quad (3.43b)$$

$$\boldsymbol{\sigma}_{e0}^+ = \epsilon_r \left( \nabla \phi_0^+ \otimes \nabla \phi_0^+ - \frac{1}{2} |\nabla \phi_0^+|^2 I \right), \quad \boldsymbol{\sigma}_{e0}^- = \left( \nabla \phi_0^- \otimes \nabla \phi_0^- - \frac{1}{2} |\nabla \phi_0^-|^2 I \right), \quad (3.43c)$$

$$\nabla \cdot (\sigma_r \nabla \phi^+) = 0, \quad \nabla^2 \phi^- = 0, \quad (3.43d)$$

$$[\![\mathbf{u}_0 \cdot \mathbf{n}]\!] = 0, \quad (3.43e)$$

$$\left[ \left[ -p_0 \mathbf{n} + \frac{1}{Re} (\mathbf{n} \cdot \nabla \mathbf{u}_0) + Ca_E \sigma_{e0} \cdot \mathbf{n} \right] \right] = \sigma \kappa \mathbf{n}, \quad (3.43f)$$

$$[\![\phi_0]\!] = 0, \quad (3.43g)$$

$$[\![\mathbf{J}_0]\!] = 0, \quad (3.43h)$$

which is the consistent with the leaky-dielectric model in [12, 11].

## 4 Numerical results

In this section, we conduct a series of numerical experiments to illustrate the validity of the established diffuse interface model. The traditional semi-implicit numerical scheme is adopted. Specifically, we add a linear stabilization factor to solve the Cahn-Hilliard equations, and the classical pressure correction method to deal with the Navier-Stokes equations. We use the Mark and Cell(MAC) finite difference to discrete the space variables, which means the scalar variables are located at the center of every mesh, however the vector is located at the center of edge. The specific semi-discrete numerical scheme in time is shown as follows,

**Step 1.** We solve the Cahn-Hilliard equation firstly with the help of stabilization method,

$$\frac{\psi^{n+1} - \psi^n}{\Delta t} + \nabla \cdot (\mathbf{u}^n \psi^n) = M \nabla^2 \mu_\psi^{n+1}, \quad (4.1a)$$

$$\mu_\psi^{n+1} = -\delta \nabla^2 \psi^{n+1} + \frac{s}{\delta} (\psi^{n+1} - \psi^n) + \frac{1}{\delta} F'(\psi^n) - \frac{Ca_E}{2} \frac{\partial \epsilon_{eff}^n}{\partial \psi^n} |\nabla \phi^n|^2, \quad (4.1b)$$

where  $s$  is the so-called stabilization factor to keep the numerical scheme more stable.

**Step 2.** The electric potential  $\phi^{n+1}$  is obtain immediately when  $\psi^{n+1}$  is known by the following Poisson equation,

$$\nabla \cdot (\sigma_{eff}^{n+1} \nabla \phi^{n+1}) = 0, \quad (4.2a)$$

$$\frac{1}{\sigma_{eff}^{n+1}} = \frac{1 - \psi^{n+1}}{2} + \frac{1 + \psi^{n+1}}{2\sigma_r}. \quad (4.2b)$$

**Step 3.** We use the pressure correction method to decoupled velocity  $\mathbf{u}$  and pressure  $p$  in Navier-Stokes equation (2.38), which means we solve an intermediate variable velocity  $\tilde{\mathbf{u}}$  shown as follows,

$$\frac{\tilde{\mathbf{u}}^{n+1} - \mathbf{u}^n}{\Delta t} + (\mathbf{u}^n \cdot \nabla \tilde{\mathbf{u}}^{n+1}) + \nabla p^n = \frac{1}{Re} \nabla^2 \tilde{\mathbf{u}}^{n+1} + \mu_\psi^{n+1} \nabla \psi^{n+1} - \frac{Ca_E}{\zeta^2} \rho_e^{n+1} \nabla \phi^{n+1}, \quad (4.3a)$$

$$\frac{1}{\epsilon_{eff}^{n+1}} = \frac{(1 - (\psi^{n+1})^2)^2}{\delta C_m} + \frac{1 - \psi^{n+1}}{2} + \frac{1 + \psi^{n+1}}{2\epsilon_r}. \quad (4.3b)$$

**Step 4.** We get the pressure  $p^{n+1}$  and velocity  $\tilde{\mathbf{u}}^{n+1}$ ,

$$\frac{\mathbf{u}^{n+1} - \tilde{\mathbf{u}}^{n+1}}{\Delta t} + \nabla (p^{n+1} - p^n) = 0, \quad (4.4a)$$

$$\nabla \cdot \mathbf{u}^{n+1} = 0. \quad (4.4b)$$

Firstly, a convergence study is carried out to varify the correctness of our codes. Then we check the sharp interface limit in Section 4.2 by choosing a relatively small values of thickness  $\delta$  and observe the result. In the next, to compare with the benchmark solution, we choose the numerical solutions in [11]. Additionally, we study the merge phenomenon with two drops located in different directions. Finally, we study the influence with the capacitance by some numerical examples.

Table 1: The discrete  $L^2$  error and convergence rate at  $t = 0.1$  with initial data (4.5) and the given parameters.

Grid sizes	Error( $\psi$ )	Rate	Error( $\phi$ )	Rate	Error( $u$ )	Rate	Error( $v$ )	Rate	Error( $p$ )	Rate
$16 \times 16$	2.3377e-02	—	8.8527e-04	—	2.4760e-04	—	4.1204e-04	—	1.7182e-02	—
$32 \times 32$	5.7835e-03	2.02	2.2773e-04	1.96	7.7879e-05	1.67	1.2048e-04	1.77	4.5426e-03	1.92
$64 \times 64$	1.4428e-03	2.00	5.7333e-05	1.99	2.2016e-05	1.82	3.3117e-05	1.86	1.1686e-03	1.96
$128 \times 128$	3.6066e-04	2.00	1.5150e-05	1.92	5.8081e-06	1.92	8.6179e-06	1.94	2.9555e-04	1.98

Table 2: The discrete  $L^\infty$  error and convergence rate at  $t = 0.1$  with initial data (4.5) and the given parameters.

Grid sizes	Error( $\psi$ )	Rate	Error( $\phi$ )	Rate	Error( $u$ )	Rate	Error( $v$ )	Rate	Error( $p$ )	Rate
$16 \times 16$	5.3663e-02	—	1.8178e-03	—	7.1054e-04	—	1.0068e-03	—	1.9289e-02	—
$32 \times 32$	1.3440e-02	2.00	4.7406e-04	1.94	2.0492e-04	1.79	2.9178e-04	1.79	7.1935e-03	1.42
$64 \times 64$	3.3507e-03	2.00	1.2254e-04	1.95	7.8757e-05	1.38	7.9105e-05	1.88	2.2039e-03	1.71
$128 \times 128$	8.3845e-04	2.00	3.5675e-05	1.78	2.5285e-05	1.64	2.0504e-05	1.95	6.1615e-04	1.84

## 4.1 Convergence test

In this section, we perform a convergence study to support the efficiency of our inhouse code. We use a uniform Cartesian grid to discretize a square domain  $\Omega = (0, 1)^2 \subset \mathbb{R}^2$ , namely the mesh size  $N_x = N_y = N$  is adopted here, and if not specified, uniform mesh is always tenable.

The initial condition is chosen as follows,

$$\psi(\mathbf{x}, 0) = 0.2 + 0.5 \cos(2\pi x) \cos(2\pi y), \quad (4.5a)$$

$$\phi(\mathbf{x}, 0) = y, \quad (4.5b)$$

$$u(\mathbf{x}, 0) = -0.25 \sin^2(\pi x) \cos(2\pi y), \quad (4.5c)$$

$$v(\mathbf{x}, 0) = 0.25 \sin^2(\pi y) \cos(2\pi x). \quad (4.5d)$$

The parameters in model are set as

$$\delta = 0.1, \quad Re = 1, \quad Ca_E = 1, \quad \sigma_r = 2, \quad \epsilon_r = 1. \quad (4.6)$$

The Cauchy error in [28] is used to test the convergence rate. In this test method, error between two different spacial mesh sizes  $h$  and  $h/2$  is calculated by  $\|e_\theta\| = \|\theta_h - \theta_{h/2}\|$ , where  $\theta$  is the function to be solved. The mesh sizes are set to be  $h = 1/16, 1/32, 1/64, 1/128$  and time step is fixed as  $\delta t = 10^{-4}$ . The  $L^2$  and  $L^\infty$  numerical errors and convergence rate at chosen time  $T = 0.1$  are displayed in Table 1 and Table 2, respectively. The second order spatial accuracy is apparently observed for all the variables.

We utilize the result to give the conservation of volume about our numerical scheme for  $\psi$  as illustrated in Fig. 1. It demonstrates the volume of  $\psi$  doesn't change over time.

## 4.2 Sharp interface limit test in one dimension

In this example, we consider the steady state solution in one dimensional situation to verify sharp interface limit of electric potential  $\phi$  in our proposed model. For simplicity, we fix the interface and assume the left interval  $(0, 0.5)$  is the inner region and the right interval  $(0.5, 1)$  is the outer region of the interface. The electric potential equation (2.34c) is used to illustrate the sharp interface limit results. The ration of two region conductivities is set to be  $\sigma_r = 2$ . Besides, the Dirichlet boundary condition  $\phi(x = 0) = 1, \phi(x = 1) = 2$  is used. With the help of continuity condition  $[\phi] = 0$  and  $[\sigma \nabla \phi] = 0$  in the sharp interface situation, it is easy to get the exact solution of sharp interface model is a piecewise linear function

$$\phi = \begin{cases} \frac{2}{3}x + 1, & x < x_0, \\ \frac{4}{3}x + \frac{2}{3}, & x \geq x_0. \end{cases} \quad (4.7)$$

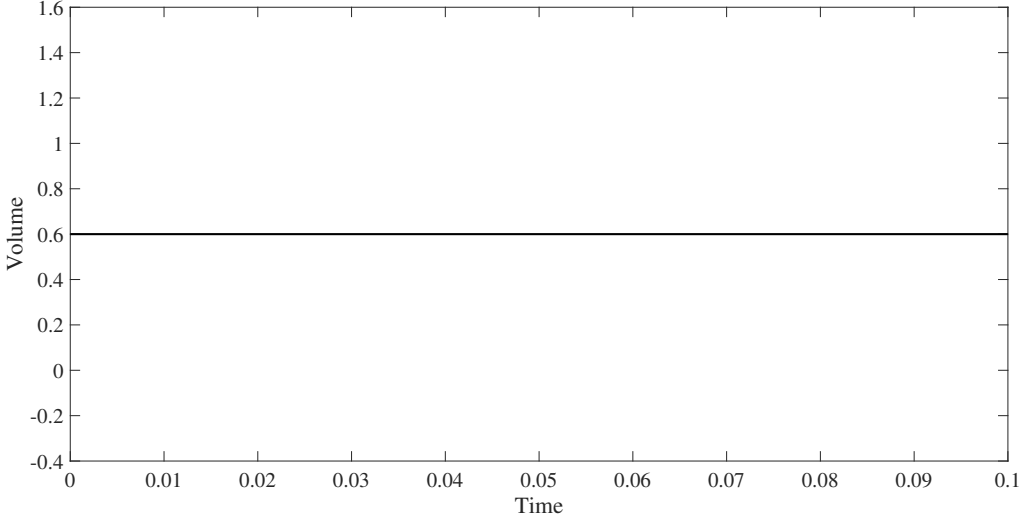


Figure 1: Conservation of volume of the numerical scheme.

In Figure 2, the exact solution (4.7) is shown in black solid line without any marker and the colored lines with different markers are the solutions of Eq. (2.34c) where the phase field function is chosen as  $\psi = \tanh\left(\frac{x-x_0}{\sqrt{2}\delta}\right)$  with different interface thickness  $\delta$ . In the bulk region, solutions of two methods fit very well. As  $\delta \rightarrow 0$ , the proposed diffusive model solutions change much sharper near the interface and converge to the sharp interface solution, which is consistent with our analysis in Section 3.

### 4.3 Comparison with the sharp interface model

In this section, we compare our diffusive interface model results with sharp interface model results conducted in [11] where a hybrid immersed boundary and immersed interface method is used to model the deformation of a leaky dielectric droplet. The 2D computational domain is set as  $\Omega = [-4, 4] \times [-4, 4]$  and the mesh size is set to be  $h = 8/256$ . The time step is chosen as  $\Delta t = 10^{-4}$  and the interface thickness is set to be  $\delta = 0.1$ . We assume the initial profile of droplet is

$$\psi(x, y, 0) = \tanh \frac{1 - \sqrt{x^2 + y^2}}{\sqrt{2}\delta}. \quad (4.8)$$

Nonflux boundary for  $\psi$  and nonslip boundary for velocity are adopted here. For the electric potential, Dirichlet boundary condition  $\phi(x, 4) = 4$  and  $\phi(x, -4) = -4$  is used on the top and bottom boundaries; the homogeneous Neumann boundary is used on the left and right boundaries. As in [11], the dielectric coefficients and electric capillary number are chosen as  $\epsilon_r = 3.5$  and  $Ca_E = 1$ , respectively. And there is no capacitance on the interface, i.e.  $C_m = \infty$  in Eq. (2.19j).

Fig. 3 shows snapshots of the droplets and flow patterns at different time  $t = 1$  (left),  $t = 5$  (middle) and  $t = 10$  (right) with three different conductivity ratio cases  $\sigma_r = 1.75$  (top),  $3.25$  (middle) and  $4.75$  (bottom) which are compared with the previous work in [11]. In each subplot, the black solid line shows the zero level set to describe the position of interface. The velocity quivers are depicted in the right half while the corresponding stream lines are shown in the left. When conductivity ratio is small  $\sigma_r = 1.75$ , the drop shape is oblate (top) and the induced circulatory flow inside the first quadrant is clockwise (from the pole to the equator). When ratio become larger, the droplet changes to be the prolate shape. The induced circulatory flow can be clockwise (middle) and counterclockwise (from the equator to the pole, bottom). The numerical results obtained by a hybrid immersed boundary and immersed interface method in [11] is shown in Fig. 4. We can see that these flow patterns are in good agreement with those from the previous work. Slight difference may be observed from the comparison due to the thickness of diffuse interface.

In Fig. 5, the charge densities  $\rho_e$  with different  $\sigma_r$  at equilibrium states are presented. In the sharp interface limit case, the continuity of current across the boundary  $-\sigma^- \nabla \phi^- \cdot \mathbf{n} = -\sigma^+ \nabla \phi^+ \cdot \mathbf{n}$  yields  $\nabla \phi^+ \cdot \mathbf{n} = \frac{1}{\sigma_r} \nabla \phi^- \cdot \mathbf{n}$ . Then, the net charge density could be calculated by  $\rho_e = -\epsilon^- \nabla \phi^- \cdot \mathbf{n} + \epsilon^+ \nabla \phi^+ \cdot \mathbf{n} =$

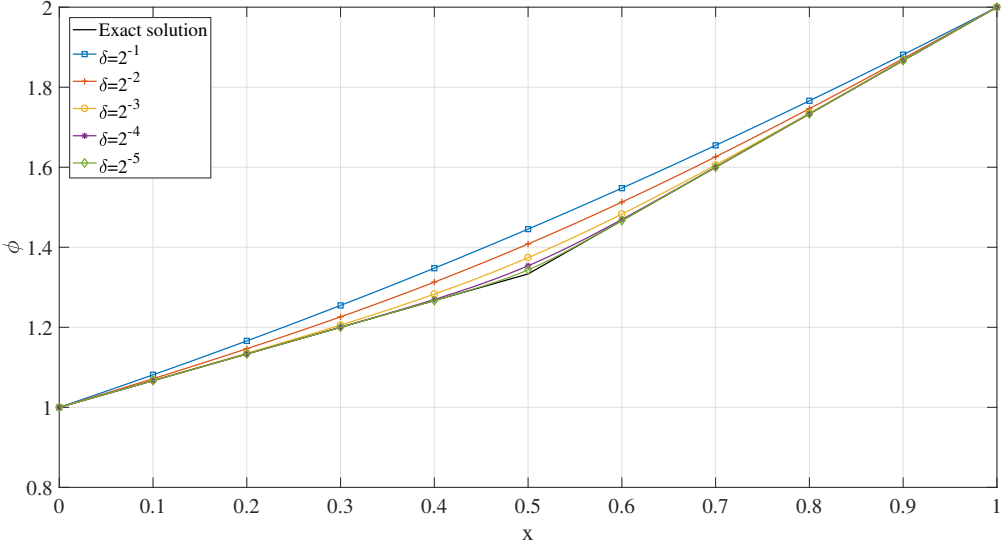


Figure 2: Sharp interface limit test of electric potential in one dimension, the fixed interface is chosen as  $x_0 = 0.5$ . The left interval is assumed as the inner region nevertheless the right interval is assumed as the outer region of the interface.

$(\frac{\epsilon_r}{\sigma_r} - 1)\nabla\phi^- \cdot \mathbf{n}$ , as in [22, 17]. Therefore, when  $\sigma_r < \epsilon_r$ , positive net charges accumulate on the top of the droplet, and negative charges are on the bottom. This can be observed in the first and second rows of Fig. 5 for the cases  $\sigma_r = 1.75, 3.25$ . When  $\sigma_r > \epsilon_r$ , the opposite is true (third row). Also, the closer  $\sigma_r$  is to  $\epsilon_r$ , the smaller the net charge is (second row of Fig. 5). The different profiles of the droplets are induced by the electric force on the droplet. As mentioned in Remark 2.1, there are two forces induced by Maxwell stress: the first term is the Lorentz force  $\mathbf{FL} = -\frac{1}{\zeta^2}\rho_e\nabla\phi$  due to the interaction of net charges with the electric field, and the second term  $\mathbf{Fp} = -\frac{1}{2}|\nabla\phi|^2\frac{\partial\epsilon_{eff}}{\partial\psi}\nabla\psi$  is due to the polarization stress. The distributions of these two forces are shown in the second and third column of Fig. 5, where the color represents the magnitude, and the arrow represents the direction of the force. It shows that the force  $\mathbf{Fp}$  is always pointing outside of the droplet since  $-\nabla\psi = \mathbf{n}$  near the interface, and the magnitude is almost the same in all cases. On the left and right sides, it becomes weaker because of the decrease of the electric field magnitude and the conservation of current across the interface (See Fig. 15 in Appendix). The Lorentz forces point to the inner side of the droplets with  $\sigma_r = 1.75, 3.25$ , and the outer side of the droplet with  $\sigma_r = 4.75$ . On the left and right sides, the magnitude of  $\mathbf{FL}$  is almost zero since there is no accumulated net charge.

In Fig. 6, we present a detailed distribution of electric force along the  $x$ -axis (top) and  $y$ -axis (bottom) for droplets with different values of  $\sigma_r$ :  $\sigma_r = 1.75$  (left),  $\sigma_r = 3.25$  (middle), and  $\sigma_r = 4.75$  (right). In all cases, the Lorentz force is negligible since the net charge density is small and the total force is outward along the  $x$  direction. When  $\sigma_r = 1.75$ , the Lorentz force is larger than the polarization force in the  $y$ -axis direction, resulting in the compression of the droplet by the electric field. Therefore, under the total electric force, the droplet appears oblate. For  $\sigma_r = 3.25$ , the polarization force is larger in the  $y$  direction. However, the total expansion force in the  $y$  direction is larger than in the  $x$  direction, and since the fluid is incompressible, the droplet is elongated in the  $y$  direction with a prolate profile at equilibrium. In the case of  $\sigma_r = 4.75$ , both the Lorentz force and the polarization force are pointing outward in the  $y$  direction, resulting in a net force that is larger in the  $y$  direction than in the  $x$  direction. As a result, the droplet is elongated in the  $y$  direction.

#### 4.4 Electro-coalescence

In this section, we conduct a series of numerical experiments to explore the electro-coalescence. Electro-coalescence refers to the process of two or more suspended droplets or particles coming into contact and merging under the influence of an applied electric field. It is a phenomenon commonly observed in various electrokinetic systems and has significant implications in fields such as microfluidics, emulsion stability,

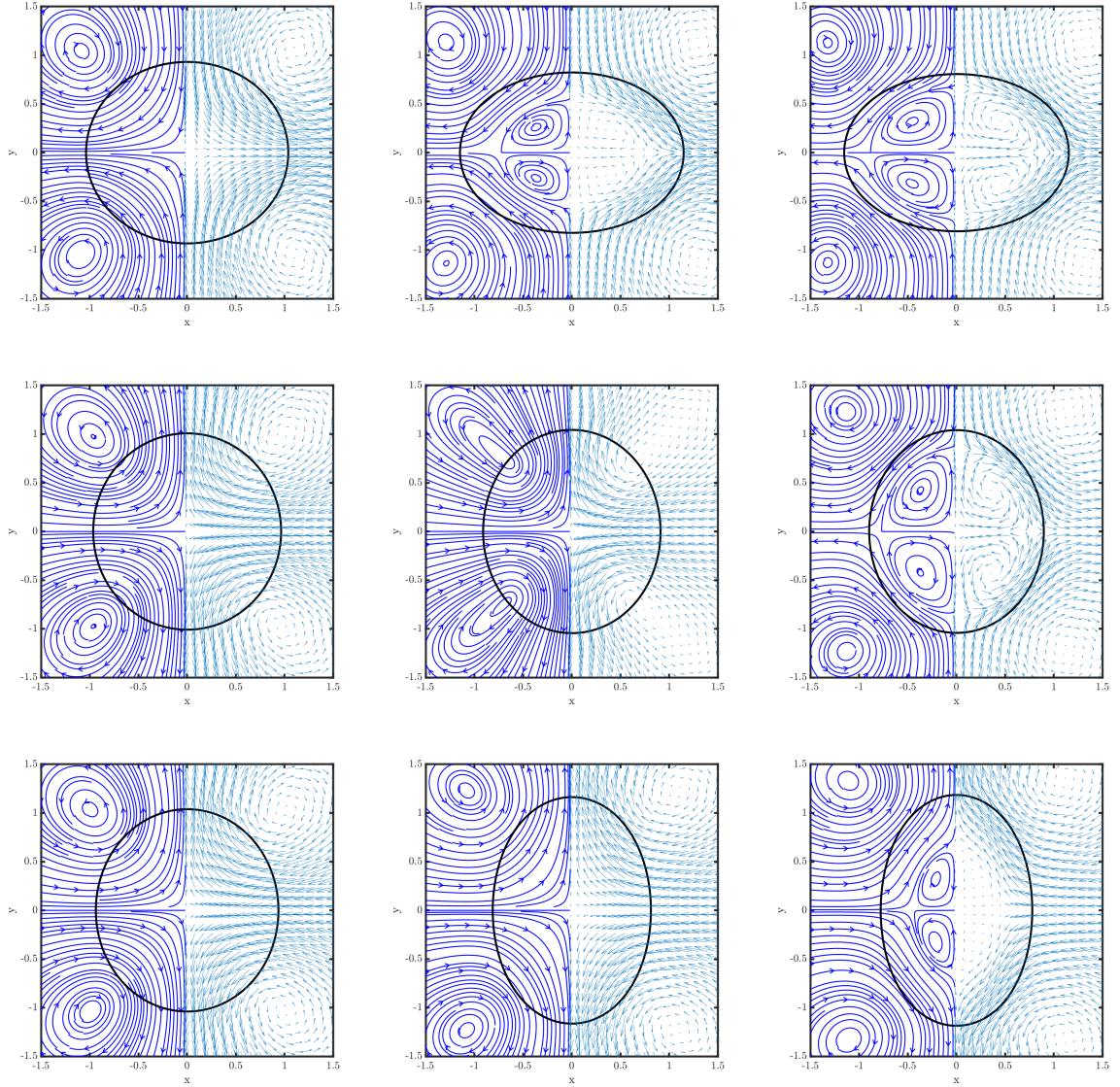


Figure 3: Drop shapes and flow patterns for  $\sigma_r = 1.75$  (top),  $\sigma_r = 3.25$  (middle) and  $\sigma_r = 4.75$  (bottom) at  $t = 1$  (left),  $t = 5$  (middle) and  $t = 10$  (right) for example 4.8 in section 4.3. The dielectric coefficient ratio is set to  $\epsilon_r = 3.5$ . The electric capillary number is chosen as  $Ca_E = 1$ . We choose the coefficients are all the same as [11] for comparison. In each subplot, the black solid line shows the zero level set of  $\psi$  to describe the position of interface, the velocity quivers are depicted in the right half while the corresponding stream lines are shown in the left.

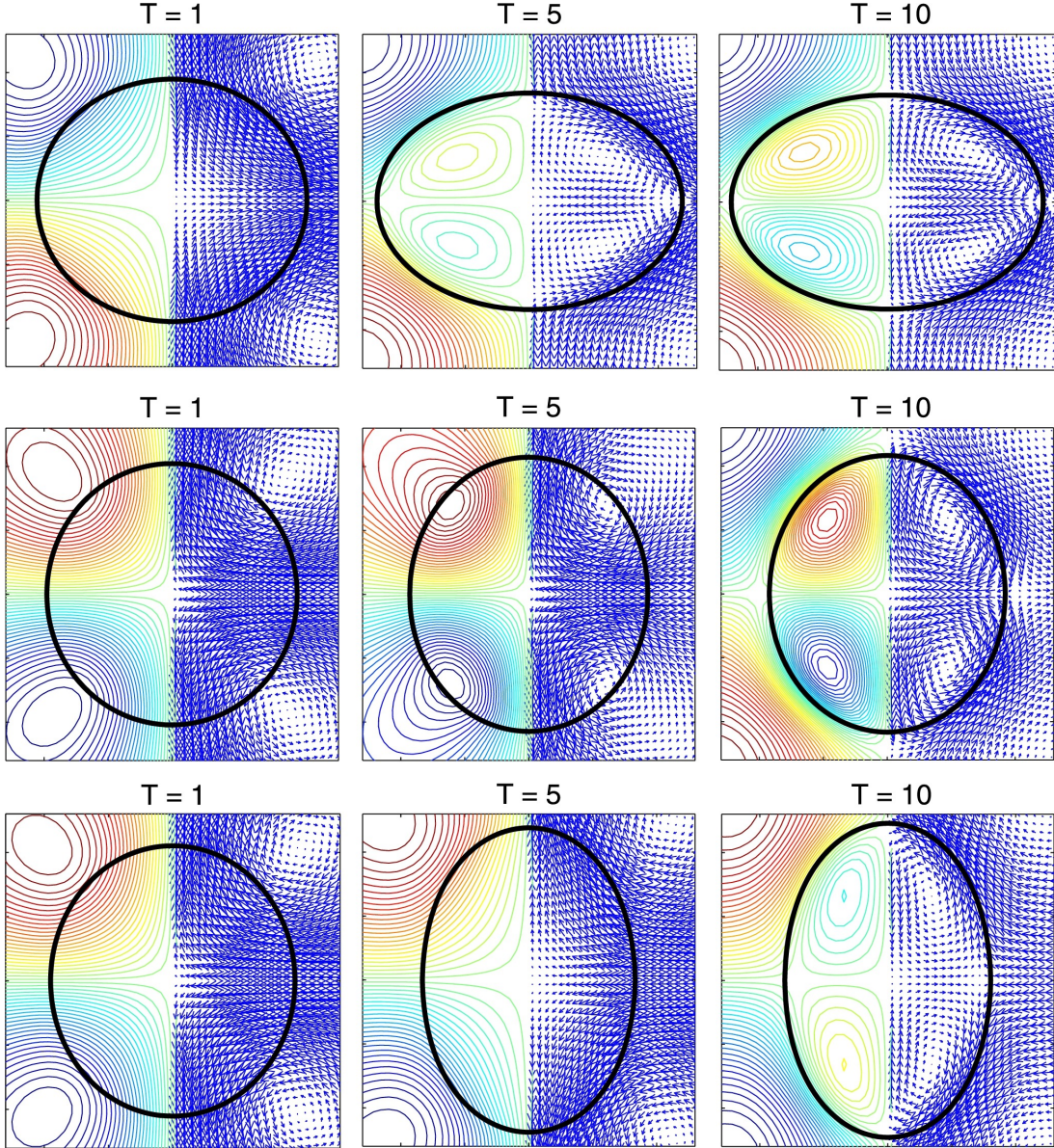


Figure 4: The numerical results obtained by a hybrid immersed boundary and immersed interface method in [11]. The black solid line is the location of interface, and left part is the stream lines and the right part is the velocity quivers. The different conductivity ratios are set as  $\sigma_r = 1.75$  (top),  $\sigma_r = 3.25$  (middle),  $\sigma_r = 4.75$  (bottom). Besides, the dielectric coefficient ratio and electric capillary are  $\epsilon_r = 3.5$  and  $Ca_E = 1$ , respectively.

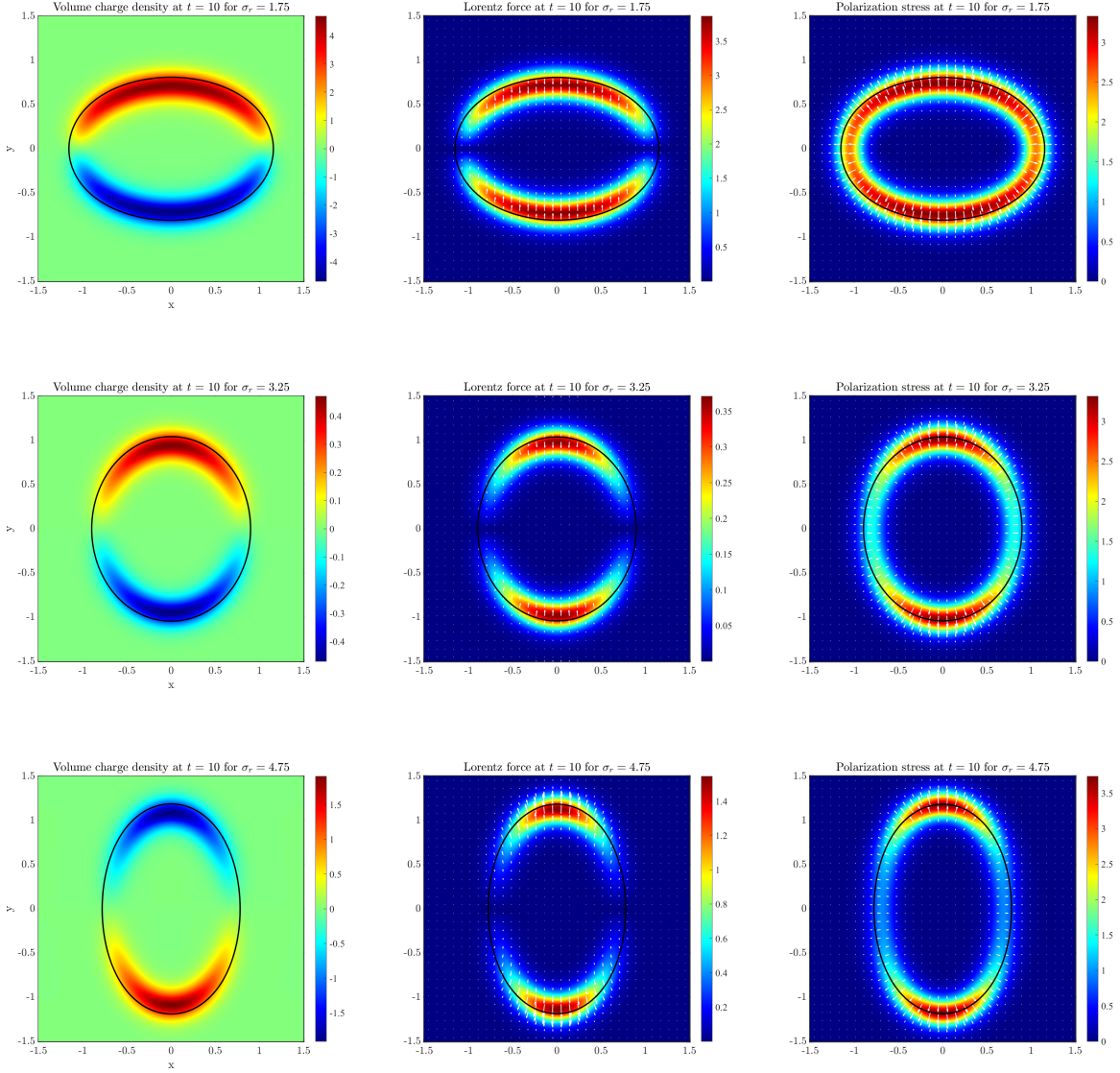


Figure 5: Distributions of charge density  $\rho_e$  (left), Lorentz electric force  $\mathbf{F}_L$  (middle) and polarization force  $\mathbf{F}_p$  (right) with different conductivity ratios  $\sigma_r = 1.75$  (top),  $\sigma_r = 3.25$  (middle),  $\sigma_r = 4.75$  (bottom) at  $t = 10$  for example 4.8 in section 4.3. The positive ions accumulate at the top of the interface when  $\sigma_r = 1.75$  and  $\sigma_r = 3.25$ , whereas the negative ions on the contrary. The positive ions accumulate at the bottom of the interface when  $\sigma_r = 4.75$ . The dielectric coefficient ratio and electric capillary are  $\epsilon_r = 3.5$  and  $Ca_E = 1$ , respectively.

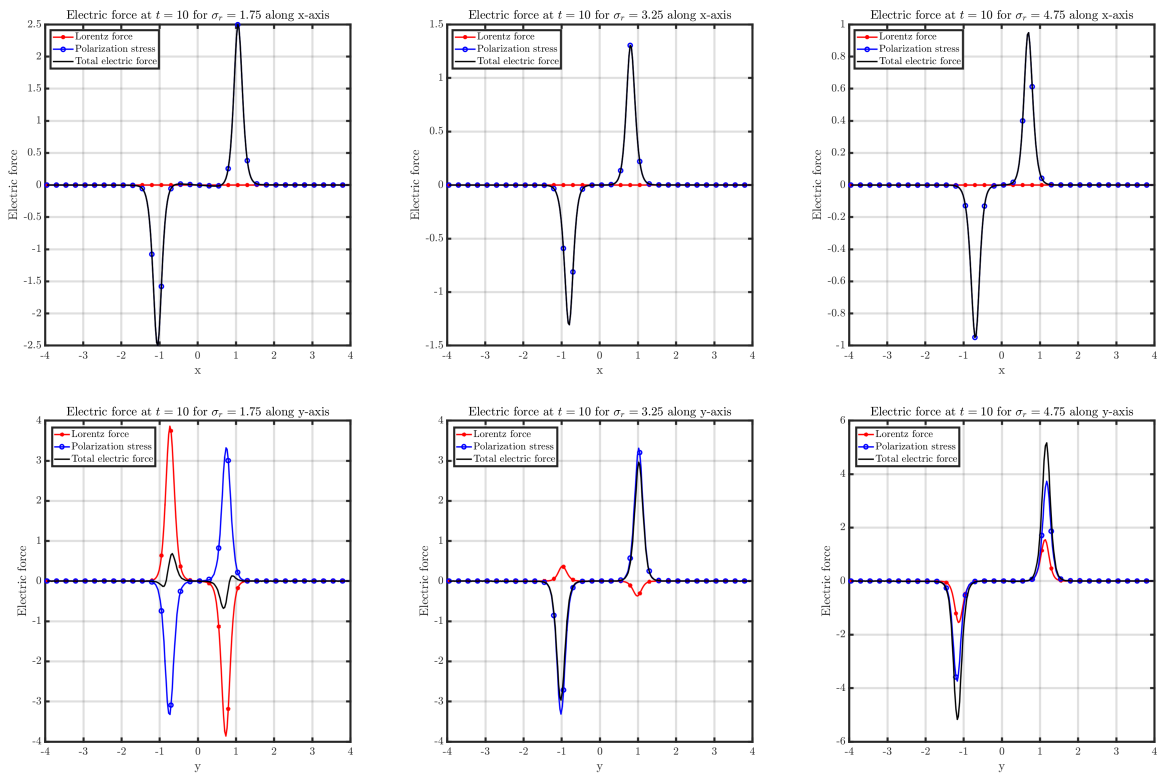


Figure 6: The electric force along x-axis (top) and y-axis (bottom) for  $\sigma_r = 1.75$  (left),  $\sigma_r = 3.25$  (middle) and  $\sigma_r = 4.75$  (right) at  $t = 10$  for example 4.8 in section 4.3. In each figure, the red solid line with star symbol shows the Loerentz force, the blue solid line with circle shows the polarization stress and the black solid line shows the total electric force. The rest parameters are chosen as  $\epsilon_r = 3.5$ ,  $Ca_E = 1$ .

and particle manipulation.

The computational domain and all the parameters are kept the same as the former section 4.3. The initial profile for double drops is shown as follows (see Fig. 7 first column)

$$\psi(x, y, 0) = \tanh \frac{1 - \sqrt{(x - 1.35)^2 + y^2}}{\sqrt{2}\delta} + \tanh \frac{1 - \sqrt{(x + 1.25)^2 + y^2}}{\sqrt{2}\delta} + 1. \quad (4.9)$$

and each of the two droplets are equal the droplet in Eq. (4.8). When  $\sigma_r = 1.75$ , due to the oblate deformation, two droplets merge together and the charge redistributed which is same as the previous session result at the equilibrium. While for the other two cases, since the deformations of droplets are prolates, the distance between two droplets is increased. The distributions of the electric forces could be found in Appendix Fig. 16-17.

In the next, we fix the conductivity ratio to be  $\sigma_r = 1.75$  and position two droplets vertically. The initial position of two droplets are set to be

$$\psi(x, y, 0) = \tanh \frac{1 - \sqrt{x^2 + (y - 1.35)^2}}{\sqrt{2}\delta} + \tanh \frac{1 - \sqrt{x^2 + (y + 1.25)^2}}{\sqrt{2}\delta} + 1. \quad (4.10)$$

As we can see in Fig. 8, due to the oblate deformation, two droplets don't merge together first. The positive ions accumulate on the top of each drop and the negative ions accumulate on the bottom of each drop. However, under the influence of the electric field, the top bubble will migrate down, and the bottom bubble will migrate up and finally the two bubbles will touch each other and merge into one droplet. The big droplet deforms from prolate to oblate and the volume charge redistribute which is same as the previous session result at the equilibrium (top). The distributions of Lorentz force (middle) and polarization stress (bottom) are also presented. The direction of Lorentz force is also from outside to inside, which is not affected by the location of ions, and the direction of polarization stress is from inside to outside. 1D distributions of forces along the line  $x = 0$  are presented in Fig. 9. In the region between two droplets, the total electric force  $\nabla \cdot \sigma_e$  is attraction force leading to two droplets approaching each other.

## 4.5 Capacitance effect

In this section, we focus on the capacitance effect acting on the drop. We consider a single drop in the applied electric field with finite capacitance  $C_m = 1, \delta^{-1}, \delta^{-2}$  and compare with the results without capacitance in Section 4.3. All the other parameters are set to be same as Section 4.3. When the capacitance  $C_m$  is set to be  $1, \delta^{-1}, \delta^{-2}$ , it means the electric permittivity near the interface  $\epsilon_m = \delta C_m$  is around  $\delta, 1, \delta^{-1}$ . The effective permittivity with different order of capacitance is shown in Fig. 10, where the finite capacitance introduces a local perturbation near the interface.

The shape behavior with different conductivity ratios  $\sigma_r = 1.75$  (left),  $\sigma_r = 3.25$  (middle) and  $\sigma_r = 4.75$  (right) with different capacitance at the final time  $t = 10$  is presented in Figure 11. The black solid lines denotes the interfaces of the droplets without capacitance for reference. Whereas the colorful dash lines are the interfaces of droplets with different capacitance  $C_m = 1$  (blue),  $C_m = \delta^{-1}$  (red) and  $C_m = \delta^{-2}$  (green). It shows that the deformation decreases as the capacitance decrease in all three cases. The distribution of the net charge is presented in Fig. 12 and Fig. 18-19 in Appendix. It shows that the distribution of net charge is affected near the interface when the capacitance is considered. With capacitance, the total net charge  $\rho_e = -\nabla \cdot (\epsilon_{eff} \nabla \phi) = -\epsilon_{eff} \Delta \phi - \nabla \epsilon_{eff} \cdot \nabla \phi$  is formed by the variation of electric field and the variation of electric permittivity. The results illustrate that the main difference is induced by the variation of the electric permittivity (third column). The derivative  $\frac{\partial \epsilon_{eff}}{\partial \psi}$  changes sign across the interface and leads to accumulation of counter-ions at the outer interface.

## 5 Discussion on time scales

In Eq.(2.27), if we introduce the dimensionless ratios

$$t_{E2M} = \frac{\tilde{t}_E}{\tilde{t}}, \quad t_{E2D} = \frac{\tilde{t}_E}{\tilde{t}_D}, \quad (5.1)$$

it could be written as

$$t_{E2M} \left( \frac{\partial \rho_e}{\partial t} + \nabla \cdot (\mathbf{u} \rho_e) \right) = \zeta^2 \nabla \cdot (\sigma_c \nabla \phi) + t_{E2D} \nabla \cdot (D \nabla \rho_e). \quad (5.2)$$

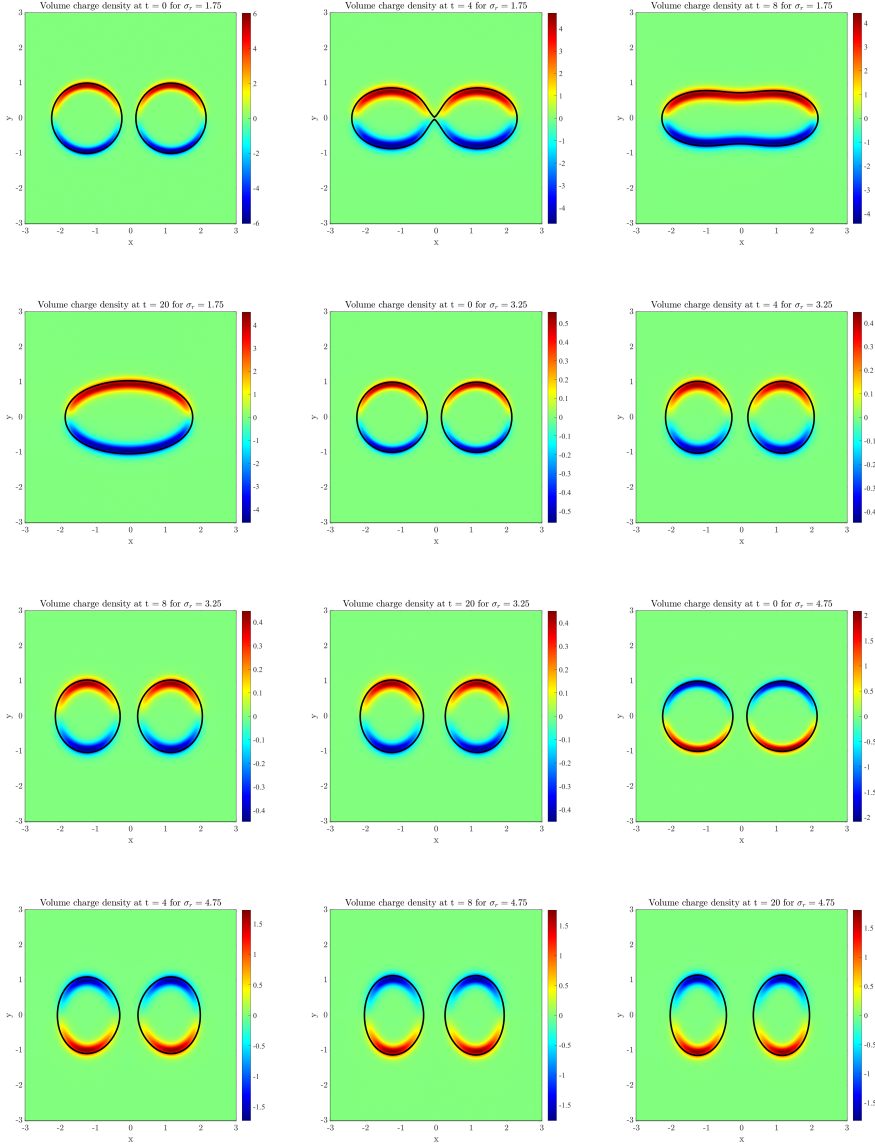


Figure 7: The merge effect for different conductivity ratios  $\sigma_r = 1.75$  (top),  $\sigma_r = 3.25$  (middle),  $\sigma_r = 4.75$  (bottom) at  $t = 0$ ,  $t = 4$ ,  $t = 8$  and  $t = 20$  from left to right, respectively for the example 4.9 in section 4.4. In each figure, the black solid line shows the zero level set ( $\psi = 0$ ) to describe the location of droplet. The rest parameters are chosen as  $\epsilon_r = 3.5$ ,  $Ca_E = 1$ .

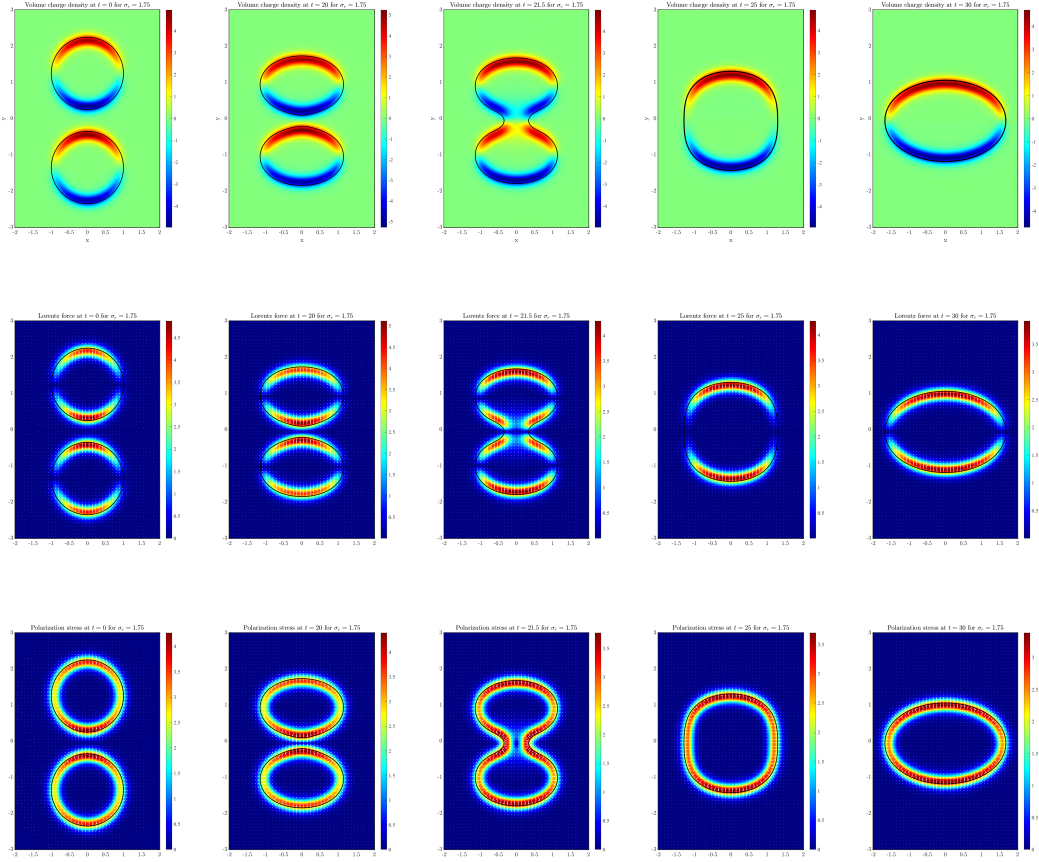


Figure 8: The merge effect for conductivity ratios  $\sigma_r = 1.75$  at  $t = 0$ ,  $t = 20$ ,  $t = 21.5$ ,  $t = 25$  and  $t = 30$  from left to right, respectively for the example 4.10 in section 4.4. In each figure, the black solid line shows the zero level set ( $\psi = 0$ ) to label the location of droplet. The volume charge density (top), Lorentz force (middle) and polarization stress (bottom) are presented. The rest parameters are chosen as  $\epsilon_r = 3.5$ ,  $Ca_E = 1$ .

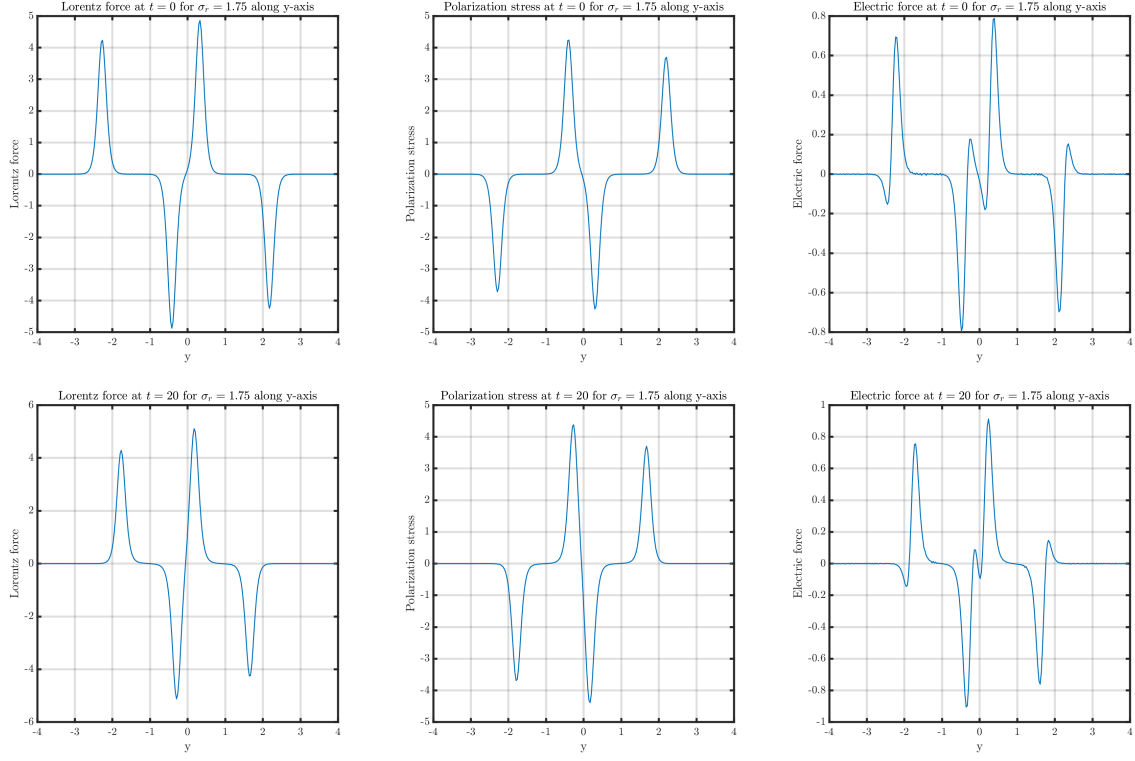


Figure 9: Electric force distribution for 2 vertical droplets with  $\sigma_r = 1.75$  along 1D line  $x = 0$  for the example 4.10 in section 4.4. Top:  $t = 0$ ; Bottom:  $t = 20$ . When  $y < 0$ , it is the force on the lower droplet;  $y > 0$ , it is the force on the upper droplet.

As we mentioned previously, as electric relaxation time is fast enough, i.e.  $t_{E2M} \ll 1$  and  $t_{E2D} \ll 1$ , the leaky dielectric model (2.30) is achieved. In this section, we would like to compare the leaky dielectric model with the net charge model (5.2) under different time scale ratios. For the convenience of discussion, we consider  $t_{E2M} = t_{E2D}$  in the following. So, we will not mention  $t_{E2D}$  no longer. The setup is same as in Section 4.3.

Firstly, we compare the phase field leaky dielectric model with a net charge model, both as approximations of the original PNP-NS-CH model, where the capacitance on the diffuse interface is not considered. In Figs. 13, 20 and 21, the influence of different time scale  $t_{E2M} = 1, \delta, \delta^2$  on droplets profiles and charge densities are shown for three conductivity ratio  $\sigma_r = 1.75, 3.25, 4.75$ , respectively. In each figure, the left column is the charge density of the leaky dielectric model with black lines for the interfaces, the second column is the charge density of the net charge model with red lines for the interfaces and last columns is the difference between two models.

For all three  $\sigma_r$  cases, it is confirmed that the leaky dielectric model provides a reasonable approximation of the net charge model when the electric relaxation is fast, i.e.,  $t_{E2M} = \delta^2$ . However, as the time ratio increases, the difference between the two models becomes larger at equilibrium due to the diffusion effect. Particularly, for the case of  $\sigma_r = 1.75$ , the droplet is prolate in the net charge model. The electric forces along the x-axis and y-axis are illustrated in Fig. 14 for  $t_{E2M} = 1$  (left),  $t_{E2M} = \delta$  (middle), and  $t_{E2M} = \delta^2$  (right). As before, the Lorentz force is negligible, and the polarization force induces expansion in the x-axis direction outward. However, in the y-axis direction, the compressed Lorentz force is weakened, and the polarization force dominates in all three cases, when the diffusion is considered, compared with the leaky dielectric model. The larger the  $t_{E2M}$ , the smaller the  $F_L$ . When the time ratio is  $t_{E2M} = 1$ , the expansion along the y-axis is larger than that along the x-axis, and the drop shape is prolate, which is completely different from the equilibrium in the leaky dielectric case. For small  $t_{E2M}$ , the equilibrium profile is oblate, which is the same as in the leaky-dielectric model, but for different reasons. In the leaky-dielectric case, it is a result of compression in the y-direction and expansion in the x-direction. When the full dynamics are considered, it is the outcome of competition between the expansion in two directions.

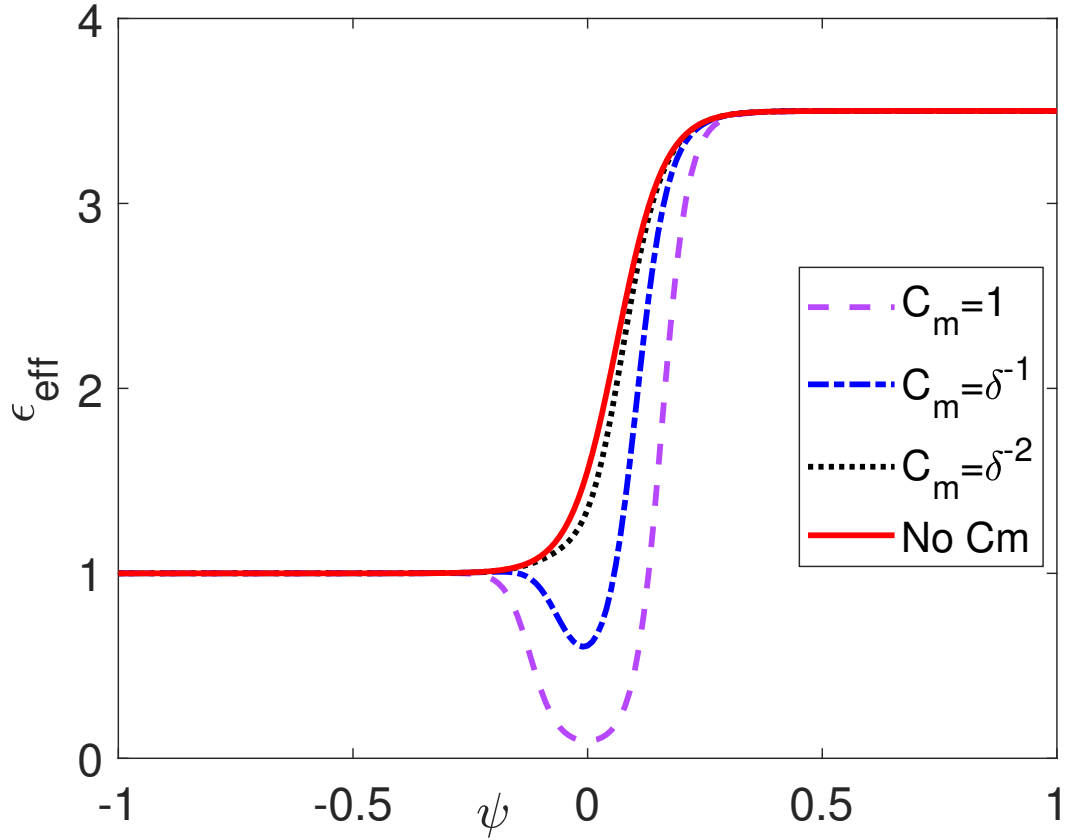


Figure 10: Effective dielectric coefficient with respect label function when  $\epsilon_r = 1.75$ . Red: without  $C_m$ ; Purple:  $C_m = \delta^{-2}$ ; Blue:  $C_m = \delta^{-1}$ ; Black:  $C_m = 1$ .

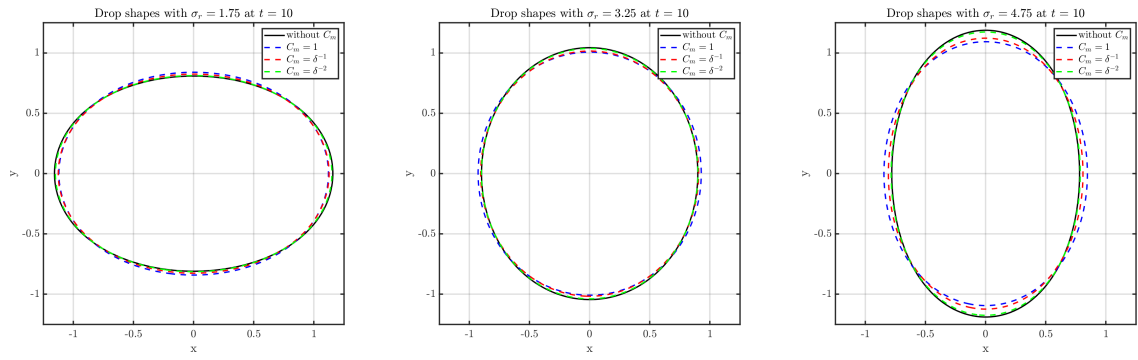


Figure 11: The behavior of drop shapes for different conductivity ratios  $\sigma_r = 1.75$  (left),  $\sigma_r = 3.25$  (middle),  $\sigma_r = 4.75$  (right) by considering different capacitances  $C_m$  at  $t = 10$ . In each figure, the solid line shows the zero level set ( $\psi = 0$ ), where the black, blue, red and green lines show the drop shape with  $C_m = 1$ ,  $C_m = \delta^{-1}$  and  $C_m = \delta^{-2}$ , respectively. The rest parameters are chosen as  $\epsilon_r = 3.5$ ,  $Ca_E = 1$ . The change of the drop shape indicates that a bigger capacitance will cause a more intense drop change.

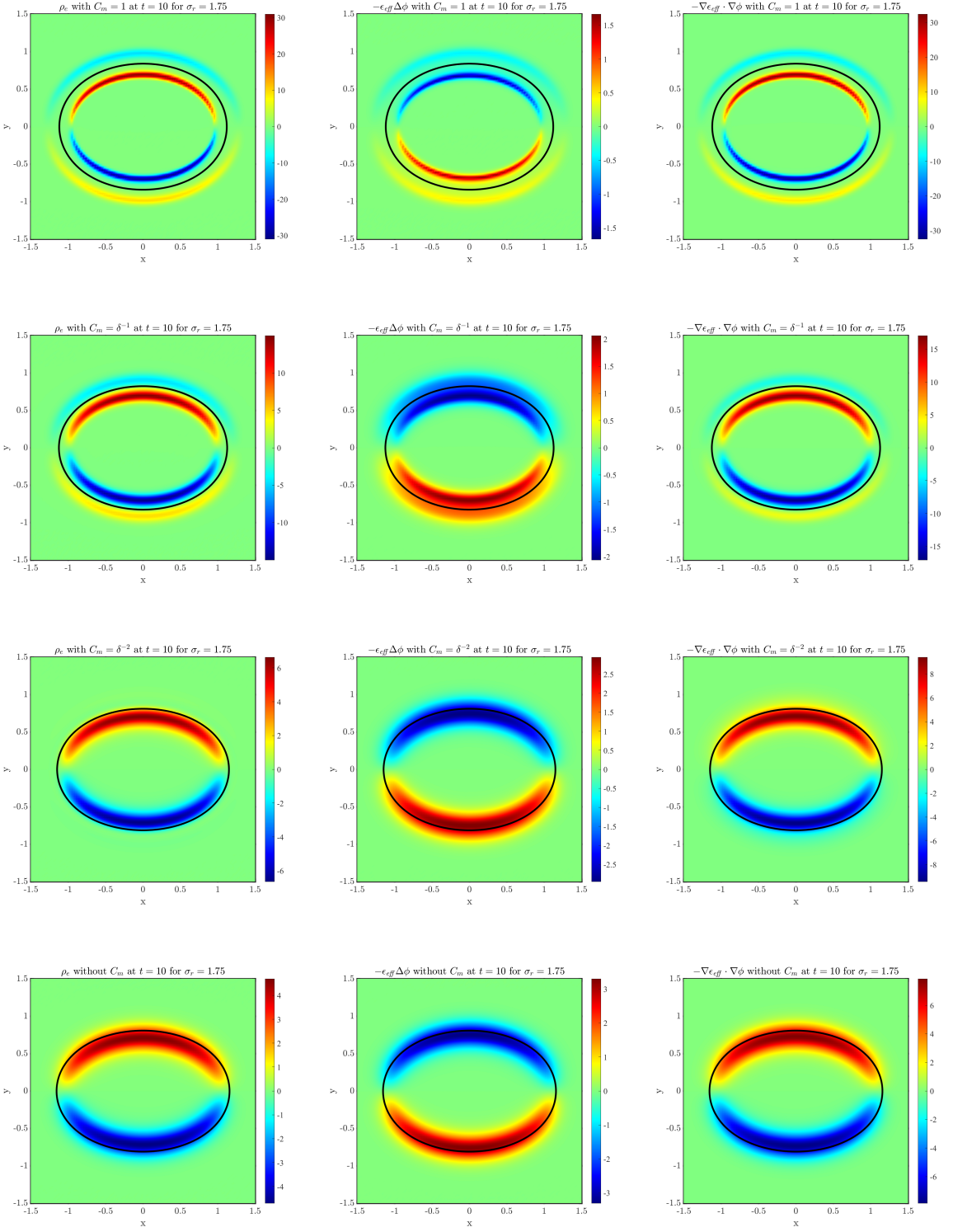


Figure 12: The net charge distribution for conductivity ratio  $\sigma_r = 1.75$  by considering different capacitances  $C_m = 1$ ,  $C_m = \delta^{-1}$ ,  $C_m = \delta^{-2}$  and no  $C_m$  from top to bottom at time  $t = 10$ . In each figure, the solid line shows the zero level set ( $\psi = 0$ ). The rest parameters are chosen as  $\epsilon_r = 3.5$ ,  $Ca_E = 1$ .

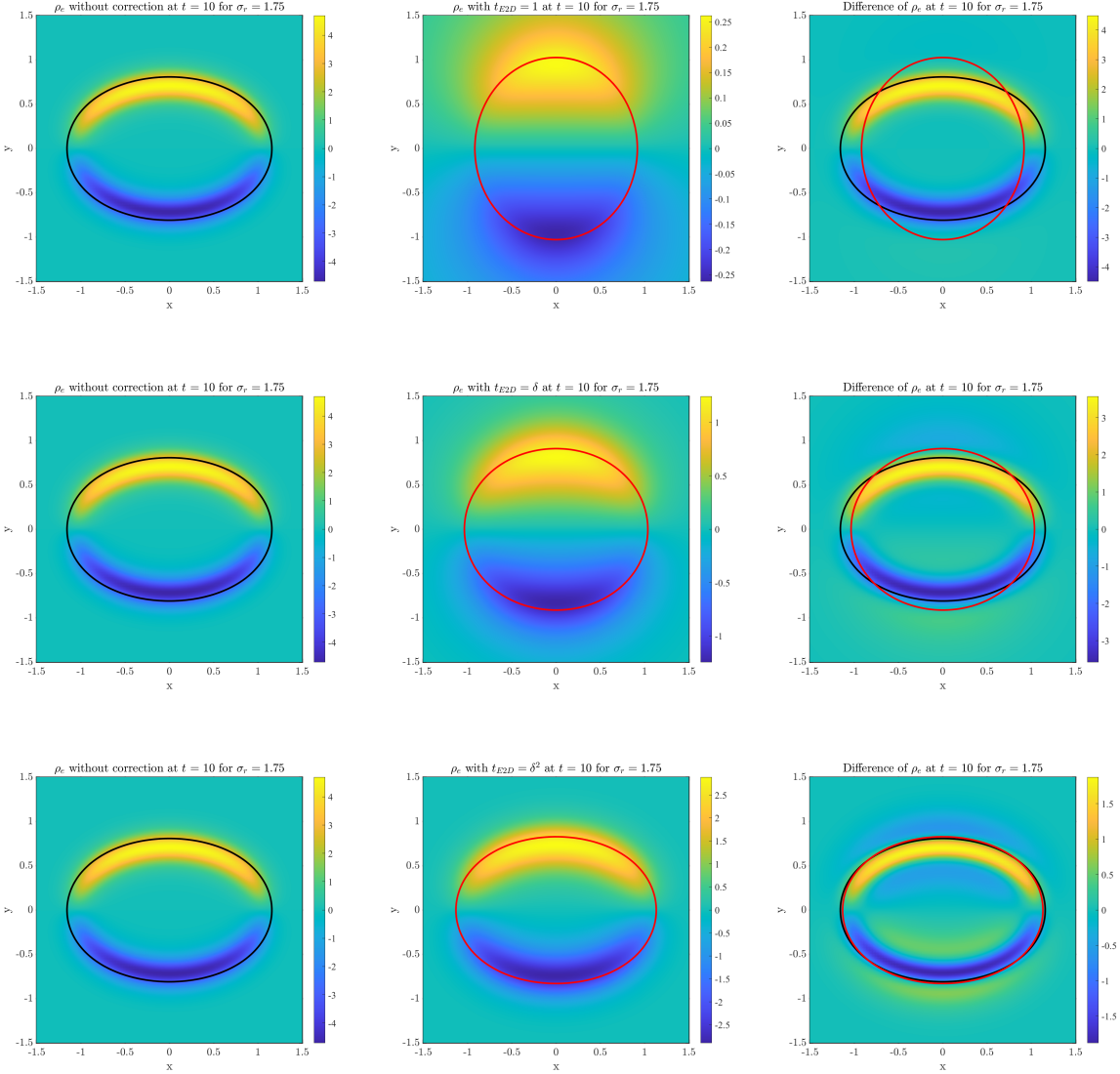


Figure 13: The comparison between leaky dielectric model (left) and net charge model (middle) at  $t = 10$ . The conductivity ratio is  $\sigma_r = 1.75$ . And the difference between them is shown in the right column. relaxation time  $t_{E2M} = t_{E2D} = 1$  (top),  $t_{E2M} = t_{E2D} = \delta$  (middle) and  $t_{E2M} = t_{E2D} = \delta^2$  (bottom) are considered here. In each figure, the solid line shows the zero level set ( $\psi = 0$ ) where the black line shows the drop shape without correction and the red line shows the drop shape with correction. The rest parameters are chosen as  $\epsilon_r = 3.5$ ,  $Ca_E = 1$ .

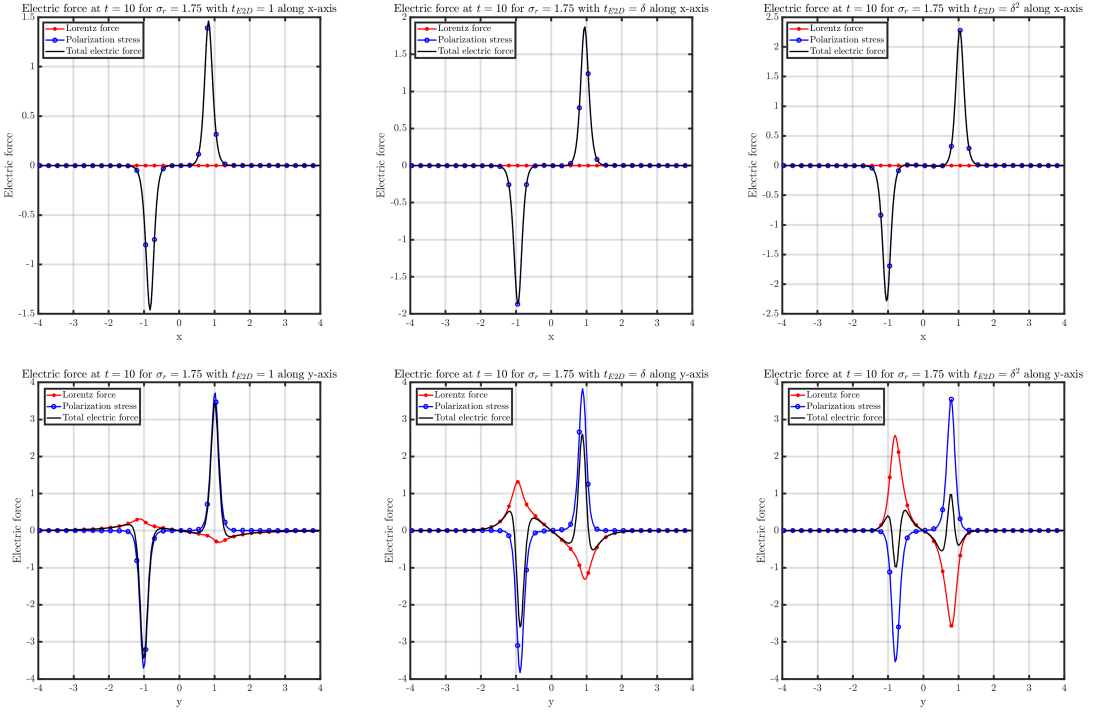


Figure 14: The electric force along x-axis (top) and y-axis (bottom) for  $t_{E2D} = 1$  (left),  $t_{E2D} = \delta$  (middle) and  $t_{E2D} = \delta^2$  (right) about conductivity ratio  $\sigma_r = 1.75$  at  $t = 10$ . In each figure, the red solid line with star symbol shows the Loerentz force, the blue solid line with circle shows the polarization stress and the black solid line shows the total electric force. The rest parameters are chosen as  $\epsilon_r = 3.5$ ,  $Ca_E = 1$ .

Figs 22-24 perform the behavior of drop shapes and distribution of the net charge for conductivity ratio  $\sigma_r = 1.75$ ,  $\sigma_r = 3.25$  and  $\sigma_r = 4.75$  by considering there is no capacitance on the interface (left) and there is capacitance on the interface (middle) about the net charge model. And the difference between them is shown on the right column. Comparing with the leaky dielectric model, the net charge model causes a lower charge accumulation on the interface due to the effect of diffusion. The capacitance effect which leads to a smaller capacitance causes a smaller deformation is also obtained for the net charge model. This result is consistent with the conclusion in section 4.5.

Figs 25-26 present the effect of relaxation time for the net charge model where capacitances  $C_m = 1$  and  $C_m = \delta^2$  are added to the interface, respectively. We choose  $t_{E2D} = \delta^2$  as the reference and the relaxation time effect is consistent with the results shown in 13.

## 6 Conclusions

In this paper, a mathematical model is developed to describe the deformation of droplets under the influence of electric field with different electric permittivity and conductivity, using the energy variation method. Specifically, the capacitance of the two-phase interface is considered using the harmonic average and the phase field function. The diffusive-interface leaky dielectric model is obtained when the electric relaxation time is sufficiently fast. After conducting careful asymptotic analysis, the sharp interface limit of this model is found to be consistent with the existing sharp interface model.

To demonstrate the effectiveness of the proposed model, a variety of numerical experiments are carried out, including the convergence test, comparison with previous sharp interface models, and deformations with topology change. The equilibrium profile of leaky dielectric droplets under a static electric field is mainly determined by the competition between Lorentz force and polarization stress. The former is induced by the accumulation of net charge, while the latter is induced by the variation of electric permittivity near the interface. The distribution of net charge is determined by the ratio between permittivity and conductivity  $\frac{\epsilon_r}{\sigma_r}$ . If it is greater than one, positive charges are accumulated near the side with higher potential and droplet is compressed to be oblate. While if it smaller than one, positive charges are

accumulated near the low potential side and the droplets is elongated into prolate shape.

Furthermore, the effect of capacitance on the interface is studied, revealing that the presence of counter-ions on the opposite side of the interfaces decreases the deformability of droplets. Finally, the impact of time scales on the deformation is discussed when the dynamics of net charge density  $\rho_e$  is considered. The results confirm that the leaky dielectric model is a reasonable approximation when the electric time scale is fast enough. However, when the electric relaxation time and macro time scale are comparable, the diffusion of free charges leads to different droplet deformations due to the decrease in the Lorentz force with dispersed distribution of net charge.

Here, we have discussed the difference between the leaky dielectric model and the net charge model. In the next step, we plan to use an efficient numerical algorithm to directly compare the net charge model with the leaky dielectric model. Additionally, we note that in the leaky dielectric model, the electric potential is continuous with different slope across the interface. However, for a vesicle, the potential is discontinuous due to the capacitance and resistance effects of the membrane, and the total current is conserved across the interface. Building on the similar ideas presented in our previous work [19], we plan to extend our model to study vesicle electrohydrodynamics [10].

Overall, this paper presents a comprehensive analysis of the phase field leaky dielectric model for electrohydrodynamics in droplet systems. Through theoretical derivations and numerical experiments, we provide valuable insights into the behavior and characteristics of these systems, advancing our understanding in this field.

## Acknowledgment

This work is partly supported by the National Natural Science Foundation of China (No. 12071190, 12201369, 12231004) and Natural Sciences and Engineering Research Council of Canada (NSERC).

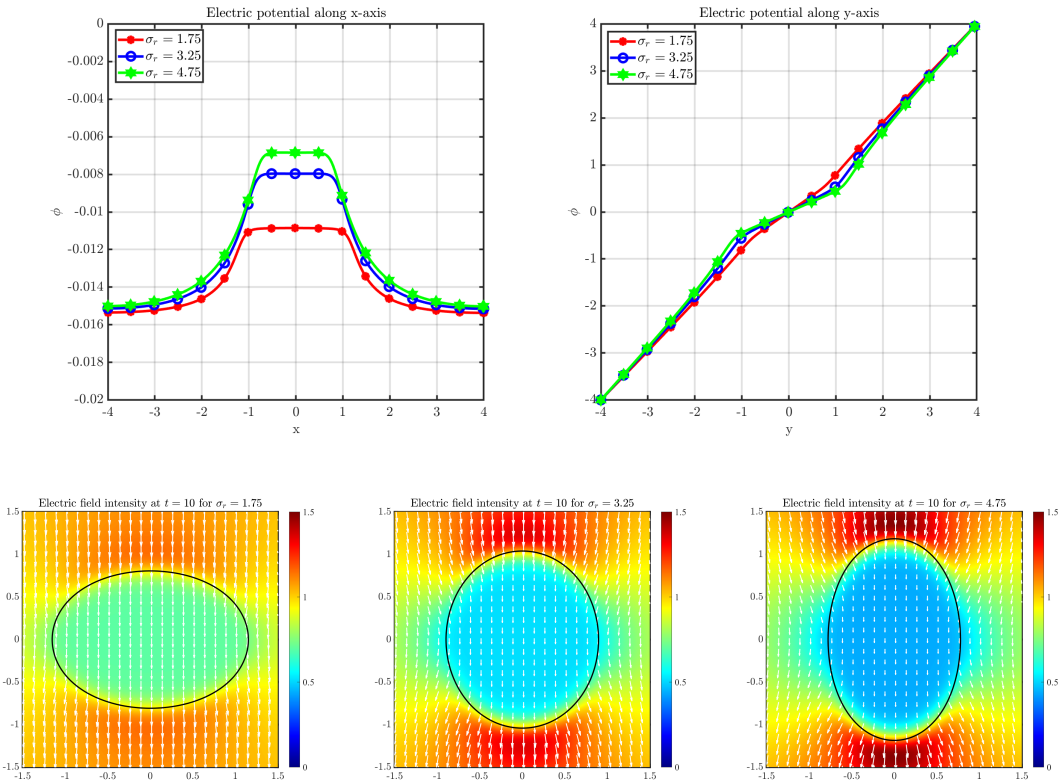


Figure 15: Top: electric potential distribution along  $y = 0$  (left) and  $x = 0$  (right); Bottom: electric field distribution in space with different  $\sigma_r$ .

**A**

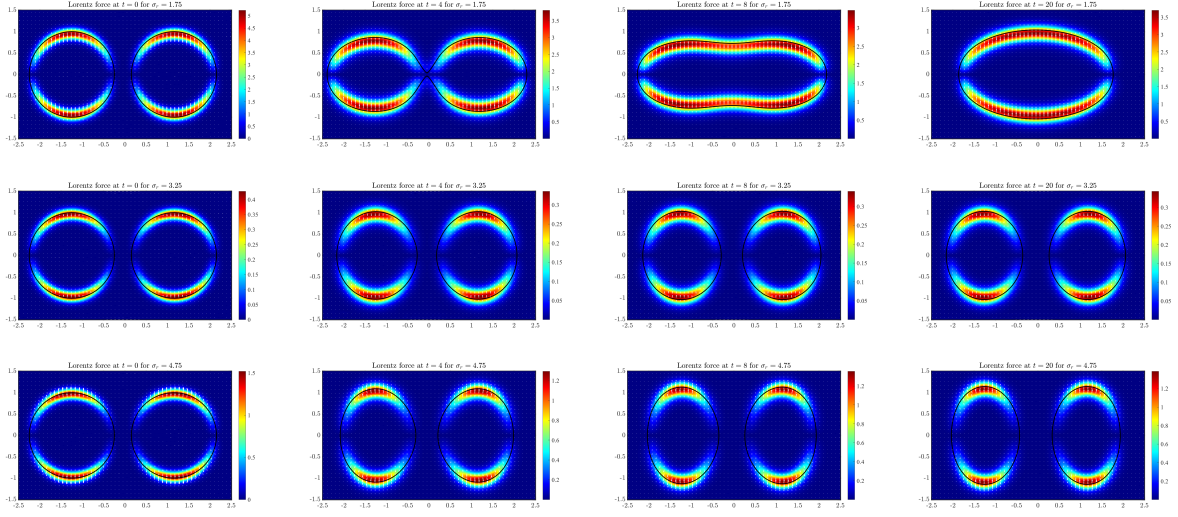


Figure 16: The Lorentz force in merge effect for different conductivity ratios  $\sigma_r = 1.75$  (top),  $\sigma_r = 3.25$  (middle),  $\sigma_r = 4.75$  (bottom) at  $t = 0$ ,  $t = 4$ ,  $t = 8$  and  $t = 20$  from left to right, respectively. In each figure, the solid line shows the zero level set ( $\psi = 0$ ). The rest parameters are chosen as  $\epsilon_r = 3.5$ ,  $Ca_E = 1$ .

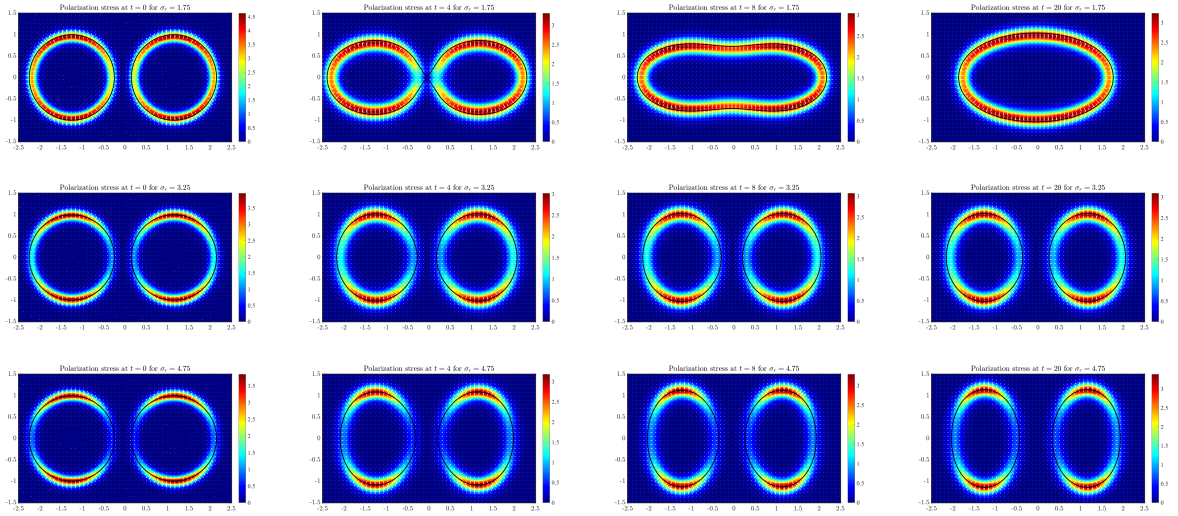


Figure 17: The polarization stress in merge effect for different conductivity ratios  $\sigma_r = 1.75$  (top),  $\sigma_r = 3.25$  (middle),  $\sigma_r = 4.75$  (bottom) at  $t = 0$ ,  $t = 4$ ,  $t = 8$  and  $t = 20$  from left to right, respectively. In each figure, the solid line shows the zero level set ( $\psi = 0$ ). The rest parameters are chosen as  $\epsilon_r = 3.5$ ,  $Ca_E = 1$ .

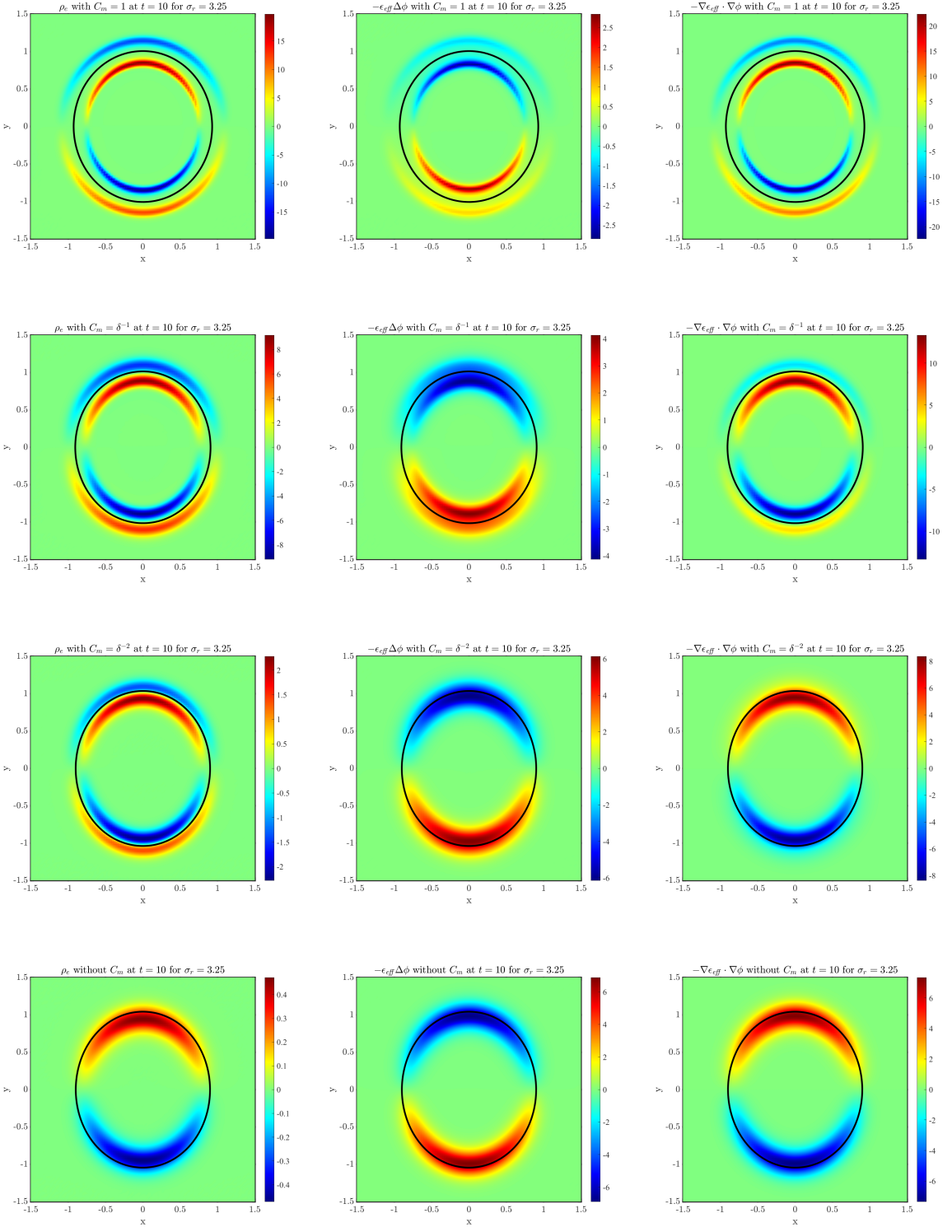


Figure 18: The net charge distribution for conductivity ratio  $\sigma_r = 3.25$  by considering different capacitances  $C_m = 1$ ,  $C_m = \delta^{-1}$ ,  $C_m = \delta^{-2}$  and no  $C_m$  from top to bottom at time  $t = 10$ . In each figure, the solid line shows the zero level set ( $\psi = 0$ ). The rest parameters are chosen as  $\epsilon_r = 3.5$ ,  $Ca_E = 1$ .

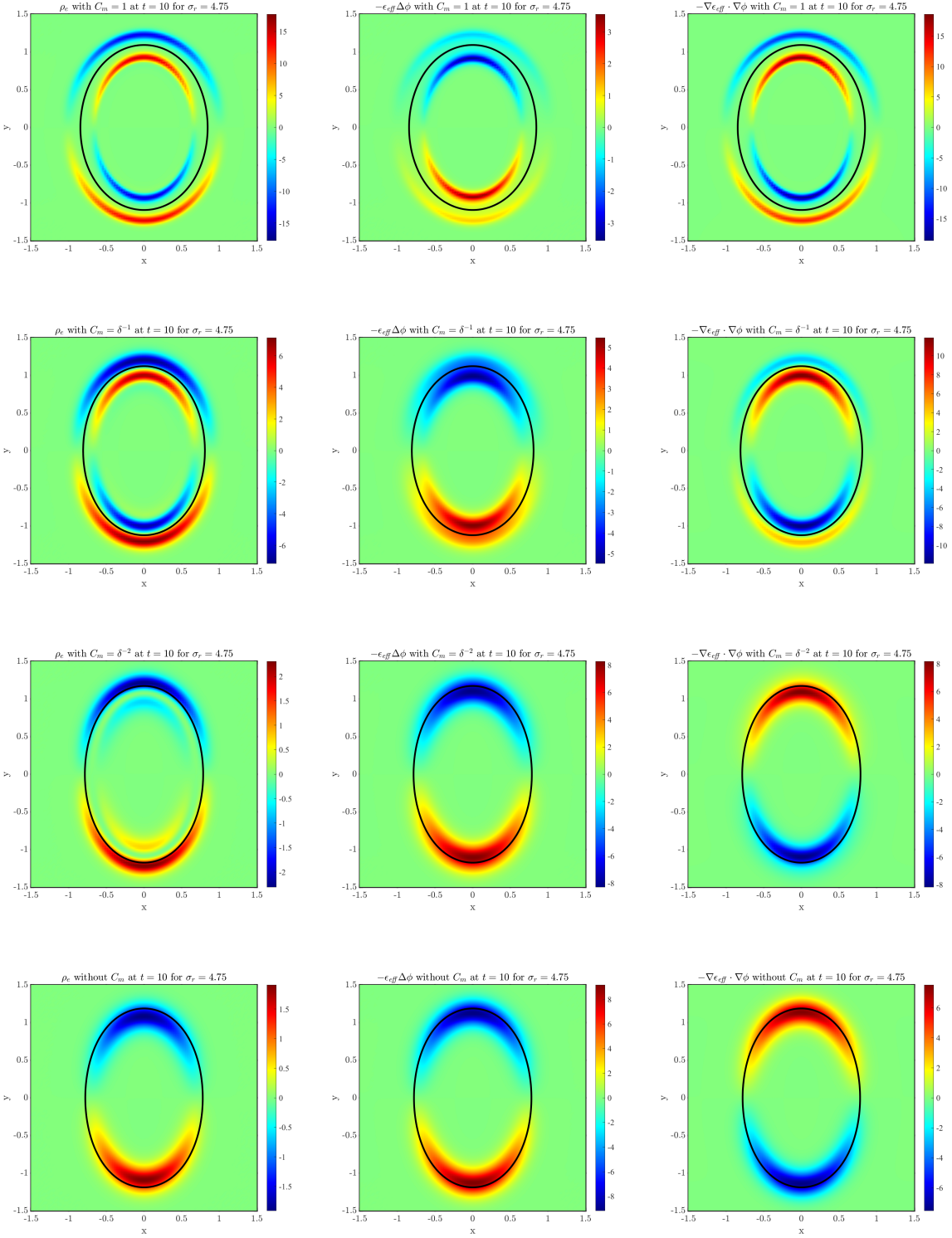


Figure 19: The net charge distribution for conductivity ratio  $\sigma_r = 4.75$  by considering different capacitances  $C_m = 1$ ,  $C_m = \delta^{-1}$ ,  $C_m = \delta^{-2}$  and no  $C_m$  from top to bottom at time  $t = 10$ . In each figure, the solid line shows the zero level set ( $\psi = 0$ ). The rest parameters are chosen as  $\epsilon_r = 3.5$ ,  $Ca_E = 1$ .

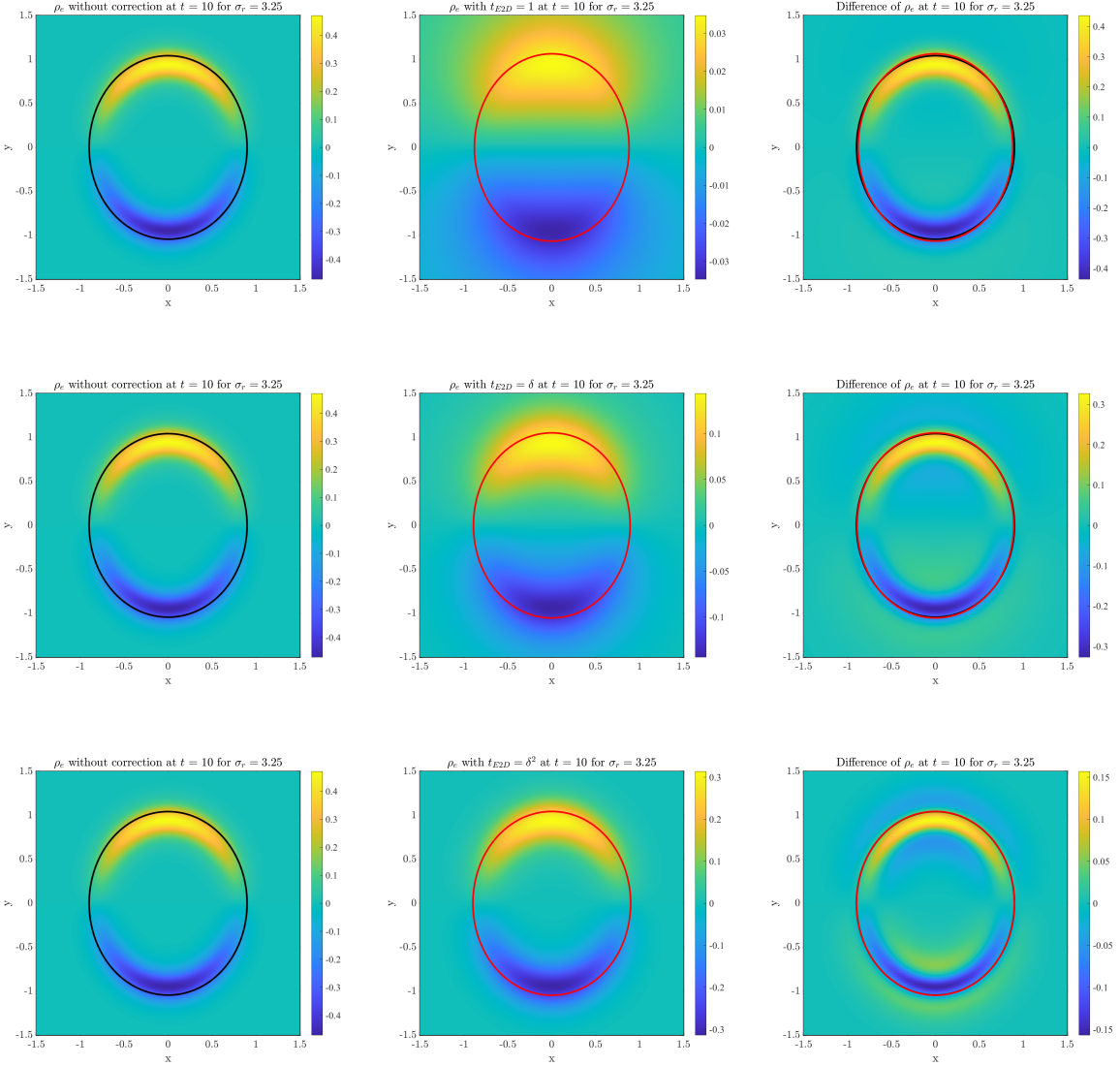


Figure 20: The comparison between leaky dielectric model (left) and net charge model (middle) at  $t = 10$ . The conductivity ratio is  $\sigma_r = 3.25$ . And the difference between them is shown in the right column. relaxation time  $t_{E2M} = t_{E2D} = 1$  (top),  $t_{E2M} = t_{E2D} = \delta$  (middle) and  $t_{E2M} = t_{E2D} = \delta^2$  (bottom) are considered here. In each figure, the solid line shows the zero level set ( $\psi = 0$ ) where the black line shows the drop shape without correction and the red line shows the drop shape with correction. The rest parameters are chosen as  $\epsilon_r = 3.5$ ,  $Ca_E = 1$ .

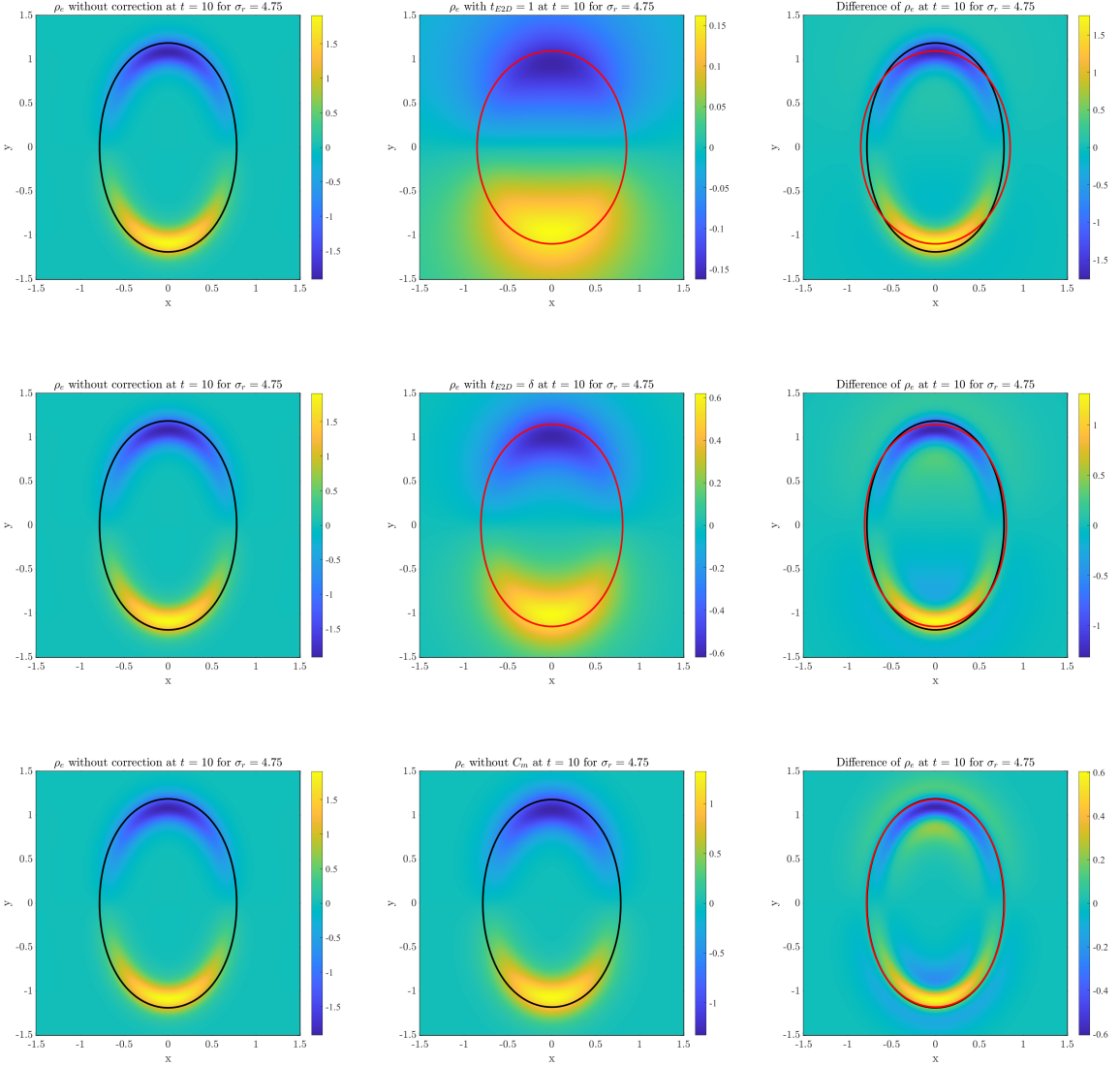


Figure 21: The comparison between leaky dielectric model (left) and net charge model (middle) at  $t = 10$ . The conductivity ratio is  $\sigma_r = 4.75$ . And the difference between them is shown in the right column. relaxation time  $t_{E2M} = t_{E2D} = 1$  (top),  $t_{E2M} = t_{E2D} = \delta$  (middle) and  $t_{E2M} = t_{E2D} = \delta^2$  (bottom) are considered here. In each figure, the solid line shows the zero level set ( $\psi = 0$ ) where the black line shows the drop shape without correction and the red line shows the drop shape with correction. The rest parameters are chosen as  $\epsilon_r = 3.5$ ,  $Ca_E = 1$ .

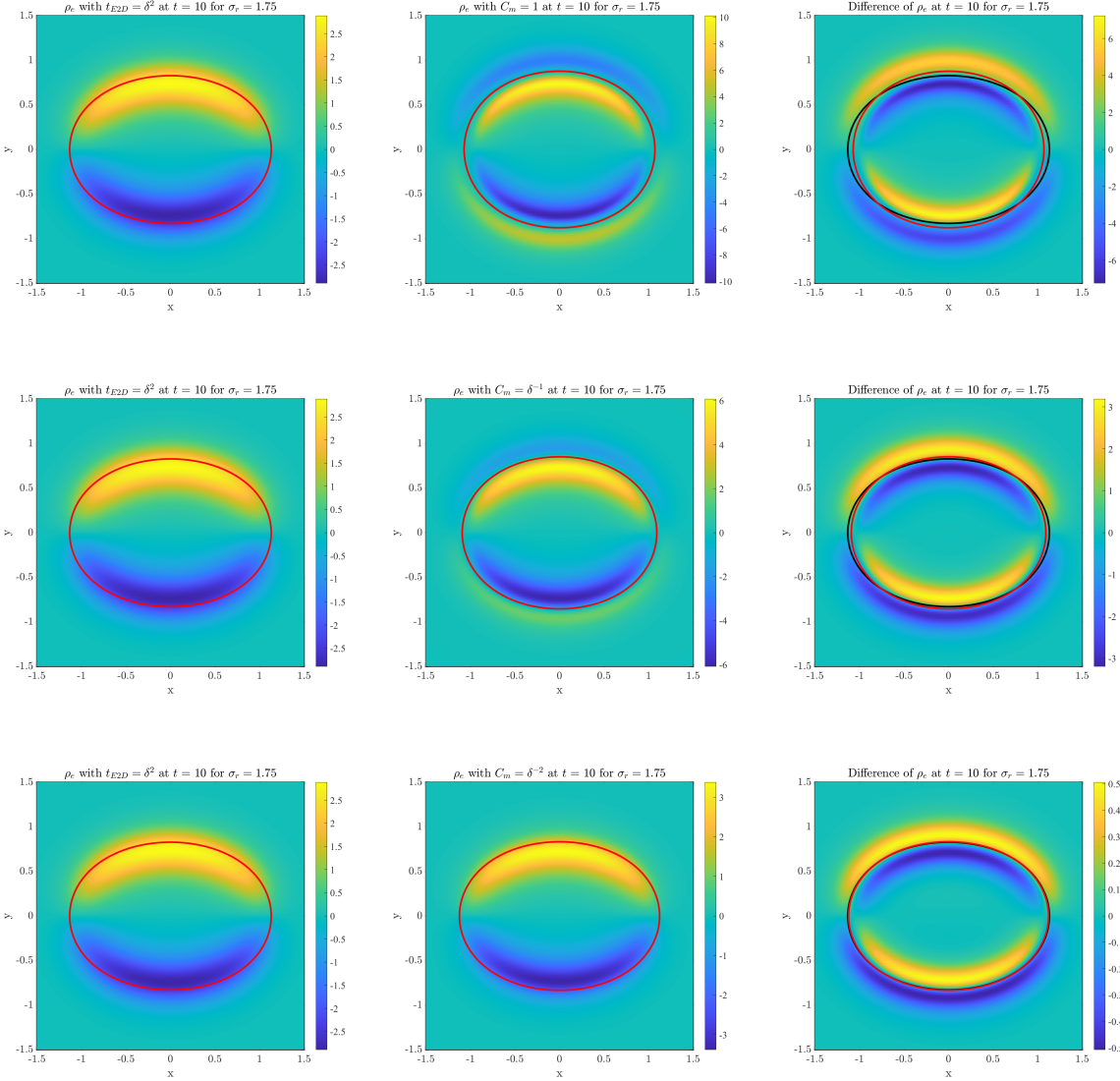


Figure 22: The effect of capacitance for the net charge model at  $t = 10$ . Conductivity ratio  $\sigma_r = 1.75$  is adopted here. We choose the situation without capacitance (left) as the reference. Three different capacitance  $C_m = 1$  (top),  $C_m = \delta^{-1}$  (middle) and  $C_m = \delta^{-2}$  (bottom) is adopted in the middle column. In each figure, the solid line shows the zero level set ( $\psi = 0$ ) where the black line shows the drop shape without capacitance and the red line shows the drop shape with capacitance. The rest parameters are chosen as  $\epsilon_r = 3.5$ ,  $Ca_E = 1$  and  $t_{E2D} = t_{E2M} = \delta^2$ .

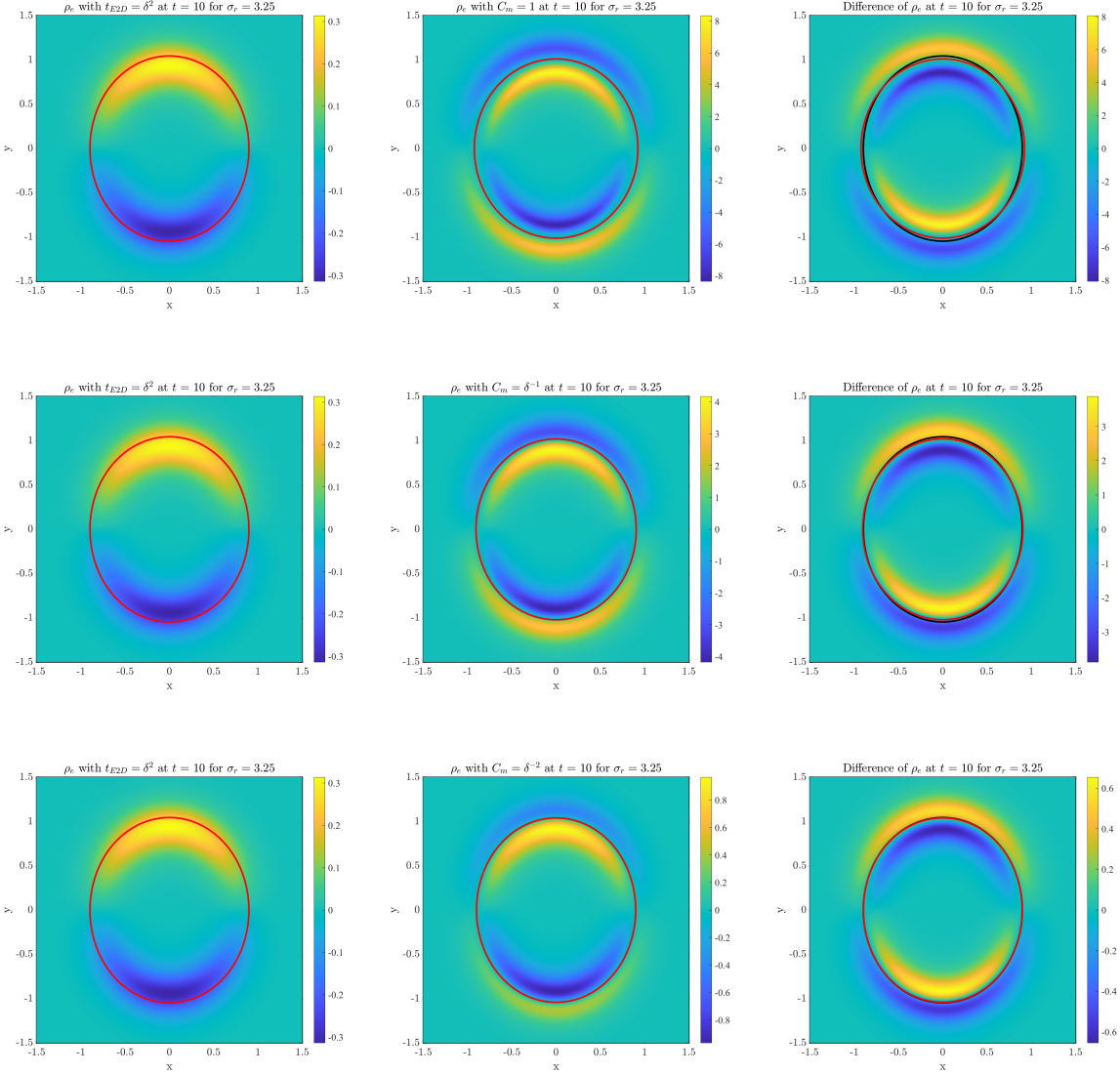


Figure 23: The effect of capacitance for the net charge model at  $t = 10$ . Conductivity ratio  $\sigma_r = 3.25$  is adopted here. We choose the situation without capacitance (left) as the reference. Three different capacitance  $C_m = 1$  (top),  $C_m = \delta^{-1}$  (middle) and  $C_m = \delta^{-2}$  (bottom) is adopted in the middle column. In each figure, the solid line shows the zero level set ( $\psi = 0$ ) where the black line shows the drop shape without capacitance and the red line shows the drop shape with capacitance. The rest parameters are chosen as  $\epsilon_r = 3.5$ ,  $Ca_E = 1$  and  $t_{E2D} = t_{E2M} = \delta^2$ .

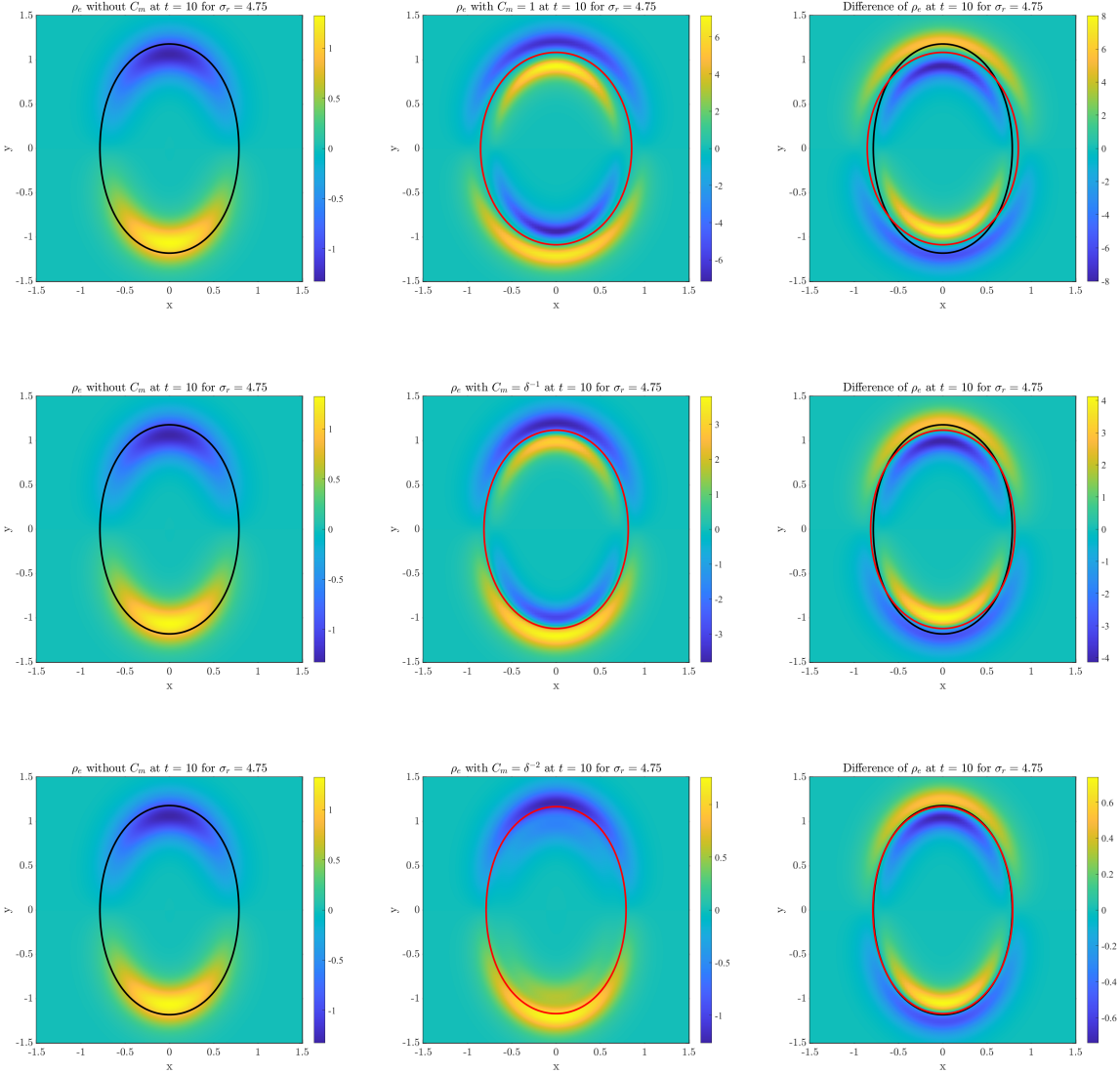


Figure 24: The effect of capacitance for the net charge model at  $t = 10$ . Conductivity ratio  $\sigma_r = 4.75$  is adopted here. We choose the situation without capacitance (left) as the reference. Three different capacitance  $C_m = 1$  (top),  $C_m = \delta^{-1}$  (middle) and  $C_m = \delta^{-2}$  (bottom) is adopted in the middle column. In each figure, the solid line shows the zero level set ( $\psi = 0$ ) where the black line shows the drop shape without capacitance and the red line shows the drop shape with capacitance. The rest parameters are chosen as  $\epsilon_r = 3.5$ ,  $Ca_E = 1$  and  $t_{E2D} = t_{E2M} = \delta^2$ .

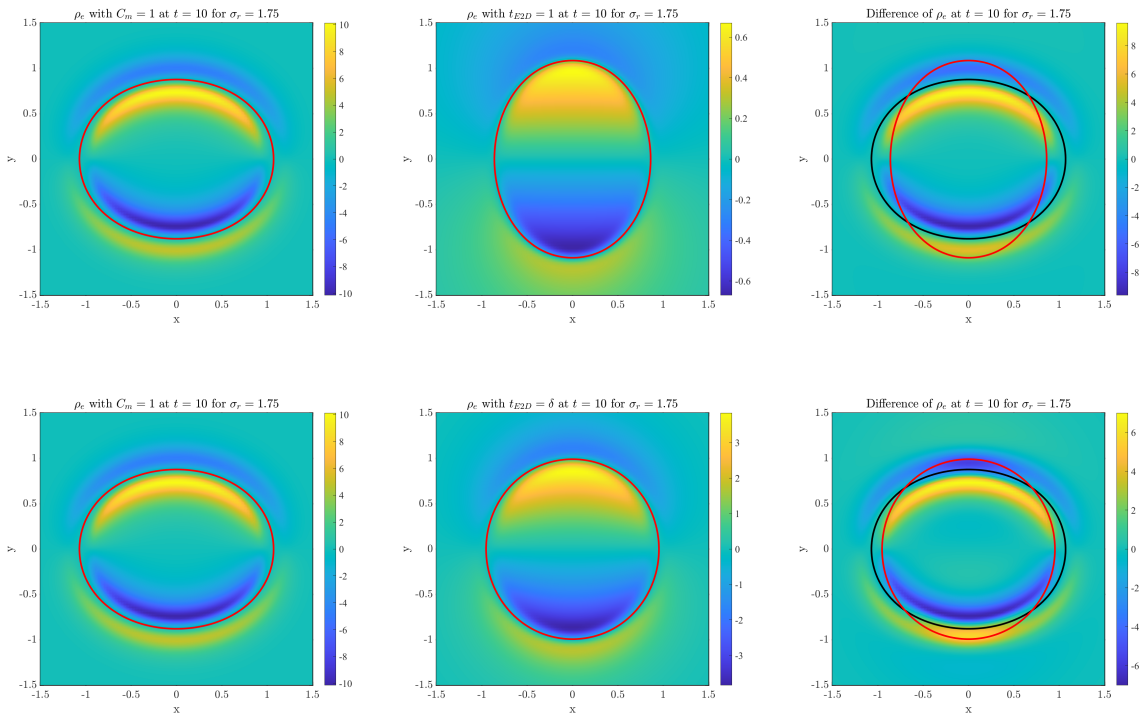


Figure 25: The behavior of drop shapes and distribution of the net charge with conductivity ratio  $\sigma_r = 1.75$  at  $t = 10$  for the net charge model. We choose  $t_{E2M} = \delta^2$  as the reference with black solid line and the results with  $t_{E2M} = 1$  (top) and  $t_{E2M} = \delta$  (bottom) with the red solid line. The rest parameters are chosen as  $\epsilon_r = 3.5$ ,  $Ca_E = 1$  and  $C_m = 1$ .

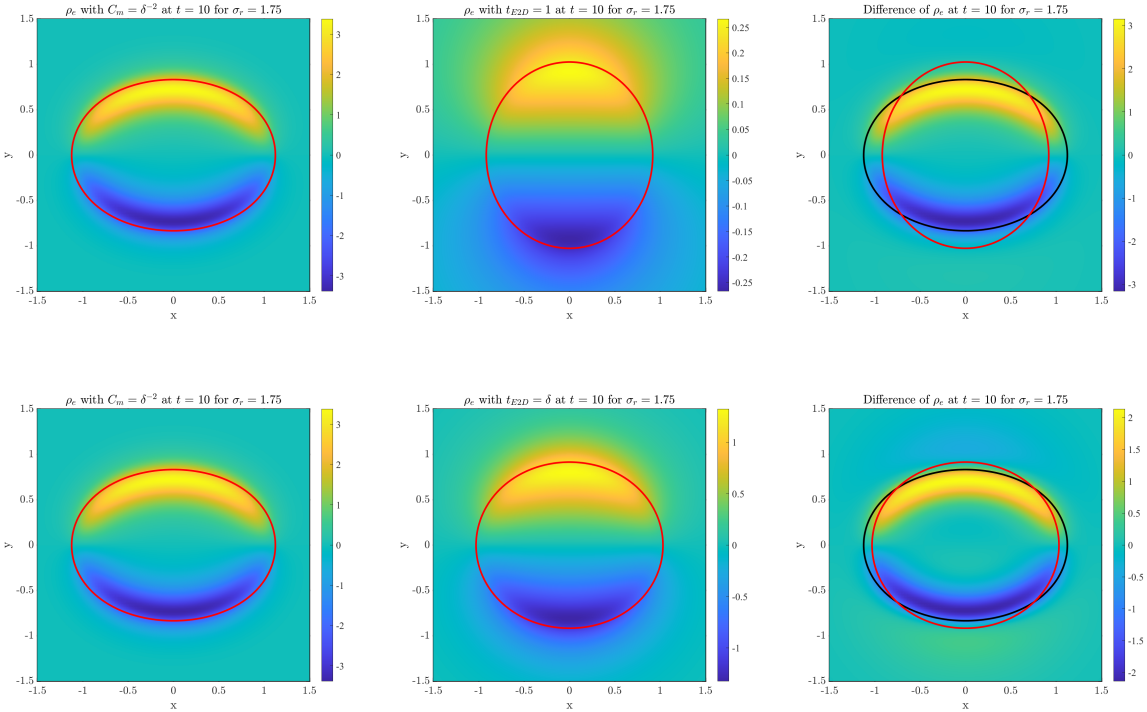


Figure 26: The behavior of drop shapes and distribution of the net charge for conductivity ratio  $\sigma_r = 1.75$  at  $t = 10$  for the net charge model. We choose  $t_{E2M} = \delta^2$  as the reference with black solid line and results with  $t_{E2M} = 1$  (top) and  $t_{E2M} = \delta$  (bottom) with the red solid line. The rest parameters are chosen as  $\epsilon_r = 3.5$ ,  $Ca_E = 1$  and  $C_m = \delta^{-2}$ .

## References

- [1] Muhammad Salman Abbasi, Ryungeun Song, Seongsu Cho, and Jinkee Lee. Electro-hydrodynamics of emulsion droplets: physical insights to applications. *Micromachines*, 11(10):942, 2020.
- [2] Muhammad Salman Abbasi, Ryungeun Song, Jaehoon Kim, and Jinkee Lee. Electro-hydrodynamic behavior and interface instability of double emulsion droplets under high electric field. *Journal of Electrostatics*, 85:11–22, 2017.
- [3] Sara Aghdaei, Mairi E Sandison, Michele Zagnoni, Nicolas G Green, and Hywel Morgan. Formation of artificial lipid bilayers using droplet dielectrophoresis. *Lab on a Chip*, 8(10):1617–1620, 2008.
- [4] Martin Z Bazant. Electrokinetics meets electrohydrodynamics. *Journal of Fluid Mechanics*, 782:1–4, 2015.
- [5] Martin Z Bazant, Mustafa Sabri Kilic, Brian D Storey, and Armand Ajdari. Towards an understanding of induced-charge electrokinetics at large applied voltages in concentrated solutions. *Advances in colloid and interface science*, 152(1-2):48–88, 2009.
- [6] Erik Bjørklund. The level-set method applied to droplet dynamics in the presence of an electric field. *Computers & fluids*, 38(2):358–369, 2009.
- [7] Mourad Boussoualem, Mimoun Ismaili, and Frederick Roussel. Influence of surface anchoring conditions on the dielectric and electro-optical properties of nematic droplets dispersed in a polymer network. *Soft matter*, 10(2):367–373, 2014.
- [8] Syandan Chakraborty, I-Chien Liao, Andrew Adler, and Kam W Leong. Electrohydrodynamics: A facile technique to fabricate drug delivery systems. *Advanced drug delivery reviews*, 61(12):1043–1054, 2009.
- [9] Yutong Cui, Ningning Wang, and Haihu Liu. Numerical study of droplet dynamics in a steady electric field using a hybrid lattice boltzmann and finite volume method. *Physics of Fluids*, 31(2):022105, 2019.
- [10] Wei-Fan Hu, Ming-Chih Lai, Yunchang Seol, and Yuan-Nan Young. Vesicle electrohydrodynamic simulations by coupling immersed boundary and immersed interface method. *Journal of Computational Physics*, 317:66–81, 2016.
- [11] Wei-Fan Hu, Ming-Chih Lai, and Yuan-Nan Young. A hybrid immersed boundary and immersed interface method for electrohydrodynamic simulations. *Journal of Computational Physics*, 282(1):47–61, 2015.
- [12] Jinsong Hua, Liang Kuang Lim, and Chi-Hwa Wang. Numerical simulation of deformation/motion of a drop suspended in viscous liquids under influence of steady electric fields. *Physics of Fluids*, 20:113302, 2008.
- [13] Rahul B Karyappa, Shivraj D Deshmukh, and Rochish M Thaokar. Breakup of a conducting drop in a uniform electric field. *Journal of fluid mechanics*, 754:550–589, 2014.
- [14] Etienne Lac and GM Homsy. Axisymmetric deformation and stability of a viscous drop in a steady electric field. *Journal of Fluid Mechanics*, 590:239–264, 2007.
- [15] Yuan Lin, Paal Skjetne, and Andreas Carlson. A phase field model for multiphase electrohydrodynamic flow. *International Journal of Multiphase Flow*, 45:1–11, 2012.
- [16] JM López-Herrera, Stéphane Popinet, and MA2764018 Herrada. A charge-conservative approach for simulating electrohydrodynamic two-phase flows using volume-of-fluid. *Journal of Computational Physics*, 230(5):1939–1955, 2011.
- [17] J R Melcher and G I Taylor. Electrohydrodynamics: A review of the role of interfacial shear stresses. *Annual Review of Fluid Mechanics*, 1(1):111–146, 1969.
- [18] Yoichiro Mori and Y-N Young. From electrodiffusion theory to the electrohydrodynamics of leaky dielectrics through the weak electrolyte limit. *Journal of Fluid Mechanics*, 855:67–130, 2018.

[19] Yuzhe Qin, Huaxiong Huang, Yi Zhu, Chun Liu, and Shixin Xu. A phase field model for mass transport with semi-permeable interfaces. *Journal of Computational Physics*, 464:111334, 2022.

[20] R Ryham, C Liu, and ZQ Wang. Electro-kinetic fluids: analysis and simulation. *Nonlinearity*, 6, 2006.

[21] Rolf Josef Ryham. *An energetic variational approach to mathematical modeling of charged fluids: charge phases, simulation and well posedness*. PhD thesis, Pennsylvania State University, 2006.

[22] D.A. Saville. Electrohydrodynamics: The taylor-melcher leaky dielectric model. *Annual Review of Fluid Mechanics*, 29(1):27–64, 1997.

[23] Ory Schnitzer and Ehud Yariv. The taylor–melcher leaky dielectric model as a macroscale electrokinetic description. *Journal of Fluid Mechanics*, 773:1–33, 2015.

[24] L. Shen, H. Huang, P. Lin, Z. Song, and S. Xu. An energy stable c0 finite element scheme for a quasi-incompressible phase-field model of moving contact line with variable density. *Journal of Computational Physics*, 405:109179, 2020.

[25] R Singh, SS Bahga, and A Gupta. Electrohydrodynamic droplet formation in a t-junction microfluidic device. *Journal of Fluid Mechanics*, 905:A29, 2020.

[26] Petia M Vlahovska. Electrohydrodynamics of drops and vesicles. *Annual Review of Fluid Mechanics*, 51:305–330, 2019.

[27] Li Wan, Shixin Xu, Maijia Liao, Chun Liu, and Ping Sheng. Self-consistent approach to global charge neutrality in electrokinetics: A surface potential trap model. *Physical Review X*, 4(1):011042, 2014.

[28] S. Wise, J. Kim, and J. Lowengrub. Solving the regularized, strongly anisotropic Cahn–Hilliard equation by an adaptive nonlinear multigrid method. *Journal of Computational Physics*, 226(1):414–446, 2007.

[29] Bowei Wu and Shravan Veerapaneni. Electrohydrodynamics of deflated vesicles: budding, rheology and pairwise interactions. *Journal of Fluid Mechanics*, 867:334–347, 2019.

[30] Shixin Xu, Ping Sheng, and Chun Liu. An energetic variational approach for ion transport. *arXiv preprint arXiv:1408.4114*, 2014.

[31] Xianmin Xu, Yana Di, and Haijun Yu. Sharp-interface limits of a phase-field model with a generalized navier slip boundary condition for moving contact lines. *Journal of Fluid Mechanics*, 849:805–833, 2018.

[32] Qingzhen Yang, Ben Q Li, and Yucheng Ding. 3d phase field modeling of electrohydrodynamic multiphase flows. *International Journal of Multiphase Flow*, 57:1–9, 2013.

[33] Qingzhen Yang, Ben Q Li, and Feng Xu. Electrohydrodynamic rayleigh-taylor instability in leaky dielectric fluids. *International Journal of Heat and Mass Transfer*, 109:690–704, 2017.

[34] Jun Zeng and Tom Korsmeyer. Principles of droplet electrohydrodynamics for lab-on-a-chip. *Lab on a Chip*, 4(4):265–277, 2004.

[35] Junfeng Zhang and Daniel Y Kwok. A 2d lattice boltzmann study on electrohydrodynamic drop deformation with the leaky dielectric theory. *Journal of Computational Physics*, 206(1):150–161, 2005.

[36] Emilij K Zholkovskij, Jacob H Masliyah, and Jan Czarnecki. An electrokinetic model of drop deformation in an electric field. *Journal of Fluid Mechanics*, 472:1–27, 2002.